INVESTIGATION OF THE EFFECT OF ORIENTATION AND HEAT TREATMENT ON THE STRESS CORROSION CRACKING SUSCEPTIBILITY OF 7050 ALUMINUM ALLOY

A THESIS SUBMITTED TO
THE GRADUATE SCHOOL OF NATURAL AND APPLIED SCIENCES
OF
MIDDLE EAST TECHNICAL UNIVERSITY

BY

GÜL ÇEVİK

IN PARTIAL FULFILLMENT OF THE REQUIREMENTS
FOR
THE DEGREE OF MASTER OF SCIENCE
IN
METALLURGICAL AND MATERIALS ENGINEERING

AUGUST 2004

Approval of the Graduate School of Natural and Applied Sciences

Prof. Dr. Canan ÖZGEN

Director

I certify that this thesis satisfies all the requirements as a thesis for the degree of Master of Science.

Prof. Dr. Bilgehan ÖGEL

Head of Department

This is to certify that we have read this thesis and that in our opinion it is fully adequate, in scope and quality, as a thesis for the degree of Master of Science.

Prof. Dr. Rıza GÜRBÜZ	Prof. Dr. Mustafa DORUK
Co-Supervisor	Supervisor

Examining Committee Members

Assoc. Prof. Dr. Kadri AYDINOL	(METU, METE)	
Prof. Dr. Mustafa DORUK	(METU, METE)	
Prof. Dr. Rıza GÜRBÜZ	(METU, METE)	
Prof. Dr. Semra BİLGİÇ	(ANKARA UNV.)	
Prof. Dr. Tayfur ÖZTÜRK	(METU, METE)	

I hereby declare that all information in this document has been obtained and presented in accordance with academic rules and ethical conduct. I also declare that, as required by these rules and conduct, I have fully cited and referenced all material and results that are not original to this work.

Name, Last name: Gül Çevik

Signature :

ABSTRACT

INVESTIGATION OF THE EFFECT OF ORIENTATION AND HEAT TREATMENT ON THE STRESS CORROSION CRACKING SUSCEPTIBILITY OF 7050 ALUMINUM ALLOY

Çevik, Gül
M.S., Department of Metallurgical and Materils Engineering
Supervisor: Prof. Dr. Mustafa Doruk
Co-Supervisor: Prof. Dr. Rıza Gürbüz
August 2004, 118 Pages

In the present work, the effect of variation in specimen orientation and heat treatment on the Stress Corrosion Cracking (SCC) susceptibility of 7050 aluminum alloy was investigated in 3,5% NaCl solution and under freely corroding conditions. For this purpose, Constant Extension Rate Tests (CERT) was performed on precracked Compact Tension (CT) specimens and the Direct Current Potential Drop technique was applied to measure the crack lengths. In addition to crack length versus time curves, the relationship between the crack growth rate and the stress intensity factor was determined. Fractographic analysis was utilized extensively to support the findings related with basic mechanisms of cracking.

The alloy was found to be in the most susceptible state in the SL orientation, in which the crack propagation direction is parallel to the rolling direction. The resistance to SCC is higher in the TS but at maximum in LT orientation where the loading direction is parallel to the rolling direction.

In the peak aging treatment, T651, alloy is susceptible to SCC in SL orientation. When the over aging treatment, T7651, is applied the resistance is increased and the two step over aging treatment, T73651, has resulted in an additional improvement in this orientation. On the other hand, the alloy showed higher resistance to SCC in TS and LT orientations in T651 condition compared to the T7651 and T73651 treatments. In these orientations, the alloy is less susceptible in T73651 condition than in T7651 treatment.

Keywords: Stress corrosion cracking, high strength aluminum alloys, specimen orientation, heat treatment, direct current potential drop technique.

ÖZ

ÖRNEKLEME YÖNÜNÜN VE ISIL İŞLEMİN 7050 ALÜMİNYUM ALAŞIMININ GERİLİMLİ KOROZYON ÇATLAMASI DUYARLILIĞINA ETKİSİNİN İNCELENMESİ

Çevik, Gül
Yüksek Lisans, Metalurji ve Malzeme Mühendisliği Bölümü
Tez Yöneticisi: Prof. Dr. Mustafa Doruk
Ortak Tez Yöneticisi: Prof. Dr. Rıza Gürbüz
Ağustos 2004, 118 Sayfa

Bu çalışmada örnekleme yönünün ve ısıl işlemin 7050 alüminyum alaşımının %3,5 NaCl çözeltisinde ve serbest korozyon koşullarında Gerilimli Korozyon Çatlaması (GKÇ) duyarlılığına etkisi araştırılmıştır. Bu amaçla Kompakt Çekme numunelerine Sabit Uzama Hızı testi uygulanmıştır. Çatlak boyları Sabit Akım Potansiyel farkı tekniği ile ölçülmüştür. Zamana karşı çatlak uzunluğuna ek olarak, çatlak büyüme hızı ile gerilim şiddet faktörü arasındaki ilişki de belirlenmiştir. Temel kırılma mekanizmalarıyla ilgili olarak, sonuçları desteklemek için kırılma yüzeyleri incelenmiştir.

Çatlak ilerleme doğrultusunun haddeleme doğrultusuna paralel olduğu SL örnekleme yönünde alaşımın GKÇna en duyarlı olduğu gözlenmiştir. Dayanç TS yönünde daha yüksektir ancak yükleme doğrultusunun haddeleme doğrultusuna paralel olduğu LT yönünde ise alaşımın GKÇna en dayançlı olduğu gözlenmiştir.

Alaşım SL yönünde ve peak yaşlandırma işlemi uygulandığında GKÇna duyarlı hale gelmektedir. İleri yaşlandırma işleminde (T7651) dayanç yükselmekte ve iki aşamalı ileri yaşlandırma işlemi, T73651, ise dayancın daha da fazla artmasını sağlamıştır. Diğer taraftan, TS ve LT yönleri T651 işleminde T7651 ve T73651 işlemlerine göre GKÇna daha dayançlı bulunmuştur. Bu yönlerde duyarlılık T73651 işleminde T7651 işlemine göre azalma göstermiştir.

Anahtar Kelimeler: Gerilimli korozyon çatlaması, yüksek dayançlı alüminyum alaşımları, örnekleme yönü, ısıl işlem, sabit akım potansiyel farkı tekniği.

to the memory of beloved Muzaffer Öztürk
whose personality is a guide & a great
inspiration to my life...

ACKNOWLEDGEMENTS

I would like gratefully to express my sincere thanks to Prof.Dr. Mustafa Doruk for his enthusiastic supervision, excellent guidance and kindness throughout this study. I appreciate to him who is a model scientist and a virtuous person.

I thank to Prof. Dr. Rıza Gürbüz for his supervision during the fractographic studies. I am indebted to him also for his support, insightful vision, and encouraging conversations.

Thanks to Prof.Dr. Filiz Sarıoğlu for her advices, guidance and positive attidute at the beginning of the study.

I am forever grateful to my parents Atike-Hamit Çevik and my brother Korhan Çevik for their endless understanding, patience and support throughout my life.

Special thanks to my friends Nevzat Akgün, Gülgün Aydoğdu, Ezgi Kotan, Hülya Arslan, Selen Gürbüz, Fatih Güner, Tufan Güngören, Ziya Esen and Kaan Pehlivanoğlu, for their support and friendship during this long journey; their understanding and encouragement when it was most required.

Thanks to the technical staff of Middle East Technical University, Department of Metallurgical and Materials Engineering, especially to Yaşar Kazanç, for their invaluable contributions to my study.

TABLE OF CONTENTS

CHAPTER 1

INTRODUCTION

Constant demands for high strength and weight reduction have been a driving force for the extensive usage of high strength aluminum alloys for the aeronautical applications. By the use of these alloys, fuel consumption is reduced in addition to the increased performance of the aircraft structures.

According to the Aluminum Association Identification system, Al-Zn-Mg-Cu alloys are named as 7000 series. 7000 series aluminum alloys have been used extensively in aircraft structures such as wing coverings, landing gear supports, fuselage structures and rivets.

It has been well established that these mechanically improved Al-alloys, especially the medium and high strength grades, suffer from the premature failure at specific environments. In such cases, cracking can occur below the stresses required for yielding. This type of brittle fracture caused by the conjoint action of corrosive environment and mechanical stress was called as Stress Corrosion Cracking (SCC).

The SCC phenomenon was first identified in the second half of 19^{th} century in the cold-drawn brass cartridge case, followed by the use of brass for the condenser tubes in electric power industry. SCC was first named as “season cracking” since SC cracks resemble the cracks in seasoned wood. Following the caustic failure of brass in ammonia SCC was then observed in steel boilers in caustics and in nitrates. Early in 20^{th} century SCC of Al-alloys in moist atmospheres was reported (1). Ever since, SCC of Al-alloys has been a problem of modern technology, especially in aeronautical engineering.

The SCC and Corrosion Fatigue studies have gained importance in recent years since especially military aircrafts are subjected to seawater by the action of wind or salt water spray from the sea during their flights at low altitudes over the sea and during take off or landing on the deck.

Alloy 7075 has been used in aircraft industry for many years. Studies to increase strength, fracture toughness and corrosion resistance of these alloys lead to the development of alloy 7050.

In addition to the development of new high strength aluminum alloys, improvement of corrosion resistance by the modification of microstructure with appropriate heat treatments have also been the subject of design studies. The T651 (peak aging) and T7651 (over aging) tempers which include the precipitation heat treatment following the solutionizing and quenching has been used extensively. Recently, in order to increase the SCC resistance, a two step over aging treatment, T73651 has been developed.

The current research aims to extend the data about the SCC behavior of 7050 alloy. Since the SCC and strength characteristics of the aluminum alloys depend strongly on the grain orientation; effects of peak aging, T651, over aging, T7651, and two-step over aging, T73651, have been investigated for 3 different crack propagation directions. In addition to the crack length (a) versus time (t) curves, the crack velocity (da/dt) versus mode I stress intensity factor (K_I) curves has been plotted for each specimen. Compact Tension (CT) specimens were tested by Constant Extension Rate Test (CERT) in 3,5wt% NaCl solution as the simulation of sea water. Crack lengths were measured by the use of Direct Current Potential Drop Technique.

CHAPTER 2

THEORY

2.1. General Characteristics of SCC

Stress Corrosion Cracking (SCC) is a time dependent process in which a metallurgically susceptible material fractures prematurely due to the synergistic interaction of a corrosive environment and a sustained tensile stress at the metal surface (2).

The tensile stress may be externally applied or may be present as the residual stresses resulting from fabrication processes, such as rolling, welding, etc., or from the heat treatments applied; and sometimes may be a combination of these conditions (2).

With the presence of a sustained tensile stress, in order for SCC to occur, threshold stress intensity, K_{ISCC}, must be exceeded. Threshold stress intensity is the critical crack tip stress intensity factor for opening mode (Mode I), below which, presumably, no failure can occur as a result of SCC (3). The threshold stress intensity values can change significantly depending on the environment.

SCC failures resemble brittle fracture; typically, there is no or little indication of metal ductility at the origin of fracture. The cracking is actually a form of subcritical flaw growth, either intergranular or transgranular, depending on the particular combination of microstructure, environment, and strain rate. However, because of compositional, mechanical and metallurgical synergism and the consequent need to consider a range of environmental variables, as well as their variations with time and their interactions with loading and metallurgical variables, it is more difficult to design against Environmentally

Assisted Cracking (EAC) than against fracture. The necessary conditions required for SCC are shown in Figure 2.1 (2).

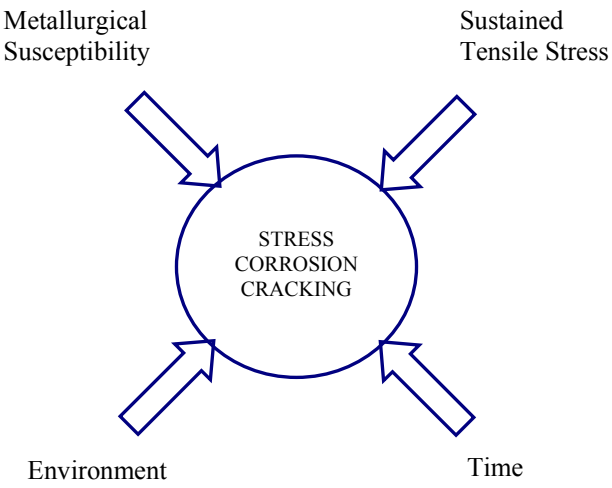

Figure 2.1. Conditions required for Stress Corrosion Cracking (2).

SCC prevention and control is problematic because it is often too difficult to control even one of the three factors; tensile stress, environment and susceptibility of the alloy.

The first factor, sustained tensile stress, is typically the most difficult to control, and for that matter, to quantify. In some cases, the stress may be an externally applied service stress. Stresses may be internal as well, such as from unequal cooling rates from high temperature, nonuniform deformation during cold working; or neglect of post-weld stress relief. If external, the best way to eliminate the effect of stress is to reduce the external load or increasing the cross-sectional area perpendicular to the applied stress. But if the stress is residual, an appropriate heat treatment must be applied to the material to eliminate these kind of stresses.

Metallurgy of the material plays an important role in the SCC beahavior. SCC resistance of a material can be increased by changing the composition of the alloy or by changing the microstructure to a more SC resistant condition by the use of proper heat treatments.To replace a SCC susceptible part with a more corrosion resistant material is not always possible because the new material may not meet strength requirements, or in order to meet strength requirements, the component might need a major redesign.

It is seldom possible to eliminate the environment responsible for a particular SCC problem totally. If possible, critical species responsible for SCC may be lowered or corrosion-inhibitors may be used to reduce the effect of environment. Isolating the environment from the material by using traditional techniques such as protective coatings may also be useful (4).

An important parameter that must be included to SCC processes in determining the mechanisms is the role of time. A quantitative determination of a SC mechanism must include not only what is happening either in metallurgical or electrochemical terms but perhaps most importantly, it must indicate the rates at which such occurences are operating (5).

2.2 Proposed Models for SCC

The SCC of Al-alloys is well documented in literature, there have been several mechanisms proposed for this phenomenon. Yet there is considerable disagreement in the scientific literature as to what mechanism causes it.

However, there are three main theories proposed for SCC of Al-alloys. These are;

- Anodic Dissolution
- Hydrogen Embrittlement
- Film Induced Cleavage

Within each of these three main theories, there are numerous submodels (6).

2.2.1 Anodic Dissolution

Anodic dissolution is sometimes called as Film Rupture Theory or Slip-Dissolution Model. According to this theory, the protective surface normally present on the metal's surface is ruptured by localized plastic deformation at the crack tip, while the film away from the tip and the non-deforming crack walls remain intact. At this time an electrolytic cell is formed, where the ruptured bare metal part is the anode and the unbroken surface film serves as the cathode. At the anodic part, anodic dissolution occurs and the crack advances. Since repassivation will occur, further plastic strain is required for the mechanism to be repeated. This behavior is repeated until fracture (7,8). In Figure 2.2, crack tip is represented schematically during anodic dissolution (9). The anodic areas are either the anodic secondary phases or the precipitate free areas which are most often arranged at the grain and subgrain boundaries and are also anodic compared with the body of the grain, as illustrated in Figure 2.3 (10).

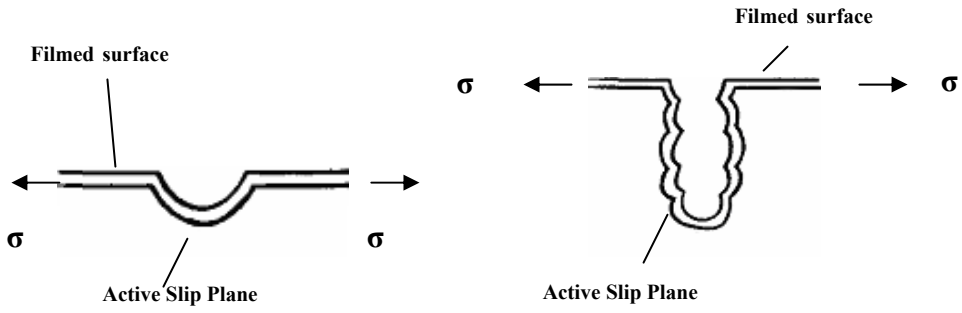

Figure 2.2 Schematic representation of crack tip during crack initiation and growth by the Anodic Dissolution mechanism (9).

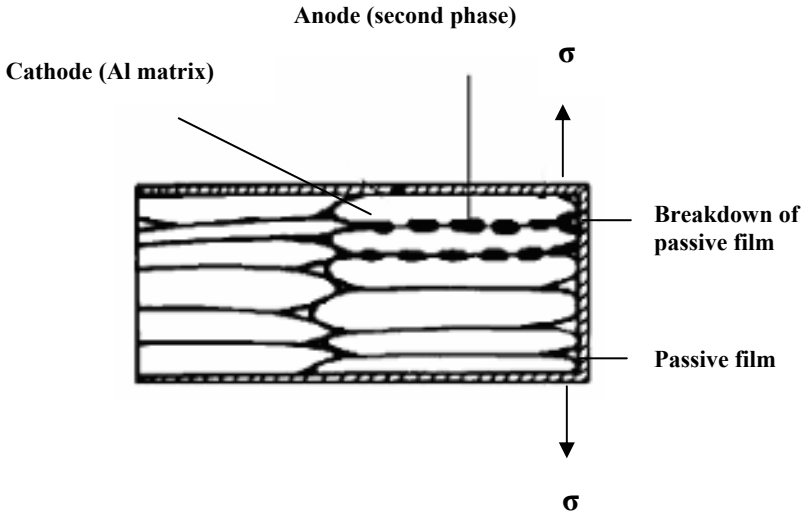

Figure 2.3 Schematic view of the intergranular stress corrosion by anodic dissolution (10).

Because of its consistence with many experimental observations concerning the effect of heat treatment on SCC susceptibility, this theory is still widely accepted, especially in the aluminum industry (11).

There have been several investigations on the anodic dissolution mechanism of aluminum alloys. These works involve the investigation of anodic dissolution mostly in electrochemical points of view. The effects of grain boundary structure and heat treatments are also studied extensively. The experimental studies involved the potential measurements and the inhibiting effect of cathodic polarization. The exact location of the localized corrosion path and the specific roles of grain boundary precipitates and the solid solutions in the grain margins depend upon the alloy type and its metallurgical condition and upon the chemical nature of the environment.

The theory of anodic dissolution as a mechanism of SCC was first proposed more than 60 years ago by Dix (12) with Mears and Brown (13) claiming that galvanic cells are set up between continuous intermetallic precipitates and

adjacent metal at grain boundaries or through paths within the grains, ensuing corrosion acting under stress to open up a crack. The role of applied stress was considered as rupturing the surface films, thereby exposing fresh metal at the crack tip and allowing reaction to continue. They supported their view by potential measurements which showed that intergranular (IG) crack sensitive paths in various aluminum alloys and also in some other metals, were anodic with respect to the grains. They also reinforced their theory with the experimental results which showed that the cathodic polarization prevented crack initiation or the growth of already started cracks. Depending on the metal, this mechanism was elaborated with certain modifications by Evans (14), Parkins (15), Hoar (16), Graf (17) and others.

A marked decrease of anodic polarization during active straining of metal wires was measured by Hoar and West (18). They supposed that an effect of this kind could act to accelerate electro-chemical action between the tip and walls of the growing cracks. They claimed that decreased anodic polarization can not be of primary importance to the SCC mechanism in the view of (I) the immunity of pure metals and various alloys which should be affected electrochemically by active strain not less than susceptible metals, except for greater overall increased area of fresh metal at surface cracks at susceptible metals and (II) the required specificity for reduced polarization. Furthermore, (III) electrochemical effects, such as discontinuous potential jumps during extension of a stressed metal specimen in an electrolyte are not confined to media which favor oxide films nor to media which cause SCC. For example, Baumel and Engell (19) found that discontinuous potentials jumps of up to 10 mV in the active direction accompanied discontinuous extension of stressed mild steel exposed to boiling 45% $CaCl_2$ (O_2 saturated) solution in which SCC did not occur, as well as in boiling $Ca(NO_3)_2$ solution in which SCC did occur.

Maitra and English(20) proposed that changes in the environment can have significant effects on localized corrosion behavior of 7075 aluminum alloy and particularly, the addition of nitrates to an aqueous solution containing chlorides

can cause IG corrosion of 7075 alloy plate in the T7351 temper; after obtaining anodic polarization curves in various chloride solutions, containing nitrates and sulphates. They attributed the increased susceptibility of the alloy to IG corrosion to the increased differences between the pitting potentials of different regions of the microstructure. They explained this feature as the difference between the pitting potential of the active grain boundary regions and the relatively noble grain interior regions increases in the presence of nitrates, thereby increasing the driving force for localized corrosion. They also proposed that the rate of grain boundary attack varies with changes in environment as a result of changes in pitting potentials which is the most important factor controlling the susceptibility to IG corrosion. As a result of their investigation, they reported not only that IG corrosion of 7075-T7351 may occur in urban environments since, generally, they are known to contain nitrates and chlorides but also the effect of sulphates and pH on the pitting potentials of the alloy in chloride + nitrate solutions is relatively small.

Joshi, Shastry and Levy (21) have investigated the effect of heat treatment on the relative amounts of the alloying elements in the grain boundaries of the aluminum alloy 7075 with Auger electron spectroscopy in a scanning Auger microprobe. They observed that both aging and solution treatments affect the distribution of these elements at grain boundaries and if identical solution treatments are employed, the aging treatment determined the solute distribution at grain boundaries and for fixed final aging treatment, the temperature of solution anneal determined the solute distribution. Their measurements showed that higher amounts of alloying elements at grain boundaries are present at the SC susceptible aging treatment T6 condition with respect to the T73 condition. They reported that SCC resistance is strongly dependent on the solute concentration at the grain boundaries which should be considered to be essential in any mechanism of IG SCC of Al-Zn-Mg alloys.

The rate of repassivation has been the subject of many investigations and is considered to be an important factor in SCC mechanism. If the repassivation

rate is too low, the crack blunts since dissolution on the crack sides will be excessive. On the other hand, if it is too high, the amount of penetration caused by crack tip dissolution is minimized. SCC process occurs at intermediate passivation rates (10, 12).

2.2.2 Hydrogen Embrittlement

There had been a broad belief among the researchers that the only mechanism causing SCC in aluminum alloys was the stress assisted anodic dissolution until the mid 70's, since SCC is frequently intergranular for these alloys. However, in recent years, numerous studies have been providing experimental evidence that hydrogen embrittlement has a significant effect on SCC phenomena in 7000 series aluminum alloys.

Hydrogen dissolves in all metals to a moderate extent. It is a very small atom, and fits in between the metal atoms in the crystals of the metal. Consequently it can diffuse much more rapidly than larger atoms. Hydrogen tends to be attracted to regions of high triaxial tensile stresses where the metal structure is dilated. Thus, it is drawn to the regions ahead of cracks or notches that are under stress. The dissolved hydrogen then assists in the fracture of the metal, possibly by making cleavage easier or possibly by assisting in the development of intense local plastic deformation. These effects lead to embrittlement of the metal; cracking may be either inter or transgranular. This kind of fracture phenomenon is called hydrogen embrittlement. The schematic view of hydrogen embrittlement is depicted on Figure 2.4 (7).

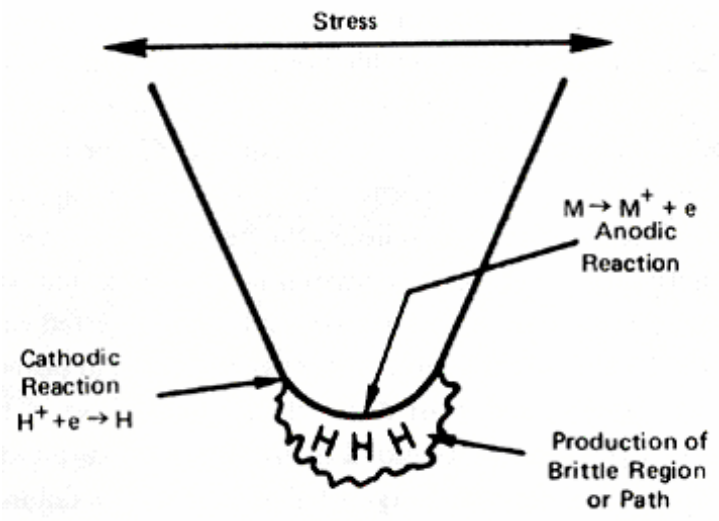

Figure 2.4 Hydrogen embrittlement mechanism for SCC. Cathodic reduction of H^+ at the tip of the crack produces hydrogen which enters the vicinity of the tip and embrittles the metal immediately ahead of and advancing crack (7).

In an investigation by Hardwick et. al. (6, 22), the 7050 and low copper 7050 alloys in the longitudinal direction were tested by two methods; first by hydrogen charging and tensile testing and second by straining electrode test. As a result of their study, they claimed that 7050 alloy was not susceptible to HE in the peak aged or over aged condition. However, the under aged 7050 and low Cu 7050 in all tempers were susceptible to HE. The authors believed that dislocation transport of hydrogen and local hydrogen accumulation at grain boundaries controlled the extent of brittle fracture.

Song et.al. (23), have investigated the relationship between grain boundary segregation and crack growth of SC and corrosion fatigue in 7050 aluminum alloy under various aging conditions. They have calculated the effects of GB segregation on the IG fracture work using a quasichemical approach. They have reported that the hydrogen content at the crack tip and the crack growth rate increase with the concentration of solid solution magnesium increasing on grain boundary; both Mg and H segregation induce the IG fracture work to

decrease. They have concluded that Mg segregation accelerates H enriching and crack propagation. It is also indicated that a Mg-H interaction occurs in the process of corrosion fatigue as well as SC. According to their theory and calculation they have postulated by using quasichemical approach, they summarized the role of Mg segregation in HIF process of 7050 alloy as: Mg segregation induces the intergranular fracture work to decrease; on the other hand, by the use of Mg-H interaction, Mg segregation enhances the amount of hydrogen absorbed, accelerates its diffusion and raises the solution degree of hydrogen on the grain boundary reinforcing, thus accelerating the crack growth of SC and CF. They have also explained that since the electronegativity difference between Mg and H atoms is larger than that between Al and H atoms, the affinity of the Mg and H atoms is larger than that of Al and H atoms. Accordingly, after the replacement of Al atoms with Mg atoms at the grain boundary, with the increasing segregation of Mg, H enrichment at the GB increases. After H enrichment at the GB, they will draw charge from Al atoms onto themselves because of the higher electonegativity of hydrogen with respect to that of aluminum. And they have explained that there is less charge available to precipitate in metal-metal bonds due to this charge transfer. Depending on the quantum theory, which postulates that the smaller the electron density, the weaker the atomic binding force; they have stated the physical nature of HE in aluminum alloys as: grain boundary segregation results in the electron density surrounding aluminum atoms to decrease and then in the reduction of IG fracture work.

Adler et.al. (24) claimed that the grain boundary precipitate characteristics has an important role on the SCC behavior. They also explained that the SCC resistance can be improved effectively by increasing the size and spacing of the grain boundary precipitates (GBPs). Since the larger GBPs can act as atomic hydrogen trapping sites which will lead to nucleate molecular hydrogen bubbles, so that the atomic hydrogen concentration at the GBs will decrease below a critical value to retard HIF. Moreover, they reported that the crack

propagation rate can significantly be reduced by larger interparticle spacing of GBPs by conventional T7 treatment on the expense of some strength.

Tsai et.al. (25) investigated the effect of grain size upon the SCCof 7475 Al-alloy plates. They applied the underaging T4, peakaging T6, two step overaging T73 and retrogression and reaging (RRA) heat treatments to the alloy, to demonstrate the effect of grain refinement on SCC resistance. They reported that grain refinement resulted in a more homogeneous slip mode and a smaller size of grain boundary precipitates to influence the SCC resistance. According to their experimental results, they reported that the more homogeneous slip mode is always beneficial for SCC resistance, however if the GBPs size was smaller than a critical precipitate size for nucleating hydrogen bubbles, the improvement of SCC due to grain refinement resulting from a more homogeneous slip, could not be obtained. In order to generate experimental data about the relationship between the SCC and HE, they conducted their experiments on both hydrogen-charged and uncharged tensile specimens for all proposed heat treatment conditions. Based on the experimental evidence showing the same tendency between the HE susceptibility and SCC susceptibility for all heat treatment conditions, they concluded that HE plays the main role to control the SCC susceptibility in the 7475 aluminum alloys.

Depending on the numerous electron microscope studies, Gruhl (6, 26) stated that neither the width of the precipitation-free zones nor the size and distribution of the precipitates in the grain boundaries can be related to the tendency to brittle fracture and susceptibility to SCC. He suggested that the diffusion of hydrogen into the grain boundaries under tensile stress reduced the cohesive strength of the grain boundaries. In his another work, Gruhl (6, 27) reviewed the literature on SCC of Al-Zn-Mg-(Cu) alloys and discredited the theory of electrochemical dissolution. He proposed that hydrogen is produced during the corrrosion and it diffuses into grain boundaries under the effect of tensile stress and embrittles the boundary. Thus the solubility of hydrogen at

the grain boundary is the critical factor. He stated that the hydrogen solubility depends on the tensile stress normal to the grain boundaries and the concentration of zinc in solid solution. The effect of tensile stress is to open up the lattice i.e. the grain boundary having a lower modulus than the matrix, and then to allow more hydrogen to diffuse inward. Another statement he made was that the increasing amount of Zn in solid solution decreased the life-time and longer aging and the addition of Cu reduces the concentration of Zn in solid solution by increased precipitation.

In a work conducted by Hermann (6, 28), the Double Cantilever Beam (DCB) specimens of aluminum alloys 7017, 7018 and 7475, all in the T651 temper were pre-exposed to a salt water solutions for several weeks and then bolt loaded and exposed to humid air at 95 percent relative humidity. The fractographic studies have shown that the crack advance was intergranular by a combination of mechanical overload shown as ductile tear ridges, elongated dimples and brittle fracture. Hermann stated that corrosion occurs during the pre-exposure to salt water, thus the passive film is attacked and hydrogen is developed and absorbed, then, the absorbed hydrogen weakens the interatomic bonds at the crack tip allowing higher crack velocity after the DCBs are stressed.

2.2.3 Combined Models

Some studies have shown that for some cases in the stress corrosion cracking process mechanism can be explained by taking into account the effect of both anodic dissolution and hydrogen embrittlement.

Hardie et. al. (6, 29) applied tensile test to the specimens of commercial 7179-T651 on which three different pre-exposure times are applied. They observed that embrittlement could be achieved by presoaking the specimen in tap water at 70°C for longer than 5 hours. Since complete recovery could be obtained by storing the specimen in lab air or in vacuum for longer than 100h, they

explained that this embrittlement was reversible. They concluded that embrittlement was due to absorption of hydrogen and recovery was due to the loss of hydrogen (or diffusion to the innocuous sites). In relation with these observations, another study with potentiostatically controlled slow strain rate tests of 7050-T73651 alloy revealed two regions of embrittlement: at strongly cathodic (hydrogen absorption) and at more anodic potentials (anodic dissolution). The author stated that at free-corrosion potentials, the two processes could overlap (30).

Magnin and Rieux (6, 31) tested smooth tensile bar specimens of weldable aluminum 7020 alloy in 3,5% NaCl solution under potentiostatic control in order to evaluate the corrosion fatigue and stress corrosion cracking behaviour. They emphasized that fatigue and anodic dissolution work together to provide microcracks for hydrogen entry into the metal which then leads to the hydrogen embrittlement.

Reboul et. al. (32) have reviewed the literature of high strength aluminum alloys in terms of responsible mechanisms for SCC. They have classified 7000 series alloys into two: first is copper lean 7000 series alloys and the second is copper rich 7000 series alloys. They stated that HE is the dominat mechanism of SCC for copper lean 7000 series alloys, however in case of copper rich 7000 series alloys, both mechanisms are involved. However, it is not clear which is not dominant in a given situation nor which microstructural features control the alloys' susceptibility.

Najjar et. al. (33) have tested 7050 aluminum alloy for three different tempers, the peak aged T6 and the over aged tempers T76 and T74 in short transverse direction, in 3% chloride solution at a strain rate of $3{,}8 \times 10^{-7} s^{-1}$. Based on the mechanical test results and similarities between microfractographic details obtained in various experimental conditions, they stated that both anodic dissolution and hydrogen embrittlement operate during the SCC process of a 7050 aluminum alloy stressed in chloride solution. The main role of anodic

dissolution is to produce critical defects which promote subsequently localized hydrogen discharge, entry and embrittlement. They concluded that the relative influence of these two mechanisms depends on the main parameters that govern cracking, i.e. the microstructure, the electrochemical potential and the strain rate.

Lee et al. (34) investigated the effect of temperature on SCC behavior of a high strength Al-Zn-Mg alloy and an Al-Li-Zr alloy in aspects of mechanisms causing SCC. They stated that the resistance and so the threshold for stress corrosion decreases with the increasing temperature. They attributed the temperature dependence of the threshold stress intensity factor to anodic dissolution mechanism. They concluded that anodic dissolution is responsible for the stage I and hydrogen embrittlement for the stage II crack propagation. Thus, by the increase in stress intensity, the mechanism changes from anodic dissolution to hydrogen embrittlement.

2.2.4 Film Induced Cleavage

The Film Induced Cleavage (FIC) Model was proposed by Sieradki and Newman (35), to explain discontinuous transgranular SCC and high transgranular SC crack growth rates. This theory postulates the presence of brittle surface films, to include dealloyed films on certain alloys and oxides on pure metals and other alloys. When a crack growing in the brittle film reaches a sufficient velocity at the film/metal interface, it will propagate further into the underlying metal . According to FIC model, the roles of anodic dissolution and hydrogen embrittlement are only to form the brittle surface film but they are not necessary to propagate cracks. Therefore, a relatively low anodic dissolution rate forms a brittle surface film and a fast growing crack in the film may penetrate for some distance into the ductile substrate metal before its growth is arrested. Then the surface film must reform at the crack tip surface before a new burst of brittle crack growth is possible. In summary, according to FIC model a low anodic current at a strained surface can enhance rapid,

discontinuous, brittle cracking (36). In Figure 2.5, the crack tip is illustrated schematically, during FIC mechanism (9).

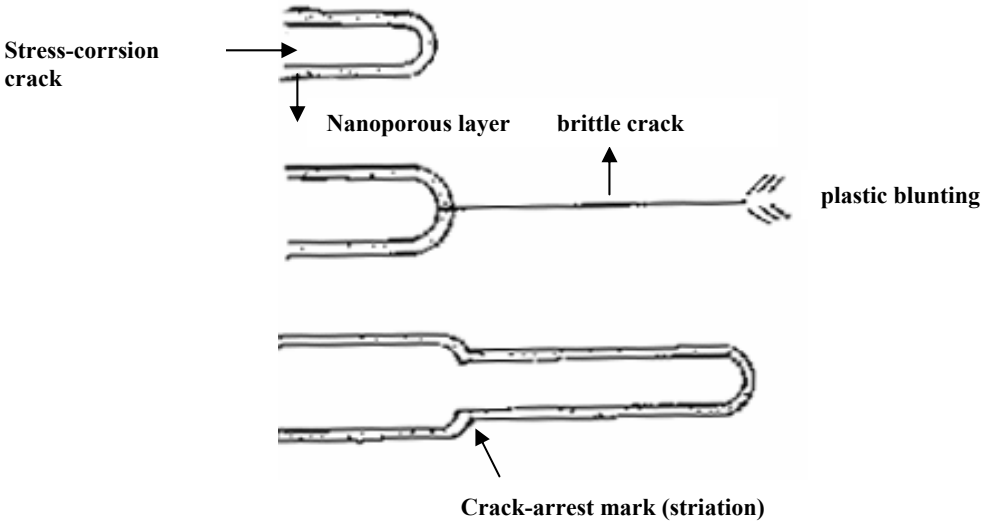

Figure 2.5 Film induced cleavage model (9).

Pugh (37) investigated the transgranular SC crack propogation in alloys by reviewing the previously proposed models and he came up with additional data. He reported that the FIC model is responsible for transgranular SC crack growth and the cleavage step formation is important in crack propagation, where intergranular SCC occurs by anodic dissolution at the crack tip.

Kanematsu, Okido, and Oki (6, 38, 39) compared three Al-Zn-Cu alloys in 0.6 N NaCl solution by a potentiostatic slow strain technique. They reported that intergranular SCC is due to the rupture of the brittle oxide film along the gain boundaries, while transgranular cracking was initiated by pitting corrosion. They used the oxide film growth to explain the effect of aging. They observed that as the aging time increased, the passive current decreased. The rapidly

growing film (higher current density) corresponded to the film, which also cracked over the grain boundary, allowing SCC.

2.3 Major Factors Affecting SCC

Stress-corrosion cracking (SCC) is affected by three factors; metallurgy of the alloy, mechanical factors and the environment. SCC behavior of a material depends on the complex interactions between these variables.

2.3.1 Mechanical Factors

A sustained tensile stress is necessary for SCC to occur. Based on the experimental evidence, it has been explained that the effect of stress in SCC is the dynamic strain it produces. And it is found that there is a threshold stress below which SCC does not occur, or at least the crack growth rate will be so slow that failure will not occur in realistic times. In Figure 2.6 a schematic illustration of time to failure with respect to the magnitude of stress is shown on a semi-logarithmic scale. As it can be derived from the figure, the SC failure will occur at shorter times when the magnitude of stress is higher (2).

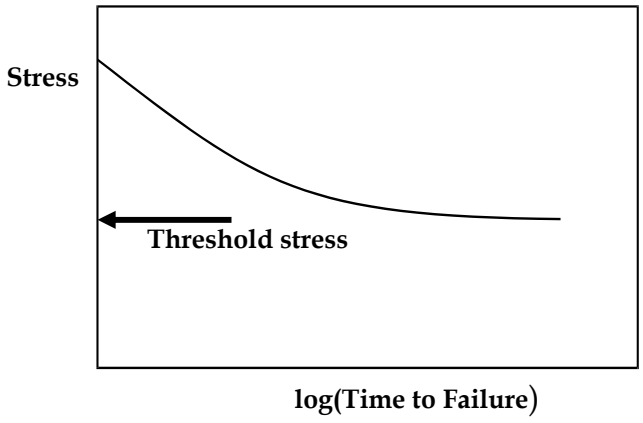

Figure 2.6 Sustained tensile stress vs log(time to failure) (2).

In service, the sustained, unintentionally induced stresses or residual short transverse or transverse stresses acting on the surface together with the corrosive environment result in SC failures. The source of residual stresses is usually the quenching of the material after solutionizing. The problem usually arises when machining operations expose the material to high residual tension stresses. At components with a complicated geometry, cooling rates may show differences at different parts during quenching because of the variations in section size or formation of steam pockets. This can cause residual surface tension stresses even without subsequent machining operations (40). Another source of stress was proposed by many investigators who are involved with high strength aluminum alloys. According to them, once a SC crack initiates, the formation of voluminous corrosion products within the crack itself can help in maintaining high stresses at the crack tip (11).

According to Linear Elastic Fracture Mechanics (LEFM) approach, the experimental studies have shown that the dominant mechanical parameter controlling SC crack growth rate in aluminum alloys is the crack tip stress intensity. The critical stress intensity that should be exceeded for SCC to occur is designated as K_{ISCC} (2, 40).

For the opening mode (Mode I), the stresses near the crack tip in an isotropic body can be represented as indicated in Equation (1.1) based on the coordinate system shown in Figure 2.7. It is worth noting that the stresses around the crack tip are fully characterized by a single parameter, called the stress intensity factor, K_I (11).

$$\sigma_x = \frac{K_I}{\sqrt{2\pi r}} \cdot \cos\frac{\theta}{2} \cdot \left(1 - \sin\frac{\theta}{2} \cdot \sin\frac{3\theta}{2}\right)$$

$$\sigma_y = \frac{K_I}{\sqrt{2\pi r}} \cdot \cos\frac{\theta}{2} \cdot \left(1 + \sin\frac{\theta}{2} \cdot \sin\frac{3\theta}{2}\right)$$

$$\tau_{xy} = \frac{K_I}{\sqrt{2\pi r}} \cdot \sin\frac{\theta}{2} \cdot \cos\frac{\theta}{2} \cdot \cos\frac{3\theta}{2}) \quad \text{..... (1.1)}$$

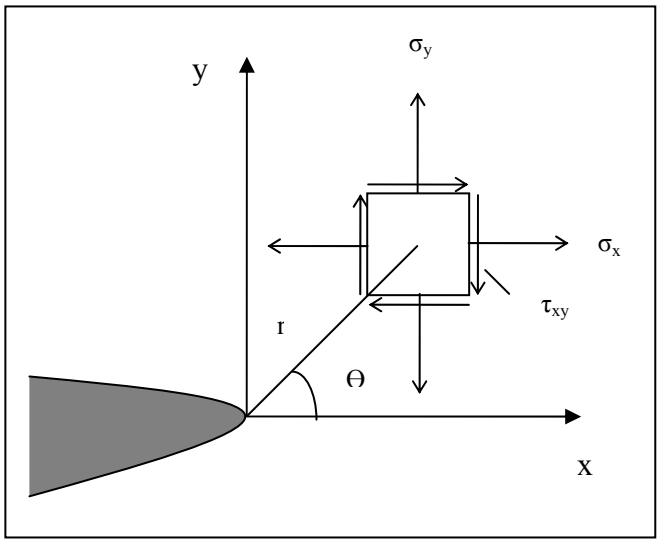

Figure 2-7 Coordinates and stress components in the crack-tip stress field (11).

However, propagating SC cracks in aluminum alloys are of course never truly elastic and there is a plastic deformation zone at the crack tip and this causes serious problems in the theoretical analysis of the experimental data. Nevertheless, the stress intensity parameter has been found to correlate well with the effect of load and specimen geometry including crack length on SC crack growth in aluminum and other alloys when it is provided that the plastic zone is small in size compared to the specimen dimensions (11, 40).

In Figure 2.8, log (da/dt) vs K_I, the effect of crack tip stress intensity on SC crack velocity is summarized schematically. The log(da/dt) vs. K_I curve is composed of three parts; Region I, the stress dependent part at low stress intensities; Region II, a stress independent part at intermediate stress intensities; and Region III, another stress dependent part at high stress

intensities. Regions I and II are typical for commercial aluminum alloys where Region III is has only been observed for high-purity and recrystallized alloys. Region I appears linear on a semi-logarithmic plot (11).

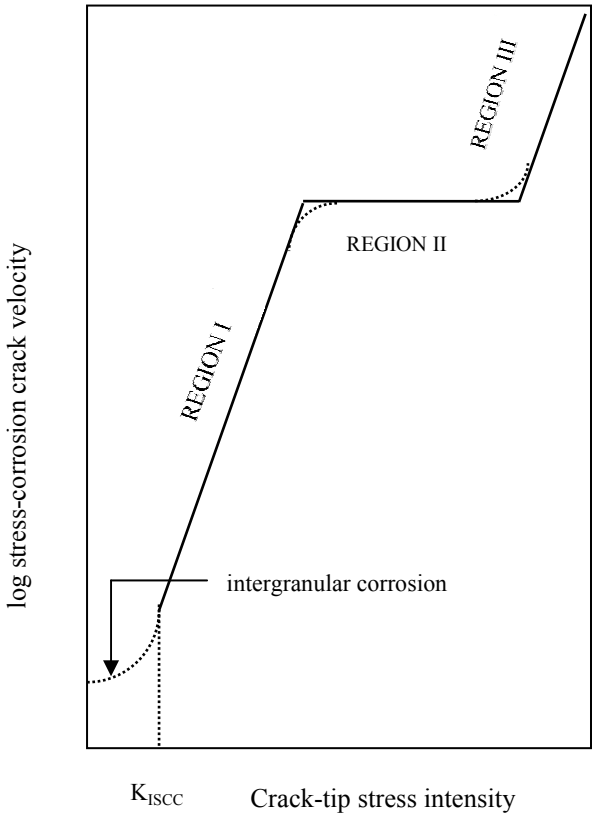

Figure 2.8 Crack growth rate vs. stress intensity factor, K_I (11).

In addition to the magnitude of stress applied and stress intensity produced at the crack tip, the state of stress has a significant importance on the SCC behaviour of a material. The effect of loading mode on SCC phenomena has been the subject of several studies. Yoda (41) investigated the SCC of a particular alloy-environment system in detail at different states of stresses such as, pure shear, plane strain, plain stress conditions and reported that the SCC behavior is different at different modes of stresses.

Since the wrought aluminum alloys have highly directional grain structures, another very important parameter effective in SCC performance is the direction of tensile stress with respect to the grain shape and orientation. The reason why SCC service failures in high strength aluminum alloys occur almost exclusively on parts with thick sections is the combination of grain flow during processing and direction of applied load in service. During forging, grains are flattened in the parting plane and during rolling in the plane of rolling. The resulting highly directional grain shape does not change during subsequent heat treatment, since the minor constituents such as Zr, Cr, and Mn form small particles of intermetallic phases which prevent the large-angle grain boundaries from moving during solution heat treatments. In thin gage material like sheet, there is normally no stress applied in the short transverse section (i.e. in the perpendicular direction to the plane of sheet) and so intergranular cracks cannot grow easily along the grain boundaries most of which are in the plane of sheet. On the contrary, in thick sections, significant residual and service stresses can exist perpendicular to the preferred plane of grain boundaries, which explains why stress corrosion cracks are mostly observed in thick sectioned parts (42).

2.3.2 Metallurgical Factors

Alloy composition and heat treatment significantly affect SCC behavior of Al-alloys. However, any isolated metallurgical parameter has not been defined yet, since testing, presentation and discussion of the metallurgical aspects of SCC of Al-alloys are difficult. The difficulty is that, variations in alloy composition and heat treatment (metallurgical variables) can affect not only the stress dependence of the crack velocity (mechanical variables), but also the dependence of the crack growth on the physical and chemical properties of the environment (environmental variables) (11).

All alloys are susceptible to some degree in specific environments. There is a generalization that susceptibility increases with an increase in yield strength in

any given alloy class. However, there exists several exceptions for this trend. For example aluminum alloys 7039 and 7079 with vastly different yield strengths exhibit identical crack velocities, both in Region I and II of the da/dt vs K_I curve. Alloys 7079 and 7075 with very similar yield strengths exhibit however quite different crack growth rates. Also, there is a general belief that materials which have higher fracture toughness are more resistant to SCC. But again there are several exceptions for this opinion. Alloys 7039 and 7079 which have definitely different K_{IC} values show similar crack growth behaviour with respect to stress intensity. So neither toughness or yield strength, alone, control the susceptibility to SCC of Al-alloys (11).

As the other pure metals, pure aluminum is not susceptible to SCC. For any given alloy system, susceptibility to SCC increases with the alloying additions. SC resistance of the ternary and higher order alloy systems, i.e. Al-Zn-Mg-Cu system, is influenced both by the total amount of alloying additions and their ratios with respect to each other. For example for the alloy 7050, high Zn/Mg ratio decreases resistance to SCC (11).

Effect of heat treatments and hence effect of microstructure on the SCC susceptibility has been the subject of many experimental investigations. For example, effect of aging temperature or aging time on SCC behavior of aluminum alloys (25, 43, 44) were studied extensively. The purpose of these studies was to find the most appropriate microstructure and so the heat treatment to supply an acceptable SCC resistance without any significant loss in strength.

Precipitation hardening is the basic heat treatment used to strengthen the Al-alloys. But the disadvantage of this method is that SCC susceptibility of the alloy increases. Supersaturated solid solutions of Al-alloys in the as-quenched condition are generally quite resistant to SCC. Precipitation hardening at ambient or higher temperatures can cause a severe increase in the susceptibility to SCC in many Al-alloys. Maximum susceptibility is observed before the peak

strength is reached during precipitation hardenening. For this condition, overaging is the solution, which improves the SCC resistance of the alloy. In Figure 2.9, based on the experimental data, Speidel illustrated the different possible ways by which the over aging increases resistance of precipitation hardening aluminum alloys to SCC; either Region I is shifted to higher stress intensities, or Region II is shifted to lower crack velocities or both. (11).

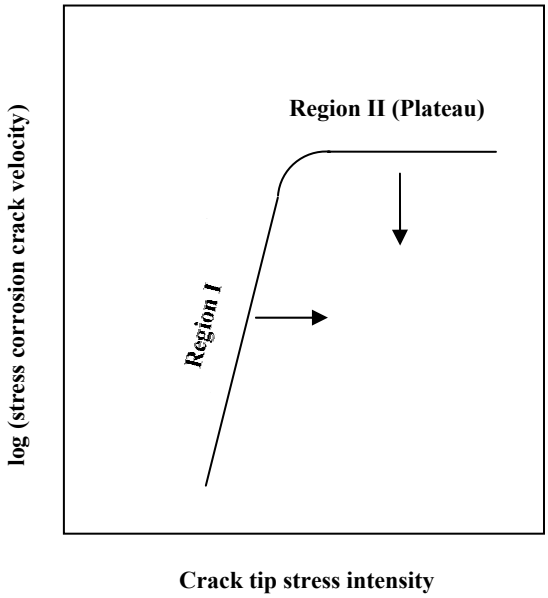

Figure 2.9 Schematic representation of possible effects of overaging on SC crack velocity in precipitation hardened aluminum alloys(11).

Precipitate Free Zones (PFZs), formed by the preferential precipitation at the grain boundaries during aging of Al-Zn-Mg alloys, are also thought to be related with SCC behavior of these alloys. Numerous studies have concerned about the relationship between the PFZ width and SCC resistance of ternary aluminum alloys. However there are no exact explanations about the effect of PFZs. Some of the investigators claimed that reducing the PFZ width will increase resistance to SCC (45), where some of them defended the opposite

view (46). On the contrary, some of the investigators believe that PFZ width is of minor or no importance to SCC resistance (47, 48).

SC cracks follow a general macroscopic path that is always normal to the tensile component of stress, regardless of whether it is intergranular or transgranular. In transgranular failure, cracks propogate across the grains usually in specific crystal planes, with low indices, such as, {100}, {110}and {210}. In the intergranular failure, cracks follow grain boundaries. Transgranular failures are less common, but the conditions for these two types to co-exist is also common (36).

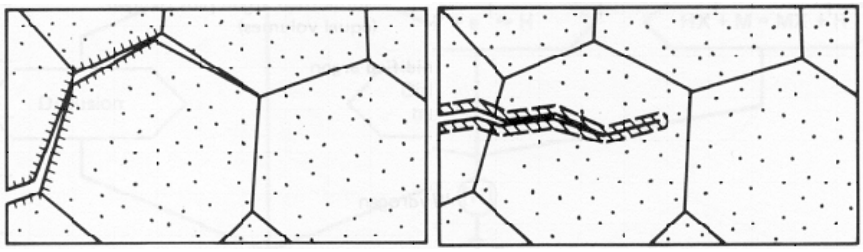

(a) (b)

Figure 2.10 Schematic view of (a) intergranular and (b) transgranular cracking (49).

2.3.3 Environmental Factors

The environment has an important effect on the nucleation and propagation of sub critical cracks in high strength Al-alloys. By changing the environment, the crack rate of an alloy may change with even more than nine order of magnitude. But it is worth noting that the SC cracks are influenced not only by the environment but also by the microstructure of the alloy and by the crack-tip stress intensity (1).

Effects of environment in physical and chemical points of view have been investigated by Speidel (11, 42). He stated that SCC cracks do not initiate or propagate in dry gases and it is the humidity in gases that causes SCC in Al alloys. It is also found that the crack growth rate increases with the relative humidity.

Aqueous solutions have been the subject of many studies. The halide ions, chloride, bromide and iodide have been observed to accelerate the growth of SC cracks. It was stated that SC crack velocity in region II of the crack velocity-stress intensity curve of alloy 7079 –T651 depends linearly on the halide ion concentration, when a certain value of concentration is exceeded (11, 42).

According to the qualitative analysis of the effect of pH on SCC of high strength Al-alloys, the occurrence of SCC in chloride containing solutions is markedly reduced as the solution is made increasingly alkaline (50). However, the solution chemistry within a narrow crack may be very different from the chemistry of the bulk solution (51).

According to a quantitative study by Tsai et. al. (52), when pH is lower than 4, intergranular corrosion assisted crack initiation occurs and when pH is higher than 10, SCC is less likely to occur in 7050-T7451 alloy exposed to 3,5 wt% NaCl solution regardless of the presence of oxygen whereas in the pH range of 4 to 10, SCC susceptibility was strongly affected by the presence of oxygen.

It has been known for many years that with the increase in temperature, SC crack growth rate increases and also crack initiation and growth occurs at lower stresses. This causes the failure of a SCC susceptible Al-alloy at shorter times (11, 53). This is why ships, aircraft and pressure vessels might suffer from SCC more severely when operating in the tropics than when operating in the polar areas (11).

The effect of applied electrochemical potential on stress corrosion crack growth of aluminum alloys has also been studied in detail, by Speidel (11). Some of the results can be summarized as follows:

● In strongly acidic solutions, the SC crack propagation rate in region II is independent of the applied electrochemical potential; i.e. cathodic protection.

● In neutral solutions, there is a potential range within which the crack velocity depends exponentially on the applied potential, and can be reduced by negative potentials. Thus, cathodic protection is possible. The potential dependence of the crack velocity is further influenced by halide ion concentration of the solution and the metallurgical parameters of the alloy.

● At very noble anodic potentials, the crack velocity is independent of the applied potential, even in solutions containing a high concentration of halide ions.

2.4 SCC Test Methods

Valid environmental characterization of materials is essential for engineers who are responsible for materials development and selection and for component structural integrity. So that, the accelerated SCC testing techniques are extensively used. The purposes of these tests can be classified into two categories. The first category is commercial (industrial) testing which intends to estimate risks or to predict serviceability of an alloy or mill product. Second one, academic testing, aims to develop an understanding of stress-corrosion mechanisms, which in turn enables the selection of more appropriate testing methods for commercial purposes. Thus the long-term objective of all stress corrosion testing is to predict the stress corrosion performance of an alloy in a given service environment (2).

There have been significant advances in the understanding of stress corrosion mechanisms and in state-of-the-art of stress corrosion testing. As the problems of SCC increased, testing methods were improved (2).

Previously, constant load or constant strain tests of smooth test specimens of various configurations were used to determine the SCC susceptibility by measuring the time-to-fracture and evaluating a threshold stress value. But later, it has been reported that undifferentiated time-to-failure data can be highly misleading, particularly when comparing high-strength alloys, in which brittle fracture occurs before stress corrosion cracking can cause significant differences in total time-to-fracture. Since the total time-to fracture is also influenced by non-stress-corrosion cracking factors such as specimen type and size, method of loading, initial stress level, and initiation behavior of the alloy; additional diffuculties have been met. Consequently, the stress-corrosion cracking ranking of materials may vary among investigators using different testing techniques. Threshold stresses and percent of specimens failing, which are important parameters in SCC comparisons, are also based on arbitrary exposure times. Test results are significantly influenced by the time required to initiate stress-corrosion cracking, which can vary widely depending on the existence and size of the flaws in the specimen. Additionally, under some conditions, random corrosion effects may override mild to moderate stress-corrosion cracking response. Hence, the test results for alloys with improved stress-corrosion cracking resistance require time-consuming exposures with attendant scatter in data. Careful interpretation is required to prevent non-stress-corrosion cracking factors from erroneously affecting test results (2).

Then two types of accelerated test techniques were developed depending on different mechanical approaches. One test technique tests and analyzes statically loaded mechanically pre-cracked specimens using linear elastic fracture mechanics concepts. In the second one, either smooth or pre-cracked specimens are tested by dynamic loading with constant extension rate (2).

2.4.1 Fracture Mechanics Approach

The use of a precracked specimens is based on the concept that large structures with thick components are apt to contain crack-like defects. When a stress-corrosion crack commences to grow, or when the specimen is provided with a mechanical precrack, classical stress analysis is not adequate to determine the response of the material subjected to stress in the presence of a corrodent (2).

The mechanical driving force for cracks can be measured with linear elastic fracture mechanics theory in terms of the crack-tip stress-intensity factor, K, which is expressed in terms of the remotely applied loads, crack size, and the geometry of test specimen. At or above a certain level of K, stress-corrosion cracking in a susceptible material will initiate and grow, whereas below that level no measurable propagation is observed (3).

The apparent threshold for the propagation of stress-corrosion cracking is designated as K_{ISCC} or K_{th}. This value defines the largest crack that can exist in a structure in the chosen environment without propagation in the form of stress corrosion cracking. Thus, in terms of linear clastic fracture mechanics theory, for a surface crack in a large plate remotely loaded in tension, the smallest crack that will propagate as a stress-corrosion crack is $a_{cr} = 0.2(K_{ISCC}/\sigma_{YS})^2$, where σ_{YS} is the tensile yield strength of the material (54).

The value a_{cr} incorporates the stress corrosion cracking resistance, K_{ISCC}, the contribution of stress levels (of the order of the yield strength) to stress-corrosion cracking due to residual or external stresses in thick component sections (54). So the application of fracture mechanics simply provides a usable method for treating the stress factor in the presence of a crack and does not provide independent information about stress corrosion cracking (2).

In LEFM approach, stress-corrosion cracking propagation rate is determined and plotted as a function of K. The test results for a highly susceptible alloy

will exhibit the general trend shown in Figure 2.8. Actual curves vary, depending upon the stress-corrosion cracking resistance and fracture toughness of the alloy. Development of such a curve (or a band if several production lots are tested) for a material provides two types of stress-corrosion cracking data that are potentially useful for predicting the behavior of large structural components for which fracture is a critical design factor. In addition to determining a K_{ISCC} value for stress-corrosion cracking propagation, indications of a "plateau velocity" can be observed. This may be regarded as an estimate of the maximum propagation rate that can be sustained in a particular material environment system. These values can be used for ranking materials that are sensitive to stress-corrosion cracking or stress-corrosion cracking environments that promote the phenomenon (2).

The use of precracked specimens permits the prediction of the stress-corrosion response in terms of flaw size and stress from laboratory tests on specimens with simple geometries. Hence, laboratory stress-corrosion cracking test results can be used in quantitative failure analysis studies and can be applied to damage-tolerant design of structural parts. Although precracking may shorten or modify the initiation period, it does not circumvent it. Thus, this method of testing also requires arbitrary and sometimes long exposure periods (2).

2.4.1.1 Static Loading

Various types of specimens and loading methods can be used to study the SCC properties of materials. There are three groups of specimens based on fracture mechanics approach; (i) Constant Load, increasing K_I specimes, (ii) Constant displacement, decreasing K_I specimes, (iii) Constant K_I specimes. The first group of specimens is exemplified by the Cantilever Bend specimens; the second, by the bolt loaded Wedge Opening Load (WOL) specimens; and the third by tapered Double Cantilever Beam (DCB) specimens. By judicious placement of loads and choice of loading conditions, increasing or decreasing K_I conditions may be obtained in any of these specimen groups. Specimens of

the first and the second groups have been commonly used for kinetic studies or K_{ISCC} determinations, or both (3).

2.4.1.2 Dynamic Loading

2.4.1.2.1 Constant Extension Rate Test (CERT)

The most recent method used for accelerating the stress-corrosion cracking process in laboratory testing involves constant extension rate tension testing of a specimen during exposure to appropriate environmental conditions, by slowly pulling to failure. The application of slow dynamic strain above the elastic limit assists in the initiation of stress-corrosion cracking (2).

Sometimes CERT is called as Slow Strain Rate Test (SSRT), since it is conducted under relatively slow strain rates. So the parameter, strain rate, will be preferred as the controlling parameter instead of extension rate when necessary.

CERT is consistent with the proposed general mechanisms of the stress corrosion cracking process, most of which involve plastic microstrain and film rupture. Based on experimental evidence, it has been suggested that the most important role of stress is the dynamic strain that it produces (55).

Slow strain rate testing is not terminated after an arbitrary period of time. Testing always ends in specimen fracture and the mode of fracture is then compared with the criteria of SCC susceptibility. In addition to its time-saving benefits, less scatter occurs in the test results (2)

The effects of stress-corrosion cracking are reflected in the load-deflection curve recorded during slow strain rate testing. Because stress-corrosion failure usually is associated with relatively little macroscopic plastic deformation during crack propagation, a comparison of the load-deflection curves for

specimens with and without stress corrosion cracking usually reveals significant differences. Crack susceptibility can be expressed by maximum load, as well as by the usual measures of ductility, elongation, and reduction in area (2).

Time-to-fracture, or fracture energy (area under the load extension curve), can also be used to indicate crack susceptibility. The results are normalized in terms of a ratio of the parameter measured in the corrodent divided by measurements taken in an inert environment under the same conditions. Thus increasing susceptibility is marked by an increasing departure from unity (2).

The use of precracked specimens in CERT in recent works, lead to the verification of stress-corrosion cracking velocities with respect to the stress intensities and threshold stresses, with modified techniques for some alloy and environment systems (55,56).

Constant extension rate test (CERT) equipment consists of a motor-driven moving cross-head in a load frame and a load cell to measure the load. Cross-head moves with a constant speed which is the measure of deformation i.e strain in the specimen (36). A schematic view of CERT system is shown in Figure 2.11.

As compared to conventional tensile test which lasts only a few minutes with a strain rate of 10^{-2} sec^{-1}, a constant extension rate test at a strain rate of 10^{-6} sec^{-1} may take nearly two days to complete. But CERT is quite fast as compared to the constant deformation and constant load tests. They may require months or even years of exposure, with no certainty that failure can not be observed at a still longer time (36).

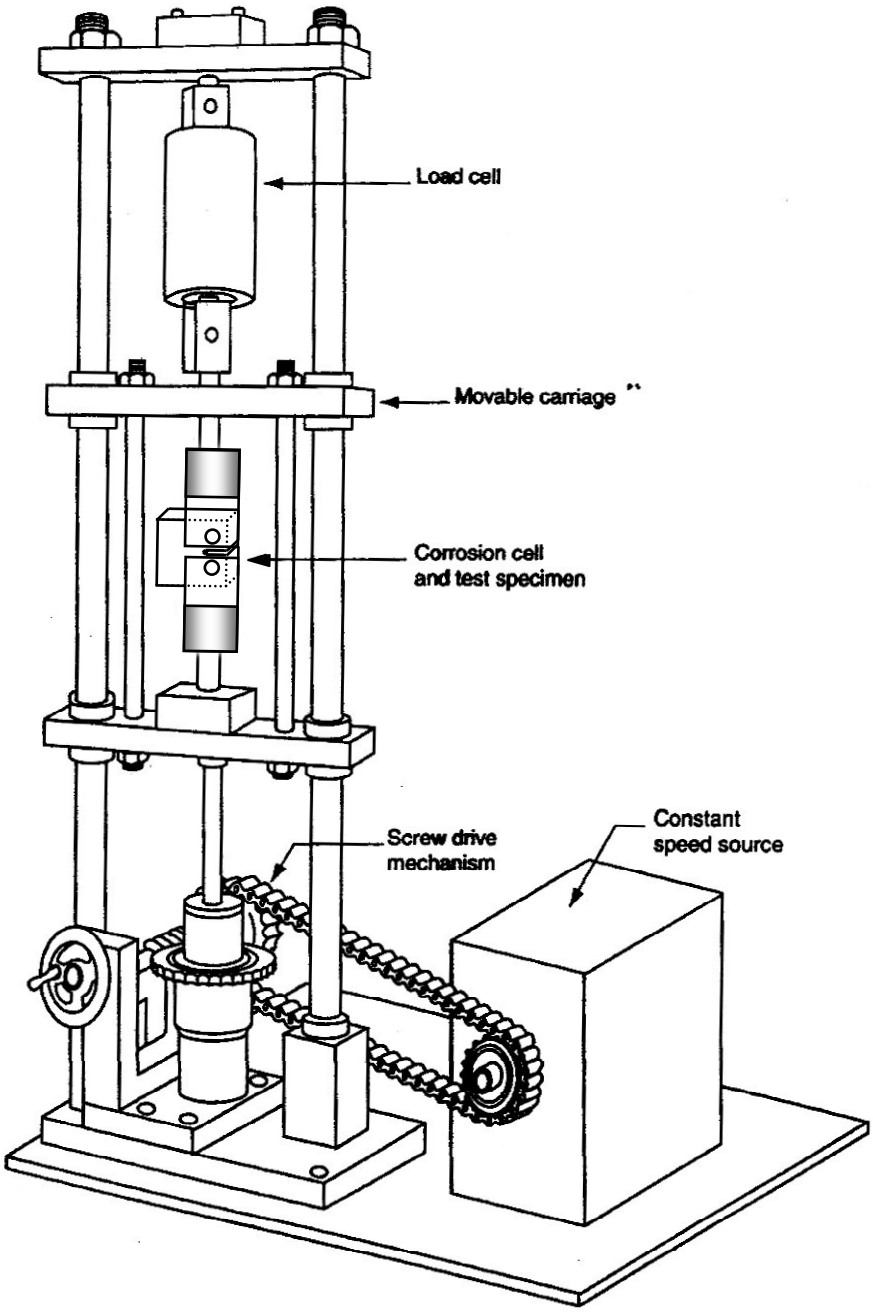

Figure 2-11 Schematic view of Constant Extension Rate Testing System (Adopted from "Principles and Prevention of Corrosion", D.A. Jones, Prentice Hall, Second Edition, 1992 (36)).

In general, the severity of SCC is a function of strain rate. Maximum severity is observed over a critical range, and the susceptibility decreases at faster and slower rates. Maximum severity is observed for strain rates of the order 10^{-6} sec^{-1} for many material-solution systems. A too rapid strain rate results in ductile failure of the specimen before significant SCC occurs. On the other hand, when the rate is so slow, repassivation occurs at the crack tip and SCC is suppressed. The absence of SCC at slow rates was attributed to film repair at the crack tip which suppresses crack growth (57, 58). A schematic view of the effect of strain rate on SCC is shown in Figure 2.12.

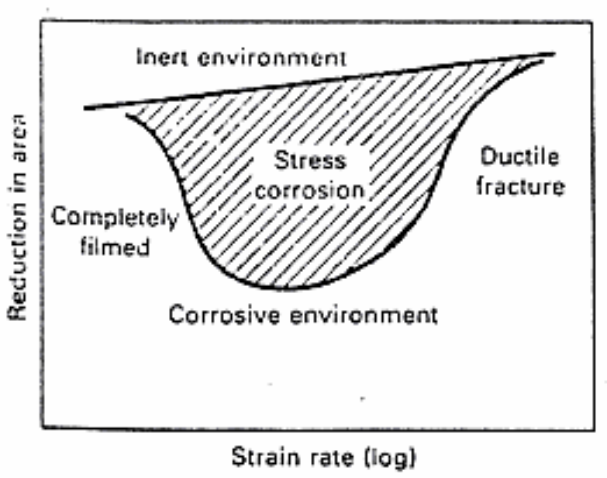

Figure 2.12 The relationship between the strain rate and the fracture behavior in terms of reduction in area (2).

Constant-displacement and constant-load methods generally require elevated temperature or solution concentration in order to accelerate laboratory testing. Accelerating agent is the continuous strain in the slow strain-rate test. So that susceptibility in simulated service conditions can be determined in the laboratory. However, the CERT is generally somewhat more aggressive than either constant-displacement or constant-load tests. Thus, the CERT is

conservative: an alloy showing resistance in this test should be resistant in service with similar corrosive conditions. But an alloy showing SCC in a CERT would not necessarily fail in service, where a forced, continuous strain is absent. However, in some instances, brittle cracking in the CERT may indicate a very long failure time in service (36).

2.5 High Strength Al-Zn- Mg-Cu Alloys

2.5.1 Composition

Aluminum-Zinc binary alloys have been the first commercial aluminum alloys. Binary alloys were used for both castings and wrought products until early 1900s. At the beginning of 20^{th} century, ternary Al-Zn-Mg alloys were developed. Following this, high strength grades of these alloys were obtained by the discovery of proper heat treatments (50).

The precipitation hardened 7000 series aluminum alloys are used when a high strength to weight ratio is important, i.e. especially in aircraft construction. The major alloying additions to aluminum are zinc, magnesium and copper for 7000 series alloys. The Zn content is usually higher than the Mg content. Because of their poor castability they are usually used as wrought products (59).

The ratio of the major alloying elements Zn to Mg is an essential factor for the mechanical performance of these alloys. An optimum strength and best response to heat treatment can be obtained with a high Zn/Mg ratio. However the high Zn/Mg ratio leads to an increase in susceptibility to intergranular corrosion and SCC. On the other hand, lower ratios give better weldability and lower quench sensitivity. The zinc-bearing constituents are also controlled by this ratio. The ratios over 2 result in the formation of $MgZn_2$ while at lower ratios, $Mg_3Zn_3Al_2$ forms. A good resistance to fatigue can also be obtained with lower Zn/Mg ratios (59).

Presence of copper improves SCC resistance of 7000 series alloys whereas it reduces the general corrosion resistance (59, 60).

In addition to the Zn/Mg ratio and amount of Cu, the total amount of alloying elements (Zn+Mg+Cu) is a controlling factor for the properties. With a total amount higher than 9 percent, high strength can be obtained with improved corrosion resistance, formability and weldability. When the total amount is in a range between 6 and 8 percent, the weldability and formability is increased with a still high strength. Below a total amount 5 to 6 percent, the SCC susceptibility tends to disappear and fabricability becomes paramount (59).

The chromium, zirconium and manganese additions also increase the SCC resistance whereas they have a limited strengthening effect. Titanium and boron are used together for grain refinement. On the other hand, iron and silicon are common impurities for these alloys but their effect is limited (59).

As observed in most other aluminum alloys, the matrix is formed of aluminum solid solutions. The other phases are dispersed in the matrix. In properly homogenized alloys, the bulk of the Zn, Cu, and Mg are in solid solution and only small amounts of their phases are visible. Most of the phases present are iron-, silicon-, manganese-, chromium-, and zirconium-bearing ones. Either $MgZn_2$ or $Mg_3Zn_3Al_2$ compounds are formed depending on the Zn/Mg ratio as mentioned before. Copper behaves similarly to zinc in the ratio and most of it dissolves in these two Zn-bearing compounds. Exceptionally, $CuMgAl_2$, CuFe or CuMn compounds are formed (59).

2.5.2 Heat Treatment of 7000 Series Aluminum Alloys

Supersaturated solid solutions of aluminum alloys in the as quenched condition are generally quite resistant to SCC. Precipitation hardening i.e. aging at ambient or higher temperature can cause a severe increase in susceptibility to SCC in many alloys. Maximum susceptibility is observed before peak strength

is reached during precipitation hardening. Further precipitation hardening beyond the peak hardness, i.e. over aging can substantially increase the SCC resistance. Thus, over aging has become the single most important metallurgical treatment to improve SCC resistance of high-strength aluminum alloys (11).

The following reaction sequence occurs for 7000 series with increasing aging time;

Supersaturated Solid Solution → Guiner-Preston Zones → η^1 → $\eta(MgZn_2)$ → $T[(AlZn)_{49}Mg_{32}]$

The presence and distribution of grain boundary phases are very sensitive to the heat treatment applied. Since the SCC in aluminum alloys generally intergranular, the chemistry and microstructures of the grain boundaries are essential. The boundary generally contains the equilibrium precipitates. For the 7000 series, the boundary is rich in $\eta(MgZn_2)$ or $T[(AlZn)_{49}Mg_{32}]$ depending on the aging condition (61).

In the peak aging condition, maximum hardness is obtained and the matrix contains semi-coherent η^1 phase. When aging time is less than the peak aged condition i.e. under aging, or higher i.e. over aging the hardness obtained is lower than the peak aged condition (61).

In many cases, unless the sample is rapidly quenched into water, the precipitates may actually nucleate during the solution heat treatment. They will initially be very fine and closely spaced. As aging proceeds, they will coarsen and their spacing will increase (61).

A depletion of Mg and Zn occurs around the precipitates $\eta(MgZn_2)$ and $T[(AlZn)_{49}Mg_{32}]$. As the aging time increases, these zones usually become

more and more depleted. These solute depleted zones are called Precipitate Free Zones (PFZs) (61).

The peak aging treatment applied to 7000 series alloys is designated as T6 and over aging as T7. As explained previously, in T7 condition, the SCC resistance is increased with the expense of some strength. Thus, over aging has become a beneficial and commercial heat treatment procedure for 7000 series and new over aging treatments, T76 and T73 has been born.

The T73 heat treatment procedure is conducted as either two-stage isothermal precipitation or as heating at a controlled rate to a single treatment temperature. The purpose is to produce GP zones that will not dissolve but transform to the η^1 precipitate when heated to the aging temperature above 150°C. Thus, either the time or the temperature of the first step or the rate of heating must be controlled to achieve this (62).

CHAPTER 3

EXPERIMENTAL

3.1 Material

In this study, the material which was tested is cold rolled plate of 7050 Al-Zn-Mg-Cu alloy. The chemical composition of this alloy is given in Table 3-1. The T73651 heat treatment was applied to the material by the supplier. This treatment consists of solutionizing at 477°C, followed by double aging at 121°C for 24 hours and at 163°C for 24 hours.

Table 3-1 Chemical composition of 7050 Aluminum Alloy in weight percentages (63).

	Al	Zn	Mg	Cu	Zr	Ti	Cr	Mn	Si	Fe	other
Min.	87.3	5.7	1.9	2.0	0.08	-	-	-	-	-	0.05
Max.	90.3	6.7	2.6	2.6	0.15	0.06	0.04	0.1	0.12	0.15	0.15

Since the plates were produced by cold rolling, similarly to the microstructure, the mechanical properties are also highly directional and vary apparently with orientation. The mechanical properties of alloy in T73651 heat treatment condition in different orientations are given in Table 3-2. The values were reported by Industrieanlegen Betriebsgesellschaft mbH, IABG, Germany (64).

Table 3-2 Mechanical properties of cold rolled aluminum 7050-T73651 (64).

Direction	**UTS (MPa)**	**σ_y (MPa)**	**E(MPa)**	**Elongation (%)**
L	510	447	72200	10
LT	519	444	73300	9
ST	502	423	72800	7

In Table 3-3, plain strain fracture toughness, K_{IC}, values determined in four orientations are given (64).

Table 3-3 Plain strain fracture toughness values for different orientations of 7050-T73651 (64).

Orientation	LT	TL	ST	SL
K_{IC}(MPa.mm$^{1/2}$)	1215	966	957	865

3.2 Compact Tension Specimens

In this study, the material was tested in three different orientations, namely, SL, TS and LT. For the compact tension type of specimens, the first letter of the designation of the orientations indicates the loading direction and second one the crack propagation direction. In Figure 3-1, the six different possible orientations are shown (65). The three orientations that was studied in this work are indicated with arrows.

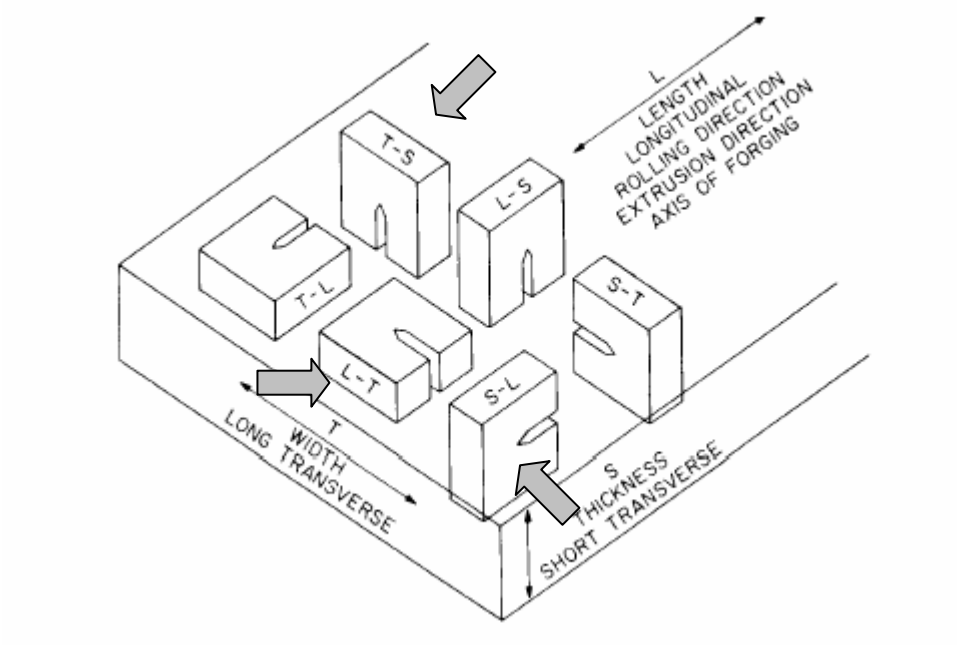

Figure 3.1 The orientations of CT specimens (Adopted from ASTM E399-90 $^{\epsilon 1}$ standard) (65).

Design of the specimens as depicted in Figure 3.2 was according to the ASTM E399-90 $^{\epsilon 1}$ standard (65), whereby, the shape and dimensional requirements for the standard CT specimens as described in this were strictly applied standard are depicted. CT specimens with a width of W = 50 mm was used in this work. Usually, the thickness is taken as W/2 to calculate the fracture toughness value in the related standard. But the same standard also proposes thickness values for alternative specimens as $2 \leq W/B \leq 4$. In this study, the thickness was selected as B =15 mm in order to obtain the plane strain condition necessary to conduct the LEFM approach for the calculation of plane strain stress intensity values. As a fatigue crack starter notch, Chevron notch was preferred as described in ASTM E399-90 $^{\epsilon 1}$ standard (65). The Chevron notch configuration is shown in Figure 3-3 (65).

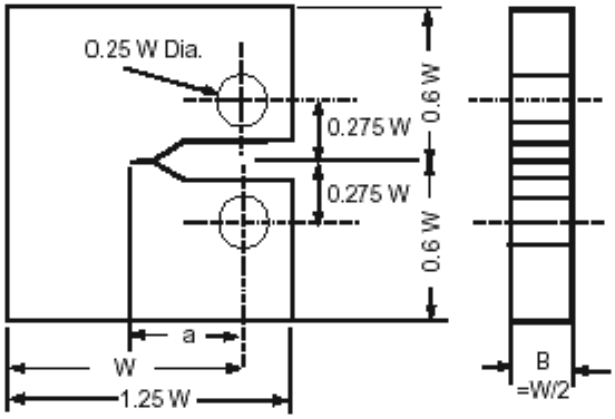

Figure 3-2 Dimension of the CT specimens according to the ASTM E 399-90 $^{\epsilon 1}$ (65).

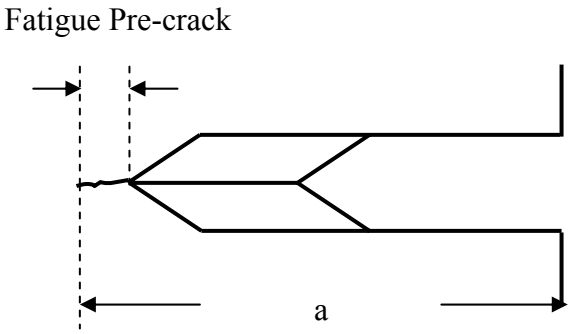

Figure 3-3 Chevron Notch (Adopted from ASTM E399-90 $^{\epsilon 1}$ standard) (65).

3.3 Heat Treatments

In the present work, the effect of three different aging treatments on the SCC susceptibility of the alloy 7050 was investigated. In addition to, T73651, which was the heat treatment of supplied material, two different aging procedures were applied following the solutionizing. The first one is the peak aging treatment, T651, which results in highest strength and second one is the over

aging treatment, T7651. Both T651 and T7651 are carried out at 121°C for different aging times.

In order to determine the peak aging time, a hardness profile was generated for aging at 121°C. For this, the 15 mm thick specimens were solutionized at 477°C for 75 minutes and then water quenched. The specimens were naturally aged at room temperature for one week. Then they were aged at 121°C for 3, 6, 12, 24, 48, 96 and 192 hours in an oil bath. After aging treatments, specimens were water quenched to avoid further precipitation and grain growth. All the agings were duplicated in order to evaluate the hardness values more accurately. The Knoop Hardness test was applied in order to obtain precise hardness values, that were converted to Brinell Hardness numbers. The resulting hardness profile is shown on a semi-logarithmic scale on Figure 3-4. As seen from this curve, aging 24 hours at 121°C gives the peak hardness value which correlates well with the suggested T651 condition by ASM in "Heat Treatment of Aluminum Alloys" (62). Thus, the treatment at 121°C for 24 hours was selected as the peak aging, T651 and aging at 121°C for 96 hours which gives a desirable decrease in hardness was selected as the T7651 condition.

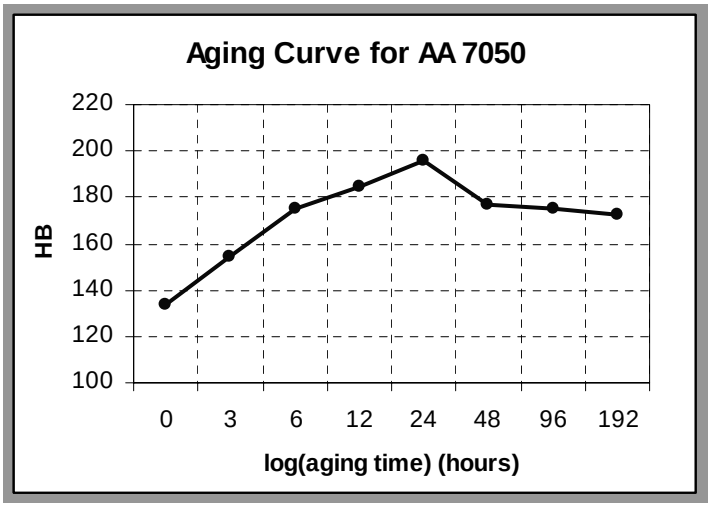

Figure 3-4 Hardness profile of alloy 7050 for aging at 121°C.

The three heat treatments applied to the alloy for each of tested orientations are summarized on Table 3-4.

Table 3-4 Heat treatment procedures applied to applied 7050.

Heat Treatment	Procedure
T73651(applied by the supplier)	solutionizing at 477°C/Water Quench/double aging at 121°C for 24 hours and at 163°C for 24 hours
T651	solutionizing at 477°C/Water Quench/aging at room temperature for 1 week/aging at 121°C for 24 hours/Water Quench
T7651	solutionizing at 477°C/water quench/aging at room temperature for 1 week/aging at 121°C for 96 hours/Water Quench

The solutionizing treatments were held in a muffle furnace and the agings were carried out in an oil bath by means of the Julabo SC device. The aging medium consisted of a silicon oil which was continuously stirred by the device to provide a homogeneous temperature distribution through the medium.

The optical micrographs of the alloy in three orientations, TS, SL and LT, for three heat treatments conditions, T651, T7651 and T73651 are depicted in Figures 3-5, 3-6 and 3-7 respectively.

As seen from the micrographs, microstructure is made up of recrystallized and polygonized grains. The lighter areas are the elongated recrystallized grains and the rest are polygonized grains. Very fine precipitations were observed being evenly distributed throughout the structure whereas larger intermetallic compounds were mostly detected among the recrystallized grains, i.e at high angle grain boundaries. It is worth noting that the recrystallized grains are flattened in the short transverse (S) direction and they are elongated in the longitudinal (L) direction due to the cold rolling process.

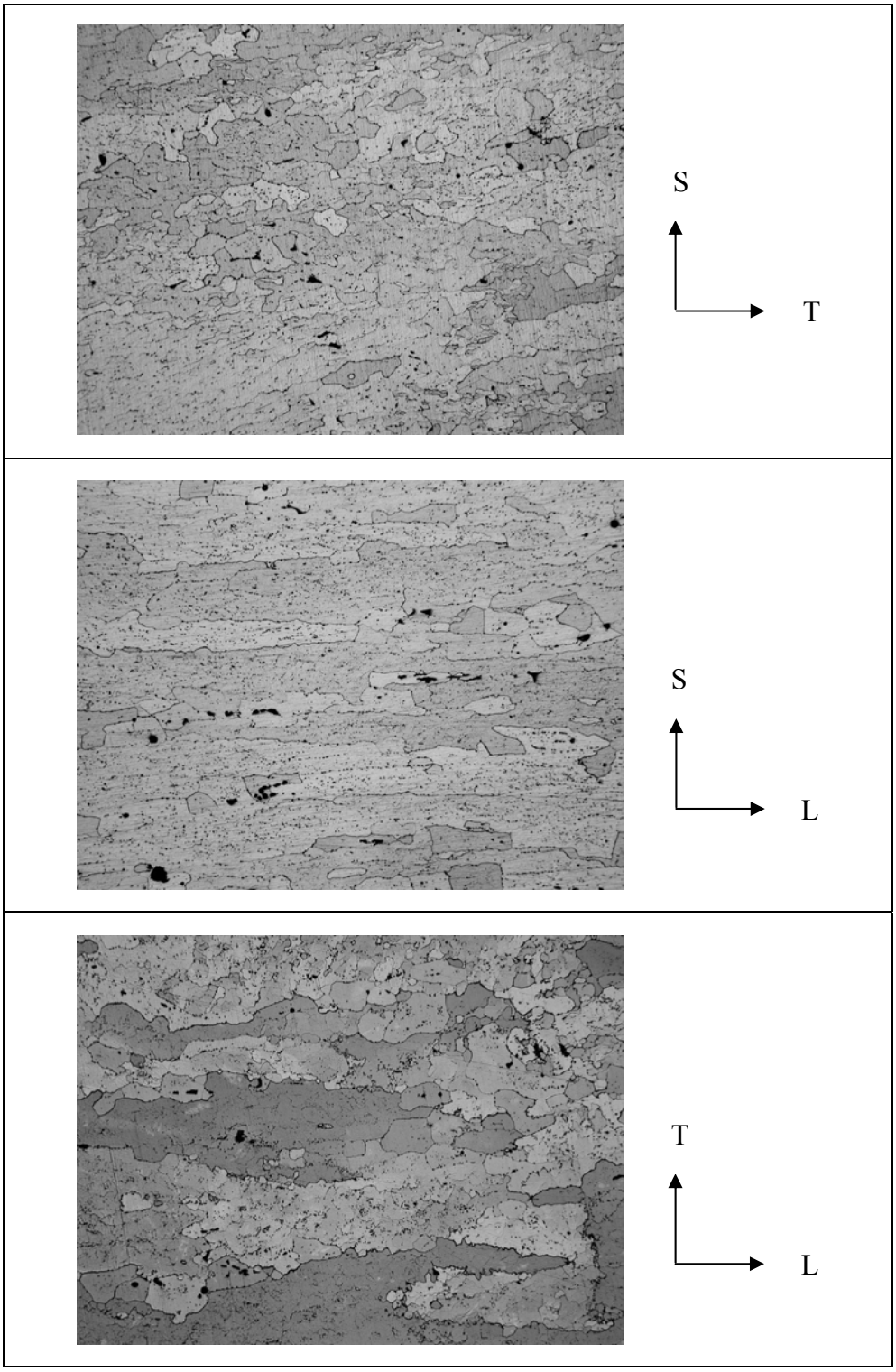

Figure 3.5 Optical micrographs for alloy 7050-T651 in TS, SL and LT orientations (X100).

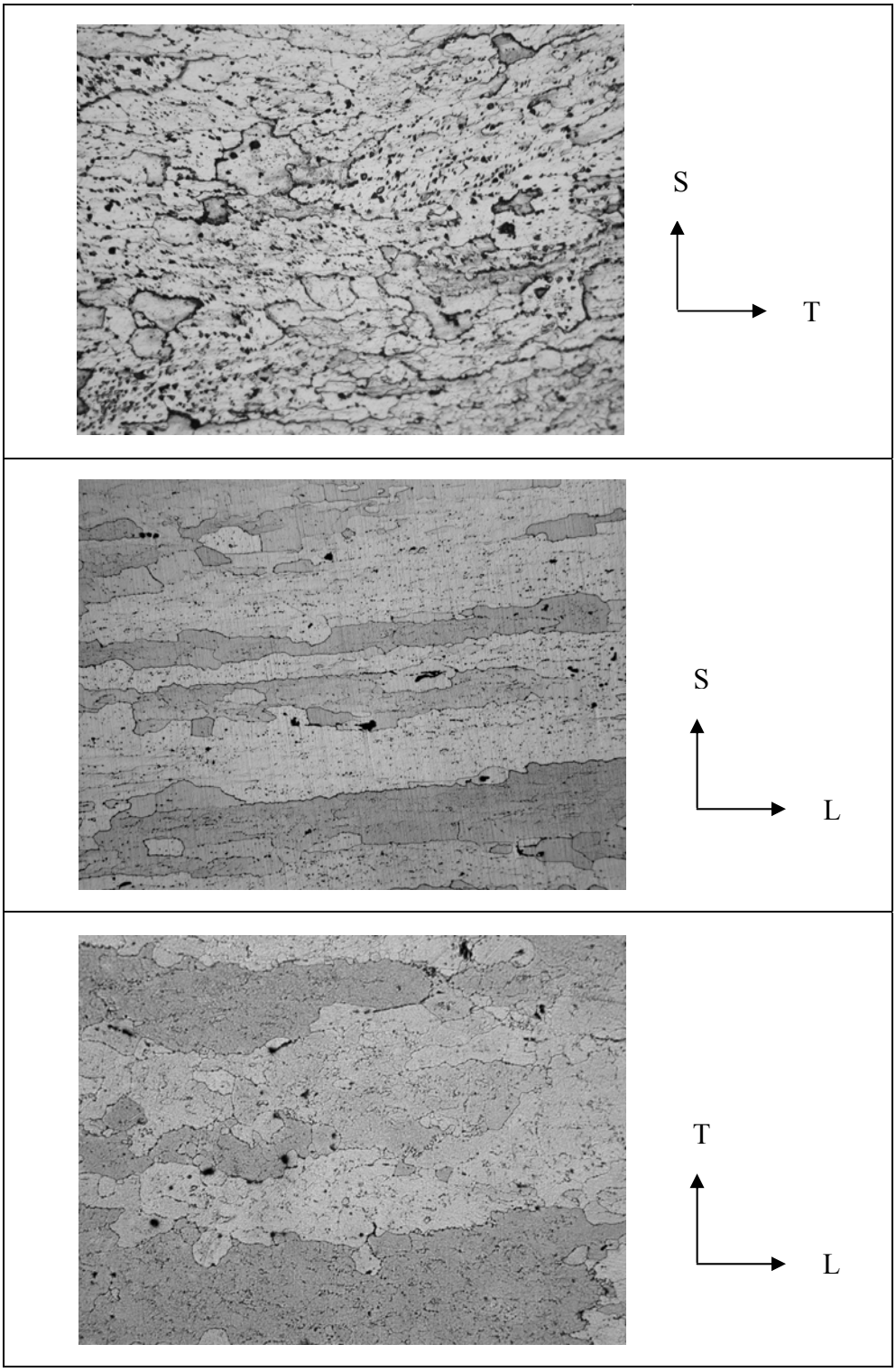

Figure 3.6 Optical micrographs for alloy 7050-T7651 in TS, SL and LT orientations (X100).

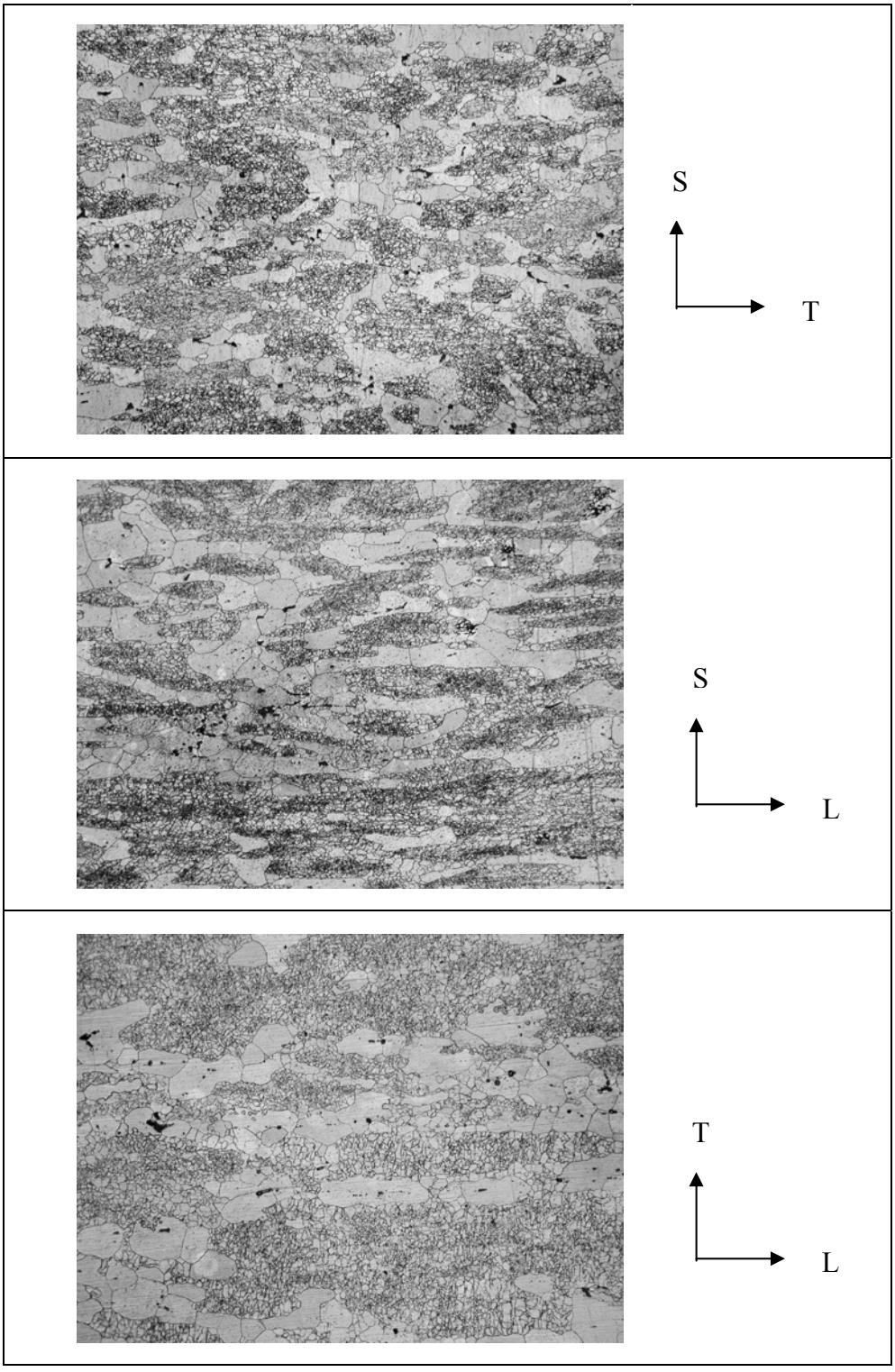

Figure 3.7 Optical micrographs for alloy 7050-T73651 in TS, SL and LT orientations (X100).

3.4 Testing Equipment

To investigate the SCC susceptibility of the alloy 7050, the fatigue pre-cracked compact tension (CT) specimens were tested in constant extension rate testing equipment. The direct current potential drop technique was used in order to measure the crack lengths. With this data, crack length versus time and crack growth rate versus stress intensity curves were plotted.

3.4.1 Constant Extension Rate Testing System

Constant extension rate test (CERT) equipment consists of a motor-driven moving cross-head in a load frame and a load cell to measure the load. Cross-head moves with a constant speed which is the measure of deformation i.e with constant extension rate in the specimen. By use of a special and a gear system the extension rate could be reduced to $5{,}66 \times 10^{-5}$ mm/sec. The load cell has a capacity of 5 tons. The stiffness off the machine was measured to be 1209,5 kg/mm. A photographic view of the CERT system that was used in this study is shown on Figure 3.8. A general view of the test system with wiring for DCPD technique is shown in Figure 3.9.

Figure 3-8 Photograph of Constant Extension Rate Testing system.

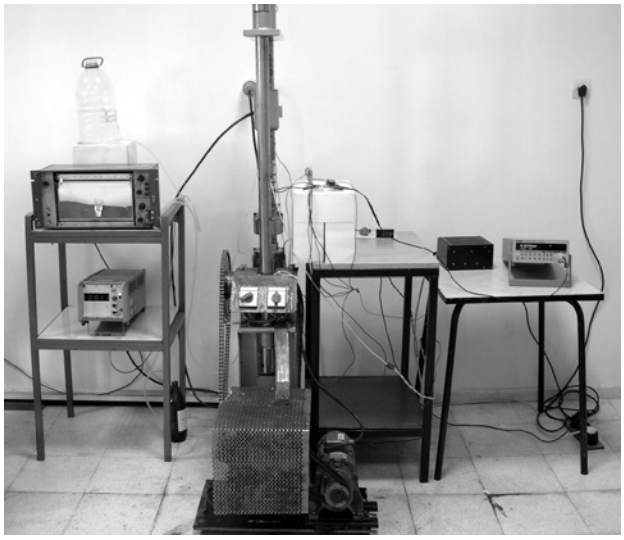

Figure 3.9 CERT with wiring for DCPD technique.

The 3,5 wt% NaCl solution at room temperature was used in this work in order to simulate the marine environment the aircraft may be exposed to during their mission. All experiments were conducted at room temperature in 3,5wt% NaCl solution under the free corrosion potential.

The specimen is exposed to corrosive medium by means of a corrosion cell made up of Plexiglas. The corrosion cell was designed in a way to permit the complete contact with the solution of moving crack up to the unstable failure of specimen. Another feature of design was to prevent the specimen holders from contacting with the medium for a galvanic action not to occur. During the experiments, the solution was circulated through the cell every half an hour with a velocity of 0,6 lt/min. The photograph of the corrosion cell attached to the specimen is given in Figure 3-10 and a detailed 3D view of the corrosion cell is shown in Figure 3-11.

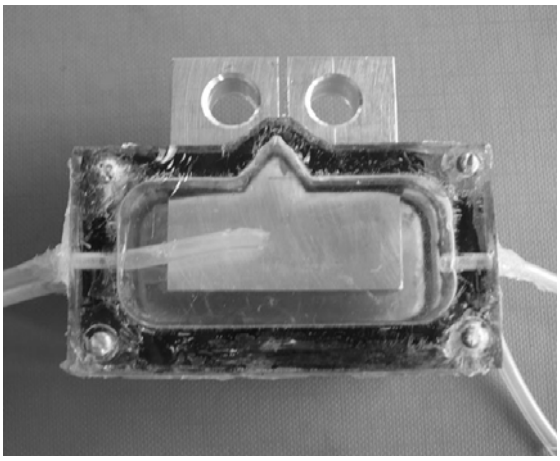

Figure 3.10 Corrosion cell attached to the CT specimen.

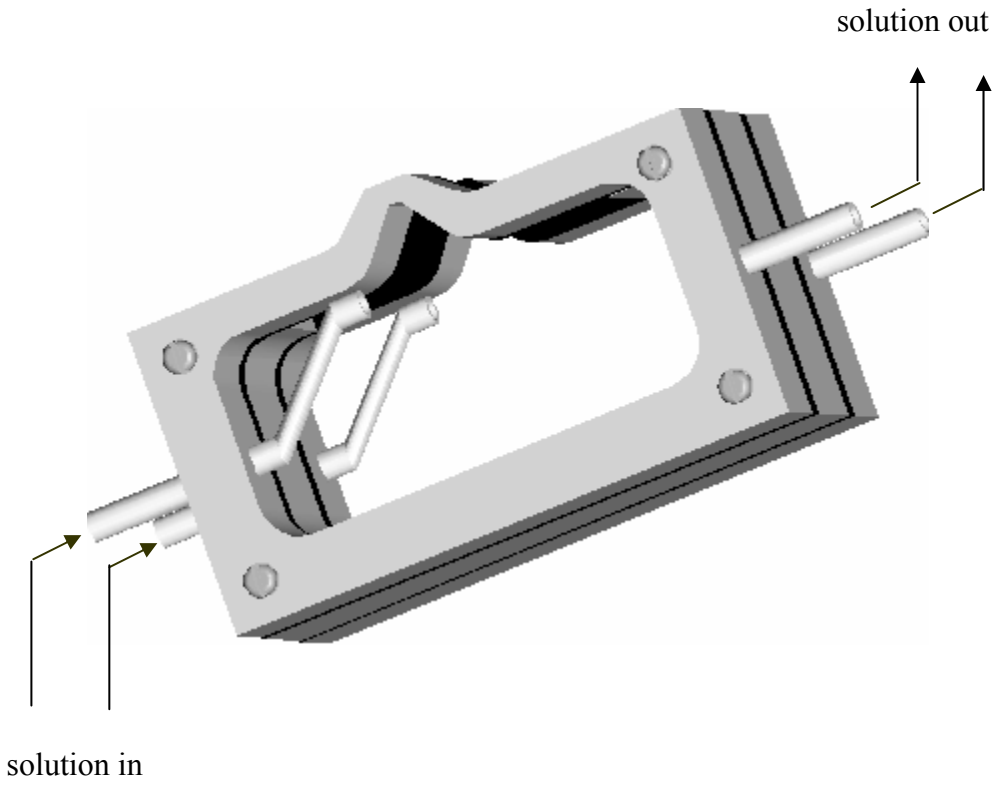

Figure 3-11 A 3D view of the corrosion cell.

3.4.2 Potential Drop Technique

The Direct Current Potential Drop technique (DCPD) is a widely accepted method of monitoring crack growth in controlled laboratory tests. The work is done by passing a constant current through the test piece and accurately measuring the electrical potential difference (EPD) across the crack surfaces. When the crack size increases, the resistance of the material and so the measured EPD value increases since the uncracked cross sectional area of the test piece reduces during crack propagation. By measuring the time-dependent change in EPD, one can derive the crack growth rate. Figure 3.12 shows the setup for DCPD measurements.

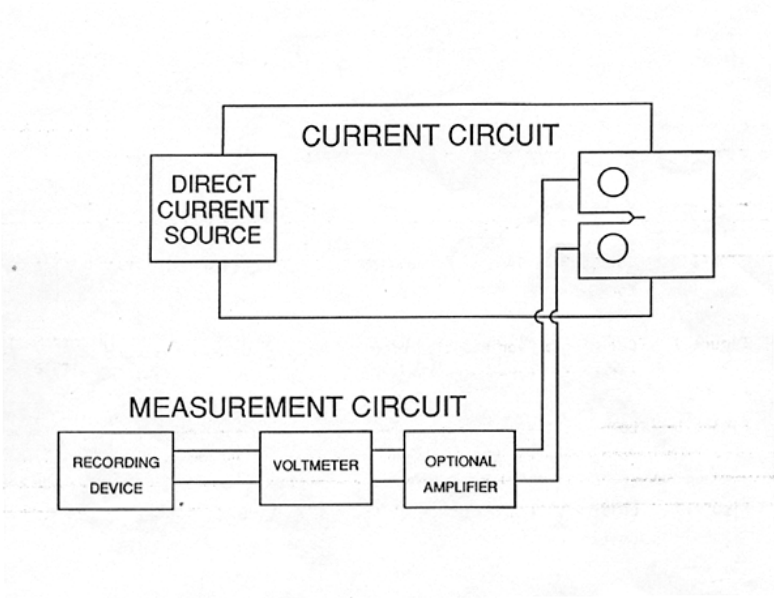

Figure 3-12 Schematic diagram of the DC potential drop system (66).

The potential drop technique has many advantages over optical measurements of crack length. It provides a total measurement, inclusive of crack front curvature and because it does not require visual inspection, tests may be conducted in any sealed environment. Generally the output is continuous which permits automated data collection and processing together with a 24 hours usage of testing machine capacity. The technique is capable of detecting small

increments of crack growth which cannot be resolved optically (67). The simple test set-ups and the possibility to derive correlation between crack length and EPD in any type of specimen by means of either analytical or numerical calculations, make the (DCPD) method to be used widely (68).

For the CT specimen geometry, Hicks and Pickard has derived a relationship between EPD and crack length. The expression of this relationship is as follows (66):

$$\frac{V}{V_0} = 0{,}5766 + 1{,}9169\left(\frac{a}{W}\right) - 1{,}0712\left(\frac{a}{W}\right)^2 + 1{,}8698\left(\frac{a}{W}\right)^3 \text{.....} \quad \textbf{(3.1)}$$

and

$$\left(\frac{a}{W}\right) = -0{,}5051 + 0{,}8857\left(\frac{V}{V_0}\right) - 0{,}1398\left(\frac{V}{V_0}\right)^2 + 0{,}0002398\left(\frac{V}{V_0}\right)^3 \text{.....} \quad \textbf{(3.2)}$$

where;

a is the crack length,
V is the measured potential at crack length, a,
V_0 is the initial potential corresponding to a/W = 0,241, and
W is the specimen width.

In order to use the above expressions, one should note that the wire connections have to be done as described by Hick and Pickard (66), that are shown in Figure 3-13.

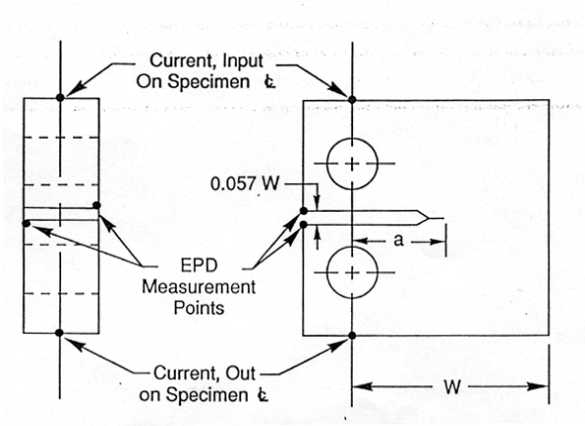

Figure 3-13 Locations of potential wire placement for Hicks and Pickard's solution (66).

It should be noted that in the Hicks and Pickard expressions, the measured EPD is referenced to a voltage, V_0, which corresponds to a particular crack length to width ratio, a/W = 0,241. Since actual measurement at this crack length is often impractical due to the CT specimen geometry, the Equation 3.1, can be used to compute this constant V_0 from any reference a/W corresponding to potential drop V. Computing V_0 in this way, accounts linearly for small changes in applied current, measured specimen dimensions, and slight errors in wire placement from sample to sample. The computed reference voltage can then be used with the second form of the equation to determine the crack length for all potential values V (66).

An accurate calibration curve is necessary to obtain correct results in the crack length measurement by DCPD technique. This calibration curve consists of a relation between V/V_0 versus a/W. Through the use of such nondimensional variables, the calibration curve becomes independent of material properties, test piece thickness and magnitude of input direct current and is mainly a function of specimen and crack geometry and the location of current input and potential measurement points (69).

The experimental calibration curve can be obtained by measuring the EPD values, V, in a single test piece where a crack length, a, is introduced by cutting slots of increasing lengths at the bottom of the notch. Measurements are taken with a constant stabilized DC current in the test solution at constant temperature (66). By making a comparison between the calibration curve obtained experimentally and the curve obtained by plotting the Equation 3.1, the validity of the found calibration curve can be tested.

In SCC testing, current leakage into the solution may result in difference in the electrochemical conditions and hence results in difference in potential measurements. However, this is not a problem in practice, since the conductivity of metals is superior over that of the most conductive electrolytes (66).

Changes in the temperature may result in proportional changes in the measured EPD values which lead to errors in crack length measurements or to increased data scatter. For example, a 3°C change in an aluminium alloy may result in 1% change in EPD signal due to the change in the material's electrical resistivity (70). Variations in current supplies may also result in a proportional scaling of the measured voltages. In order to compensate for these effects, voltage measurements can be normalized by dividing the voltage of the active EPD location by the voltage at some reference location (71). This ratio compensates for changes in both applied current and sample temperature. Crack length resolution can also be increased by the use of the reference voltage measurement. Ideally, the reference measurement should be conducted on the test sample in a location which is not affected by the changes in crack length. However, this is not always possible in practice. For example, it is highly unlikely that a suitable location on the CT specimen can be found which has a sufficient signal level, but which is not affected by changes in crack length. For this reason it is beneficial to use an alternate sample of the same material and in the same current path and environment. In this case, the EPD values are divided by the ratio V_{ref}/V_{ref0}, where V_{ref} is the reference probe

voltage measured at the same time as the EPD crack voltage is measured and V_{ref0} is the initial reference probe voltage (66).

3.4.2.1 Application of DCPD to CT Specimens

In this study, the CT specimens were wired as described by Hick and Pickard, with some modification. A reference specimen was used in order to compensate for the temperature changes. The design and dimensions of the reference specimen was prepared identical to the test specimen.

The DCPD wiring applied in this work is shown on Figure 3.14. The test specimen and reference specimen are placed on the same circuit. A direct current source of 40 A capacity was used. The EPD measurements were carried out by employing the Keithley 197A model nano-voltmeter.

The current input and voltage output wire placements applied in this work are shown on Figure 3.15. The current input wires consisted of 2,5 mm diameter and 14awg copper cables that were fastened to the specimen by the M4 screws. A Plexiglas insulator was placed between the fastening lug and the specimens through which the positioning errors associated with the broad surface contact of the fastener were minimized.

Gold-plated brass pins having a 1,0 mm diameter were attached to the specimens at the EPD measurement points. The voltage wires then attached to these pins by soldering to obtain a reliable joint. A 0,5 mm diameter two-conductor twisted and shielded cable was used between the test sample and the differential amplifiers. Silicon rubber sealant was placed over the pins and solders to strengthen the connection and to supply a thermal insulation.

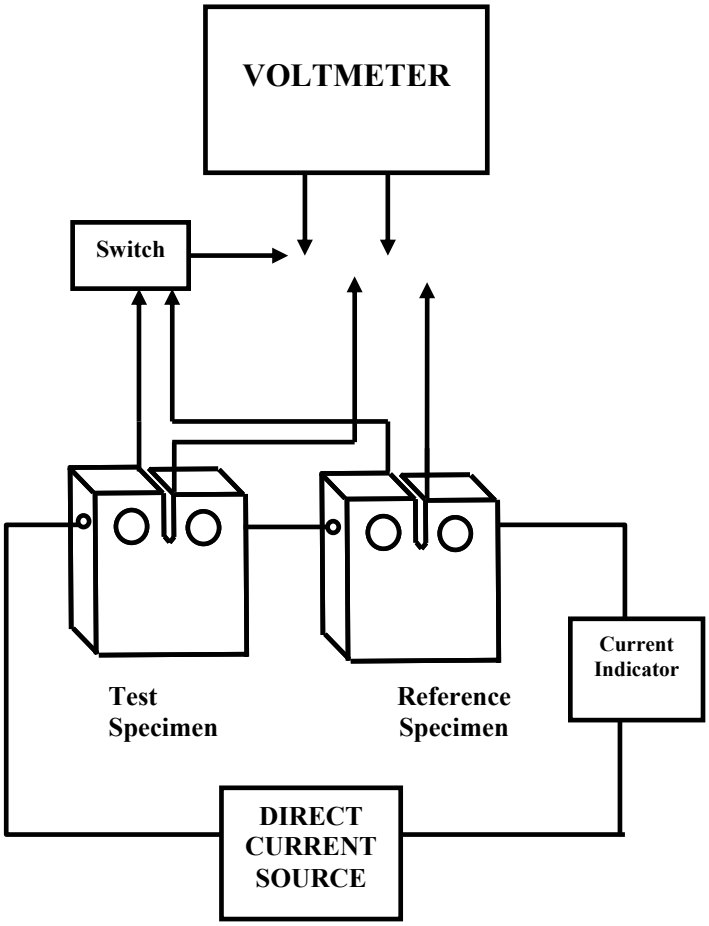

Figure 3-14 Wiring diagram for DCPD technique.

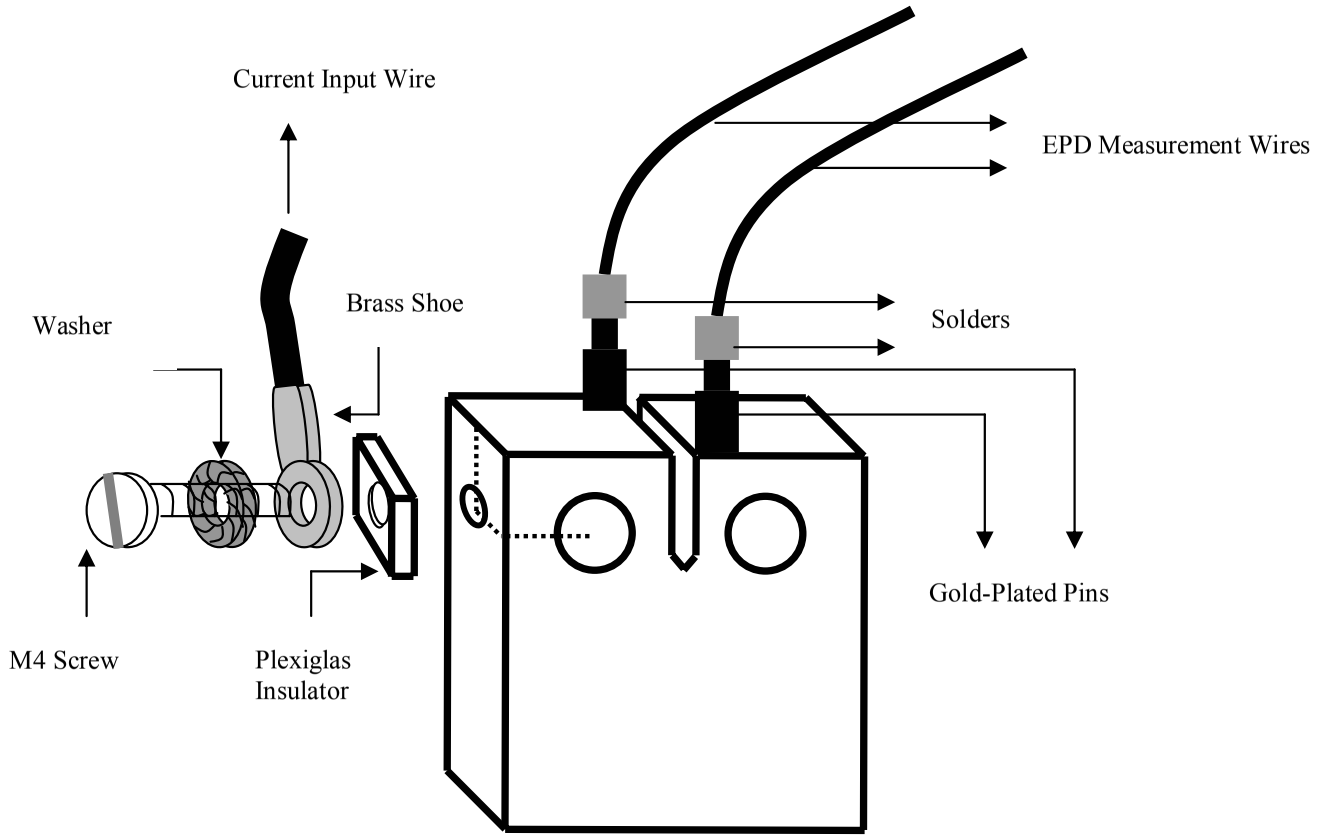

Figure 3.15 Current input and voltage output wire placements for DCPD technique.

In the present study, the EPD measurement points did not exactly met the Hicks and Pickard's configuration. Due to the Chevron notch, the distance between the two EPD measurement points is not equal to 0,057W and, was adjusted to 7 mm which corresponds to 0,14W. However, this modification did not result in any measurement errors as it will be indicated by the calibration curve (Figure 3.17), since the reference potential, V_0, corresponding to a/W = 0,241, was calculated for the EPD measurement points placement of this study.

To avoid any noise caused by the instrumentation and the testing machine, the voltmeter and the voltage measurement wires were grounded, to secure the accuracy of the EPD measurements.

Since a reference specimen was used, Hick and Pickard expressions can be modified followingly by including the ratio, V_{ref}/V_{ref0}:

$$(\frac{V}{V_0})(\frac{V_{ref_0}}{V_{ref}}) = 0{,}5766 + 1{,}9169(\frac{a}{W}) - 1{,}0712(\frac{a}{W})^2 + 1{,}8698(\frac{a}{W})^3 \text{ …… .. } \textbf{(3.3)}$$

and

$$(\frac{a}{W}) = -0{,}5051 + 0{,}8857(\frac{V}{V_0}\frac{V_{ref_0}}{V_{ref}}) - 0{,}1398(\frac{V}{V_0}\frac{V_{ref_0}}{V_{ref}})^2 + 0{,}0002398(\frac{V}{V_0}\frac{V_{ref_0}}{V_{ref}})^3$$

…… **(3.4)**

A photograph of the test and reference specimens adapted to testing equipment is given in Figure 3.16.

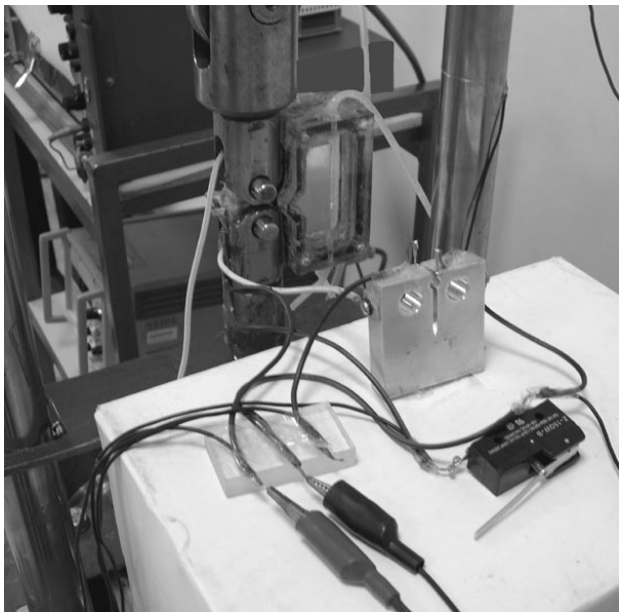

Figure 3.16 The test and reference specimens.

For the crack length measurements by DCPD technique, a calibration curve was generated. For this purpose, two CT specimens identical to the test specimens were prepared, the first one being the calibration specimen and the second one the reference specimen. In the calibration specimen, the crack length was increased artificially by cutting 0,5 mm dip slots starting from the tip of the notch. EPD measurements are taken for each slot with a constant stabilized DC current of 15 A, as it was used throughout the experimental work.

Making use of the EPD values from both the calibration specimen, V, and from the reference specimen, V_{ref}, at each a value with 0,5 mm increment, Equation 3.3 was applied to determine the V_{ref0} /V_0 ratio corresponding to a/W = 0,241. After this, Equation 3.4 was used to find the corresponding a/W ratios at relavent V and V_{ref} values. Calibration curve obtained experimentally and the curve which can be derived from the Hicks and Pickard solution were plotted on the same graph in Figure 3.17, showing excellent agreement between them.

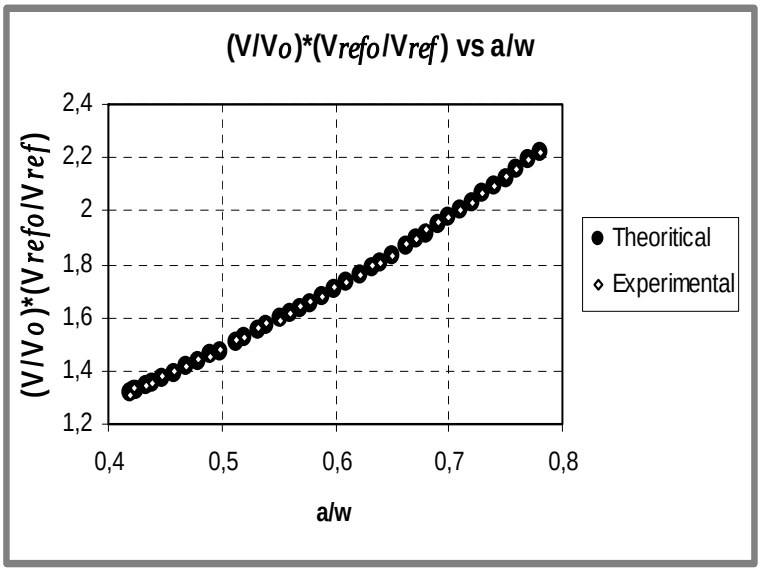

Figure 3.20 Comparison of the experimentally determined calibration curve to the theoretical one plotted from Hicks and Pickard equations.

3.5 Conduction of Experiments

The specimens were fatigued in order to obtain a sharp fatigue pre-crack that satisfies the requirements of ASTM E399 standard. For this purpose closed-loop servo-hydraulic MTS Testing Machine with a 10 tons capacity was used. A frequency of 10 Hz was applied and the load amplitudes were selected for the stress intensity conditions given in ASTM E399 standard. During fatigue pre-cracking, the crack lengths were measured at both surfaces with a travelling microscope.

Before CERT, all specimens were exposed to 5% NaCl solution for 72 hours for the incubation of corrosion process. The pre-cracked CT specimens were tested under tension with a constant extension rate of $5{,}66 \times 10^{-5}$ mm/sec in CERT equipment .All of the tests were conducted in 3.5% NaCl solution under free corrosion potentials. The heat treatment conditions and the specimen orientations that were covered in this work are given in Table 3.5.

Table 3.5 Test specimen orientations and heat treatment conditions.

Heat Treatment Condition	Specimen Orientation
T73651	LT, TS, SL
T651	LT, TS, SL
T7651	LT, TS, SL

During the tests, the EPD values of the test specimens (V) and the reference specimen (V_{ref}) were recorded against the time together with load. A direct current of 15 A has been used during the experiments.

Since the calibration curve has correlated well with the Hicks and Pickard polynomials, the crack lengths were derived from Equation 3.4.

By the use of data obtained, crack length (a) versus time (t) and load (P) versus time (t) graphs were plotted. A curve fitting method was applied to fit a-t and P-t curves to a multiple term polynomial function with the aid of Mathcad 2001 program. The derivatives of the a-t curves were evaluated at relevant test times to plot the crack growth rate (da/dt) versus stress intensity (K) curves. The derivatives were determined by the method of least squares. The stress intensity values were calculated according to the formula given by ASTM-E399-90 standard (69):

$$K = \frac{P}{B\sqrt{W}} f(\frac{a}{W}) \quad \text{.....} \quad \textbf{(3.5)}$$

$$f\left(\frac{a}{W}\right) = \frac{\left[(2+\frac{a}{W})(0{,}886+4{,}64\frac{a}{W}-13{,}32(\frac{a}{W})^2+14{,}72(\frac{a}{W})^3-5{,}6(\frac{a}{W})^4\right]}{\left[1-(\frac{a}{W})^3\right]}$$

..... **(3.6)**

where

K is stress intensity,

P is load,

B is specimen thickness,

a is crack length, and

W is specimen width.

The plotted da/dt versus K curves were also regressed by fitting to multiple term polynomial functions by the use of the same program.

3.6 Fractographic Analysis

Fractographic analysis has been carried out by the use of Scanning Electron Microscope (SEM). After the CERT, the specimens were cleaned by alcohol. Before microscopic examination, the specimens were cut into the desired size for SEM investigation, that were then ultrasonically cleaned in acetone to remove the undesired extraneous materials that may have deposited on the fracture surfaces after testing. The specimens were examined in SEM by secondary electron imaging at 20 keV excitation.

CHAPTER 4

RESULTS AND DISCUSSIONS

4.1 Summary of Results

The crack lengths (a) were measured by the use of DCPD technique and recorded against time (t). With these data, a vs. t graphs were plotted for each specimen. The curves were then smoothened by fitting to polynomial functions.

In addition to the crack lengths, the load values were also recorded against time, during testing. Similar to the a vs. t curves P vs. t curves were also smoothened by the same method.

The crack growth rate (da/dt) values were derived by taking the derivatives of the smoothened a-t curves by the method of least squares and stress intensity (K_I) values were calculated by Equation 3.5, in order to plot the da/dt vs. K_I curves on a semi-logarithmic scale. The da/dt vs. K_I curves were then fitted to multiple term polynomial functions.

In Figures 4.1 to 4.9, the da/dt vs K_I graphs together with a-t and P-t curves for each heat treatment condition and specimen orientation are represented.

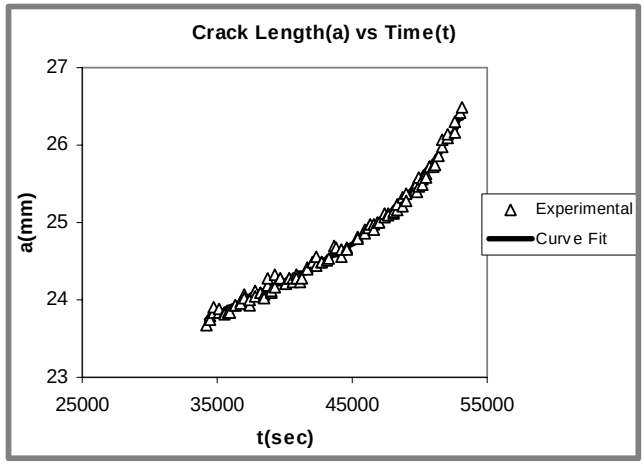

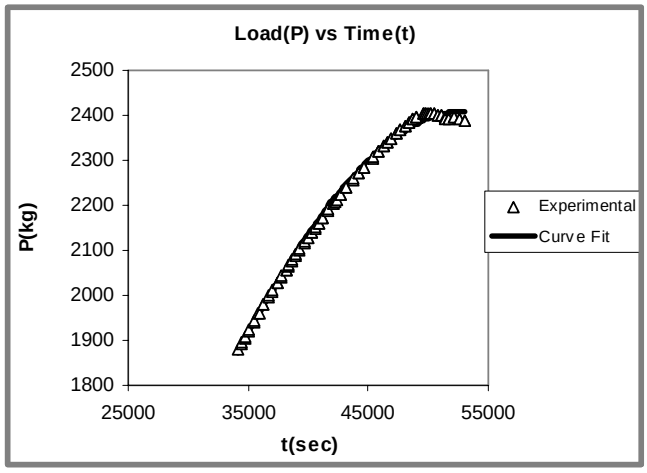

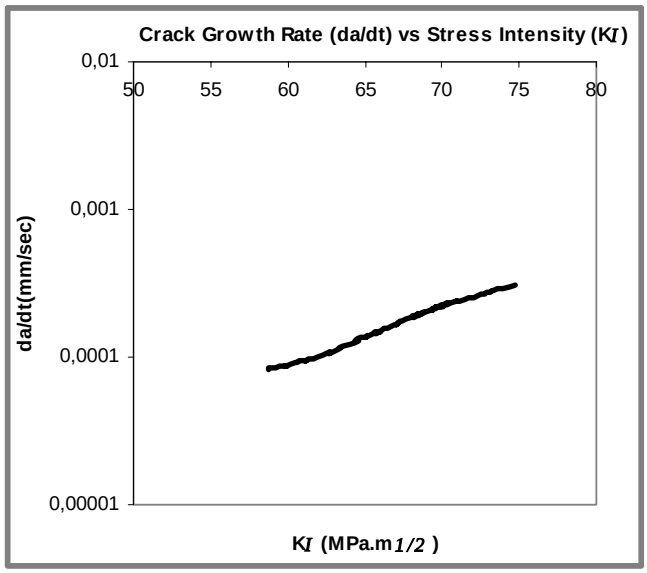

Figure 4.1 A vs. t, P vs. t and da/dt vs. K_I graphs for aluminum alloy 7050-T651 tested in LT orientation .

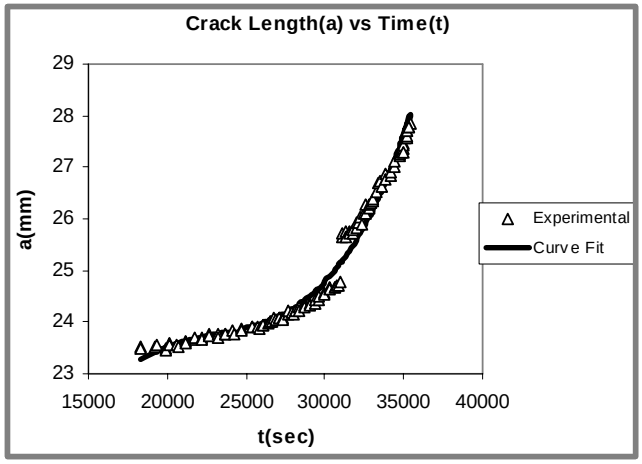

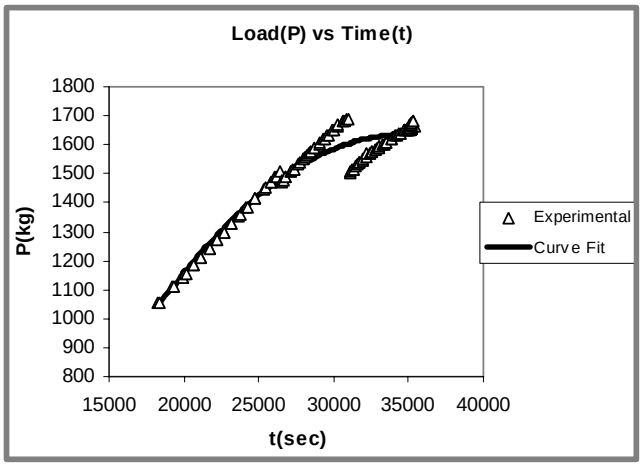

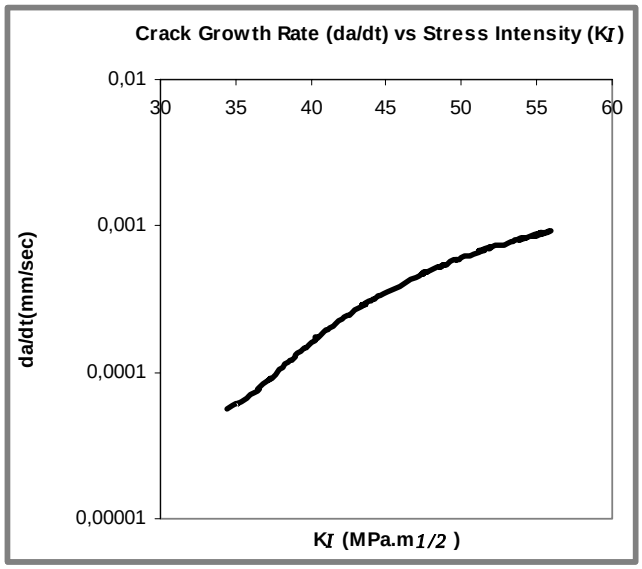

Figure 4.2 A vs. t, P vs. t and da/dt vs. K_I graphs for aluminum alloy 7050-T7651 tested in LT orientation .

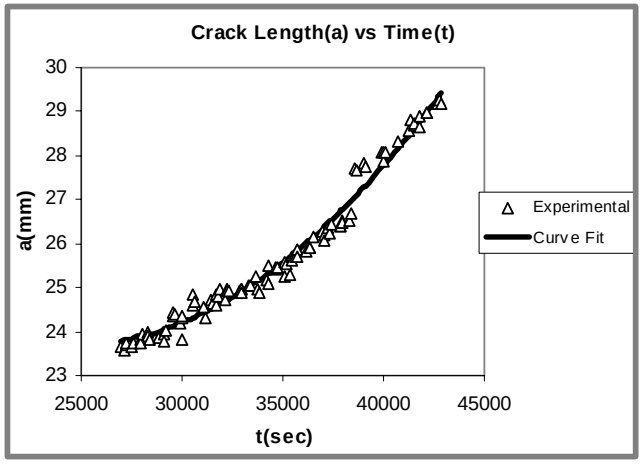

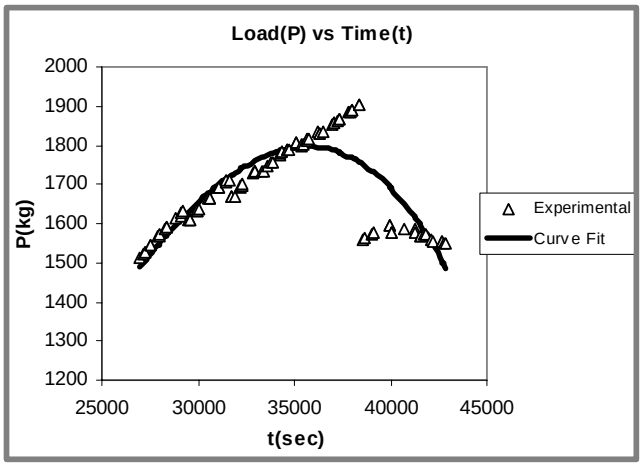

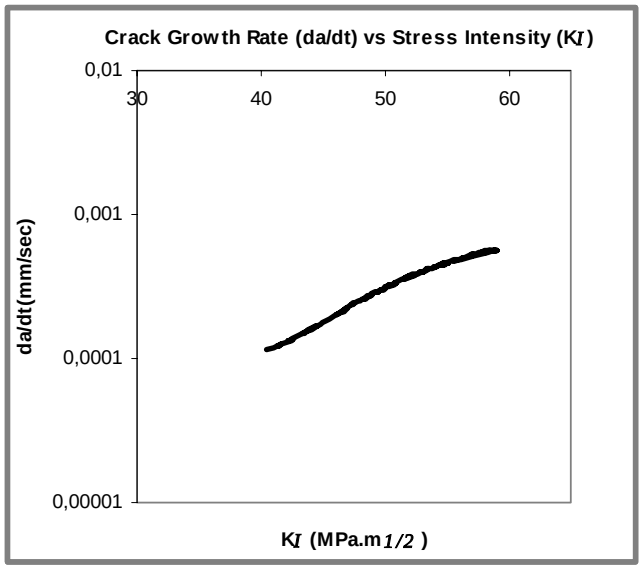

Figure 4.3 A vs. t, P vs. t and da/dt vs. K_I graphs for aluminum alloy 7050-T73651 tested in LT orientation .

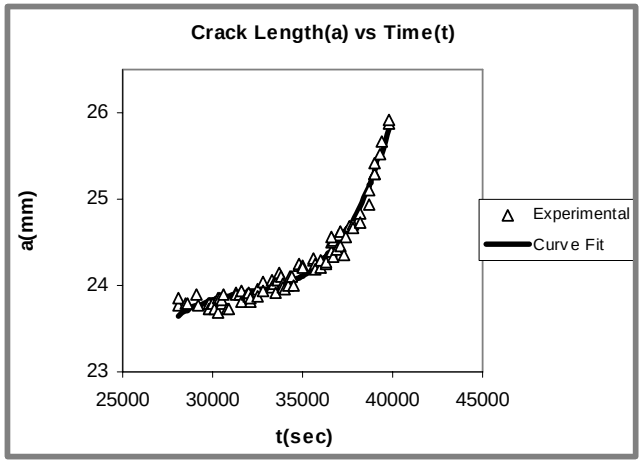

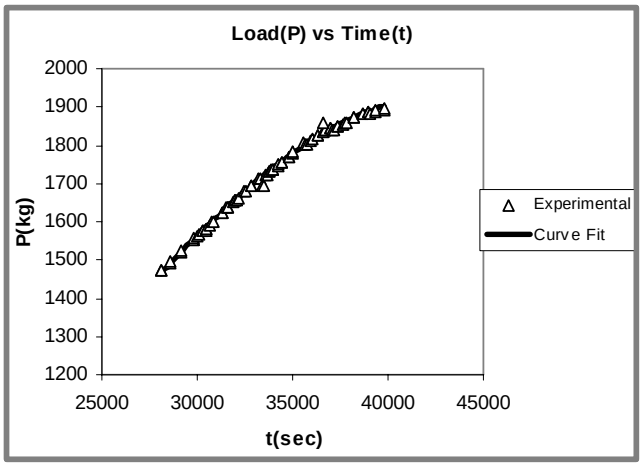

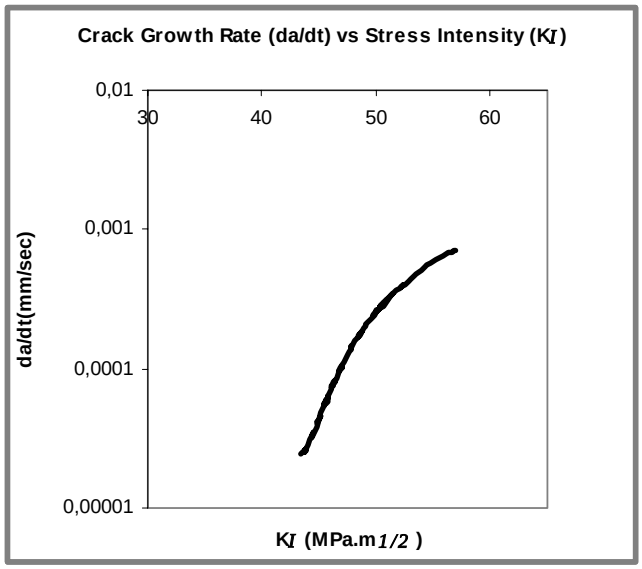

Figure 4.4 A vs. t, P vs. t and da/dt vs. K_I graphs for aluminum alloy 7050-T651 tested in TS orientation .

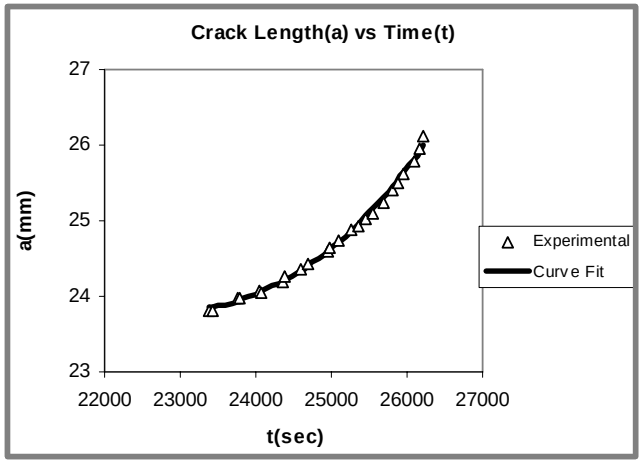

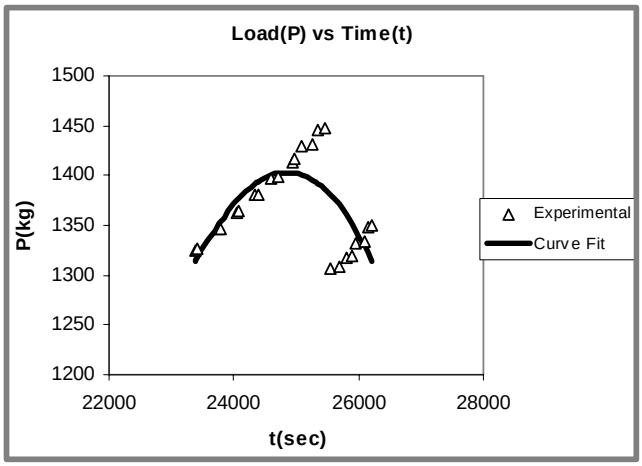

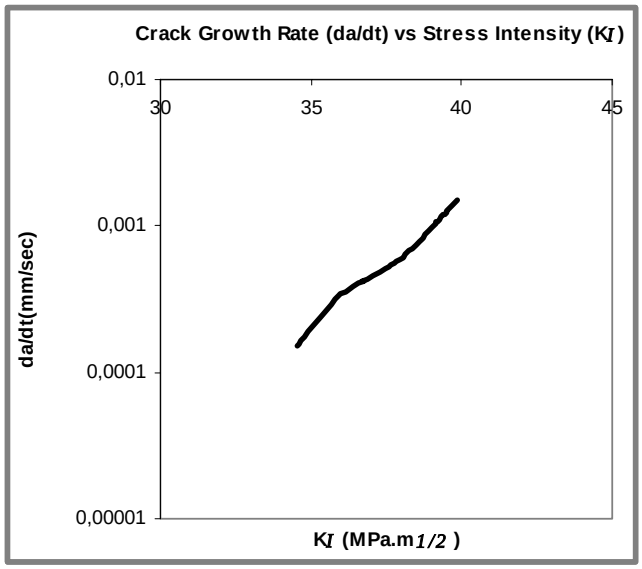

Figure 4.5 A vs. t, P vs. t and da/dt vs. K_I graphs for aluminum alloy 7050-T7651 tested in TS orientation .

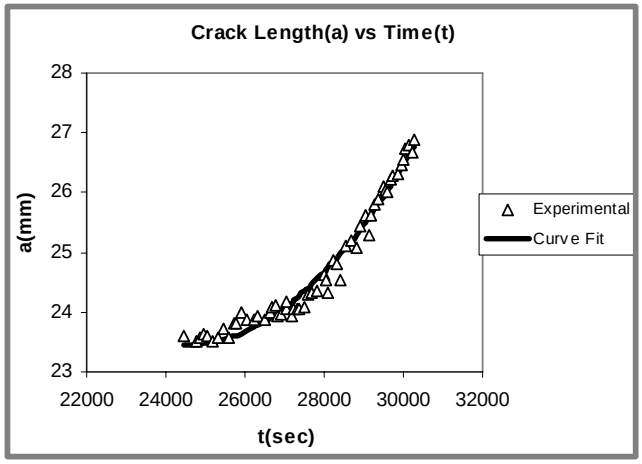

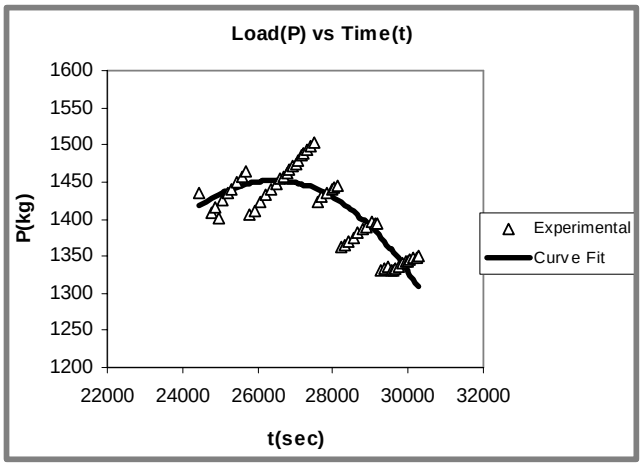

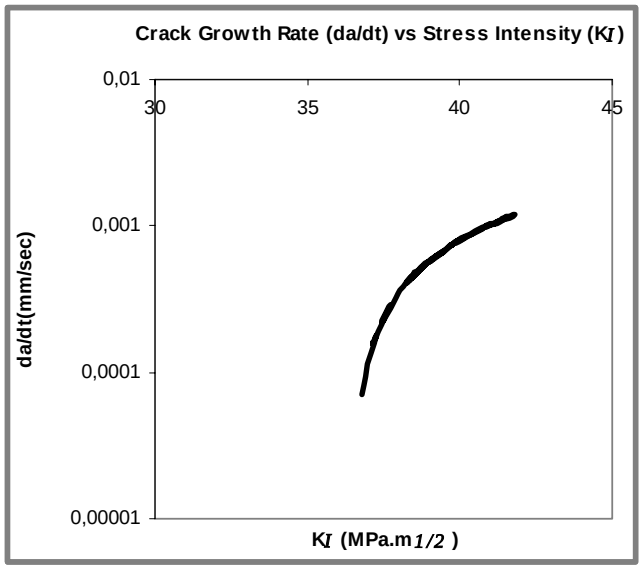

Figure 4.6 A vs. t, P vs. t and da/dt vs. K_I graphs for aluminum alloy 7050-T73651 tested in TS orientation .

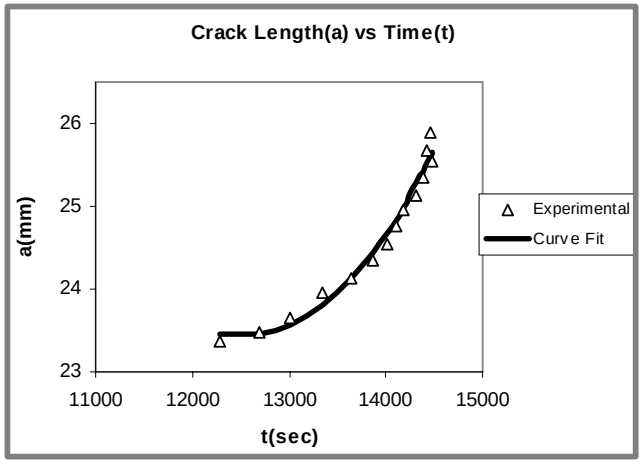

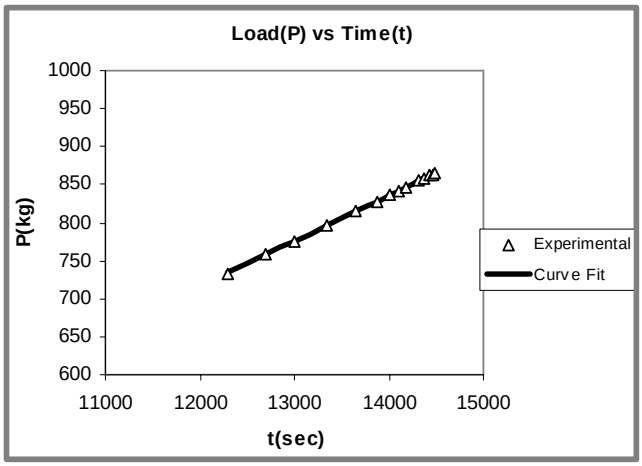

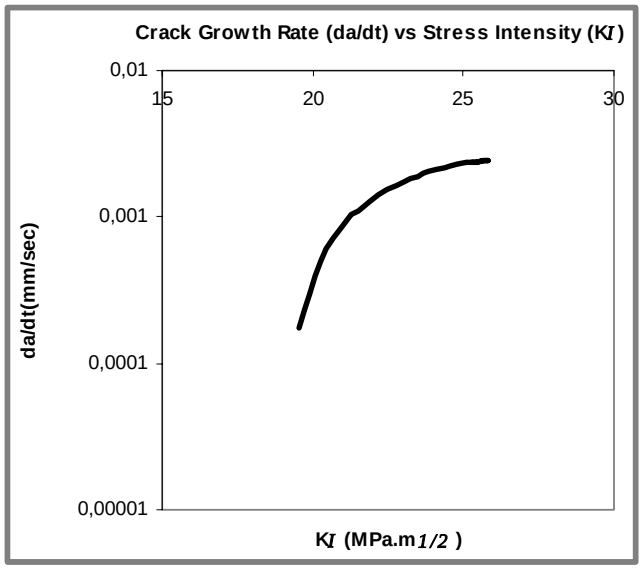

Figure 4.7 A vs. t, P vs. t and da/dt vs. K_I graphs for aluminum alloy 7050-T651 tested in SL orientation .

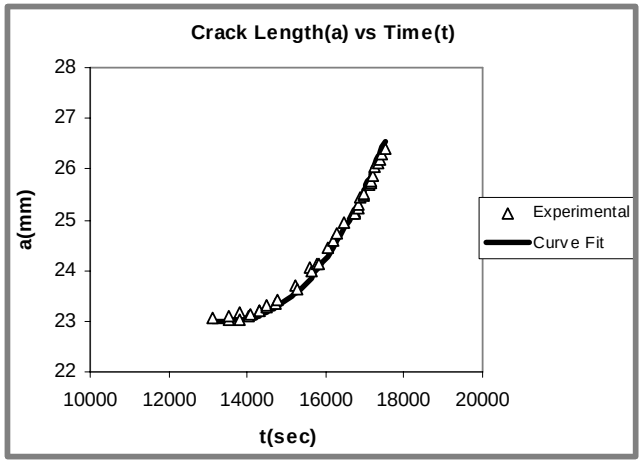

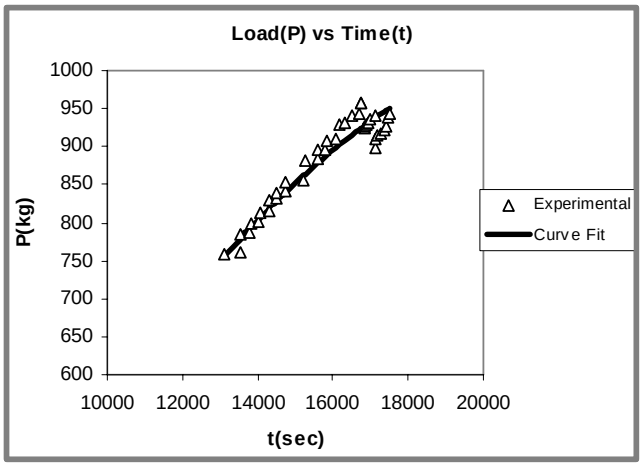

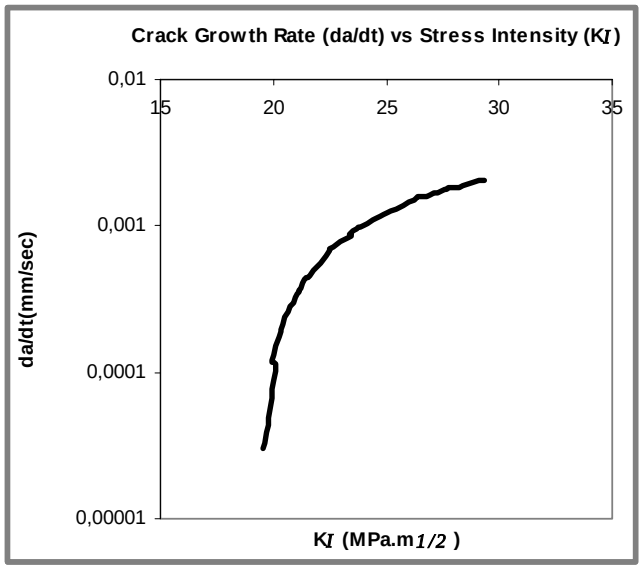

Figure 4.8 A vs. t, P vs. t and da/dt vs. K_I graphs for aluminum alloy 7050-T7651 tested in SL orientation .

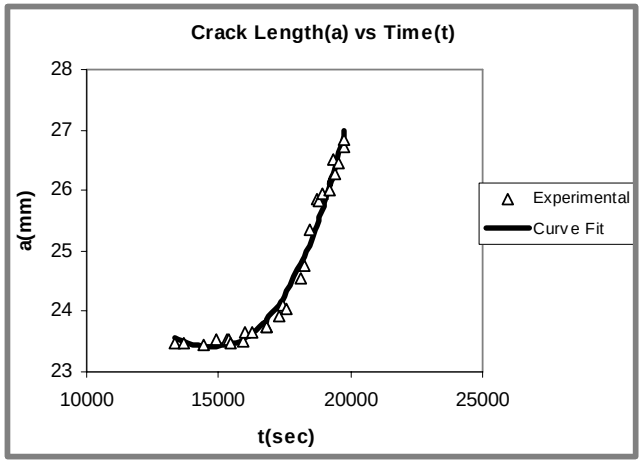

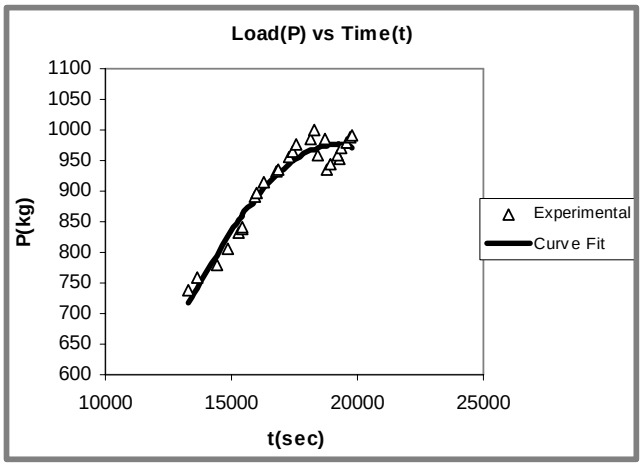

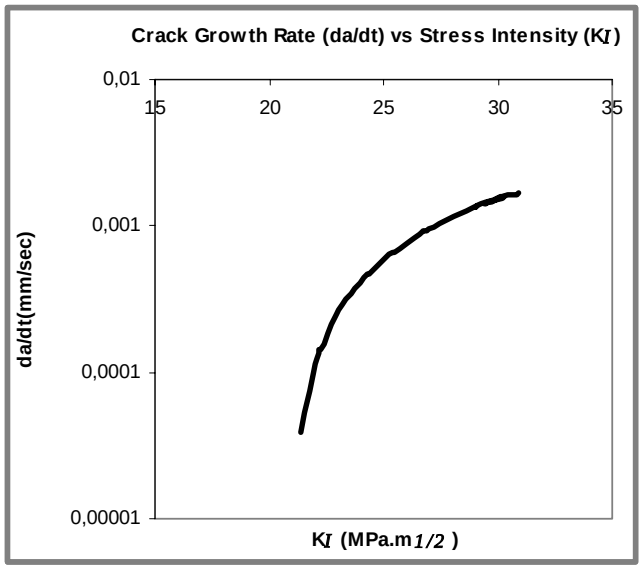

Figure 4.9 A vs. t, P vs. t and da/dt vs. K_I graphs for aluminum alloy 7050-T73651 tested in SL orientation.

4.2 Effect of Orientation on SCC Characteristics of 7050 Aluminum Alloy

Based on the experimental results it is evident that SCC characteristics of the alloy is strongly dependent on the loading and crack propagation directions. The effect of orientation under SC conditions was discussed by the comparison of the a-t, P-t and da/dt- K_I curves. Experimental results were also quantatively summarized in terms of critical crack length at fracture point (a_c), time to failure (t_f), maximum load (P_{max}) and maximum stress intensity (max. K_I) the material can withstand ultimately and the maximum crack velocity (max. da/dt). Table 4.1 demonstrates the as-told terms for all test conditions.

Table 4.1 Summary of experimental results.

Heat Treatment	Specimen Orientation	a_c(mm)	t_f	P_{max}	max da/dt(mm/sec)	max K_I(Mpa.$m^{1/2}$)
T651	**LT**	26,35	53080	2408	$3{,}08.10^{-4}$	74,8
	TS	25,84	39840	1902	$7{,}12.10^{-4}$	56,9
	SL	25,65	14480	865	$2{,}415.10^{-3}$	25,8
T7651	**LT**	27,86	35300	1640	$9{,}2.10^{-4}$	55,9
	TS	26,0	26220	1402	$1{,}494.10^{-3}$	39,9
	SL	26,55	17500	950	$2{,}064.10^{-3}$	29,3
T73651	**LT**	29,43	42880	1796	$5{,}46.10^{-4}$	58
	TS	26,77	30275	1451	$1{,}186.10^{-3}$	41,7
	SL	26,98	19760	976	$1{,}7.10^{-3}$	30,9

Figures 4.10 to 4.12 show the a-t curves of LT, TS and SL orientations on the same graphs for different heat treatment conditions. It is evident from the figures that the material fails at shorter times when the crack propagation direction is parallel to the rolling direction L i.e. SL orientation. On the other hand, when the material is loaded parallel to the rolling direction i.e. LT orientation, time to failure increases apparently. If the material is loaded in the long tranverse orientation and the propagation direction is short transverse i.e

TS orientation, the failure time is increased when compared to the SL orientation but still lower than that of the LT.

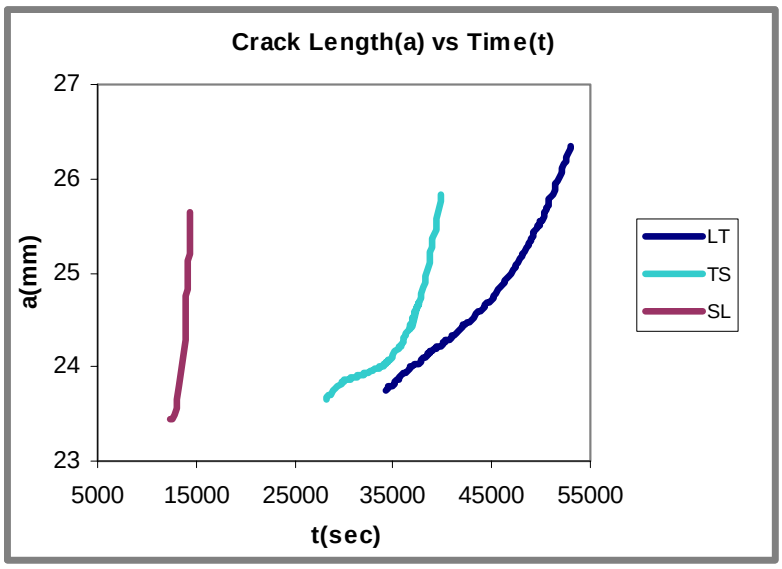

Figure 4.10 The a-t curves of 7050-T651 alloy in LT, TS and SL orientations.

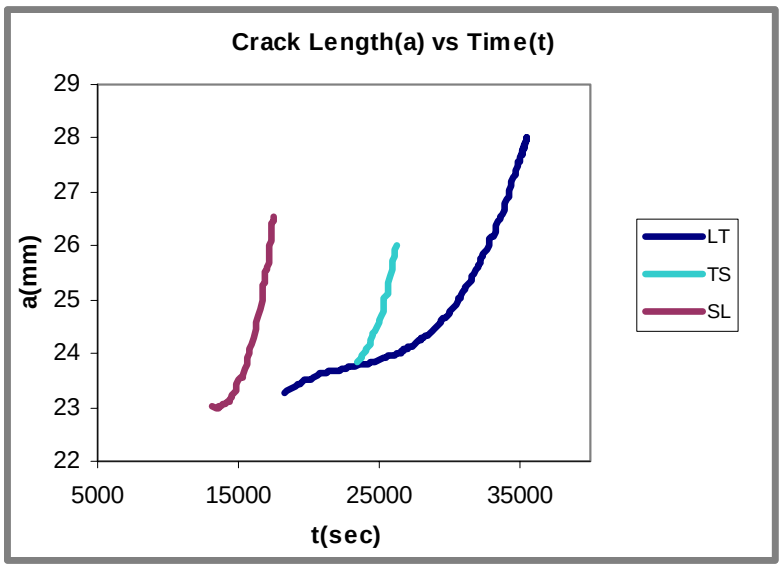

Figure 4.11 The a-t curves of 7050-T7651 alloy in LT, TS and SL orientations.

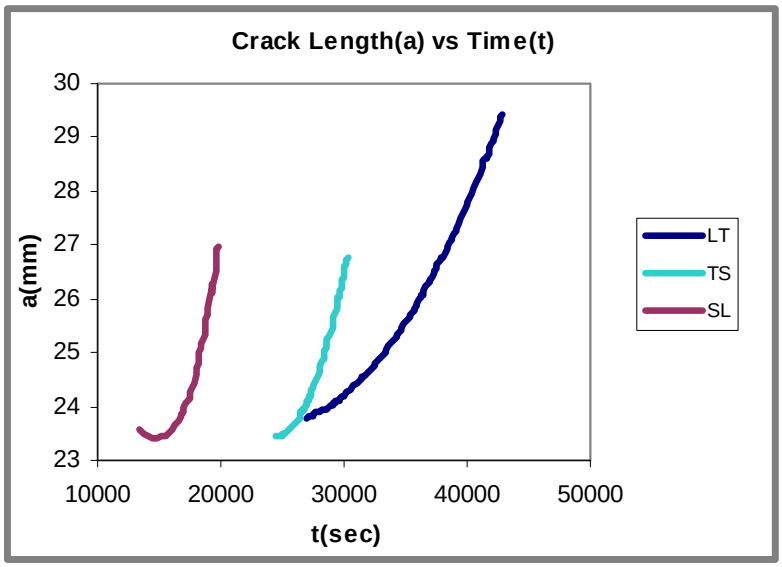

Figure 4.12 The a-t curves of 7050-T73651 alloy in LT, TS and SL orientations.

The effect of orientation is similar at different aging conditions with a variation of severity. The terms related to SCC charateristics can be compared by using the data in Table 4.1. At the peak aging condition, T651, the ratio of time to failure for LT orientation to that of SL is 3,67 where it is 2,02 and 2,2 for T7651 and T73651 conditions respectively. This ratio for LT to TS is 1,33, 1,35 and 1,42 for T651, T7651 and T73651 conditions respectively.

Another parameter included in Table 4.1 is the critical crack length, a_c at which the unstable fracture was initiated. For T651 condition the a_c values are the highest for LT and lowest for SL orientation. On the other hand, in the T7651 and T73651 conditions, a_c is higher in SL orientation compared to the TS orientation with a difference of 0,55 and 0,21 mm respectively. However a_c can not be regarded solely as a parameter to determine the SCC resistance. The crack growth characteristics is determined by stress intensity which is a function both of the crack length and load (Equation 3.5). The precrack length is also important for comparing the a-t curves. The precrack lengths of TS and

SL orientations for T7651 condition were 23,86 and 23,01 mm whereas it was slightly different for T73651. It is sure that a specimen containing a long precrack will propagate at lower loads when the required stress intensity value is reached.

As a result, by examining the a-t curves, it can be concluded that the SCC resistance of LT orientation is superior to TS and SL.

The da/dt-K_I curves for LT, TS and SL specimen orientations are plotted on the same graphs in Figures 4.13 to 4.15 for different heat treatment conditions.

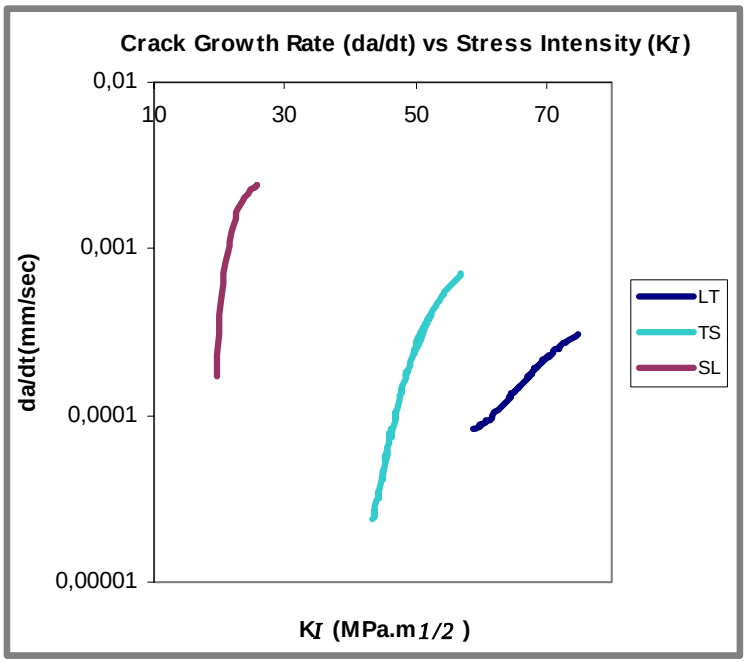

Figure 4.13 The da/dt-K_I curves of 7050-T651 alloy in LT, TS and SL orientations.

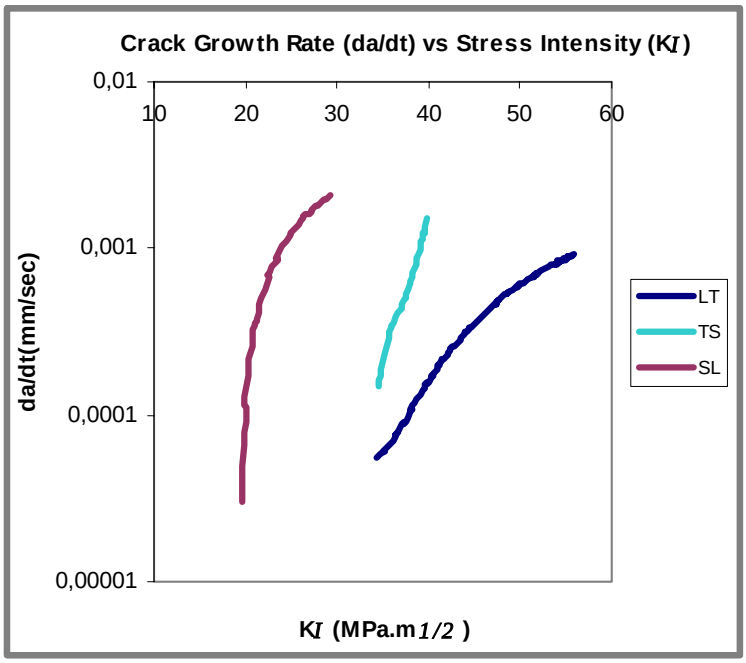

Figure 4.14 The da/dt-K_I curves of 7050-T7651 alloy in LT, TS and SL orientations.

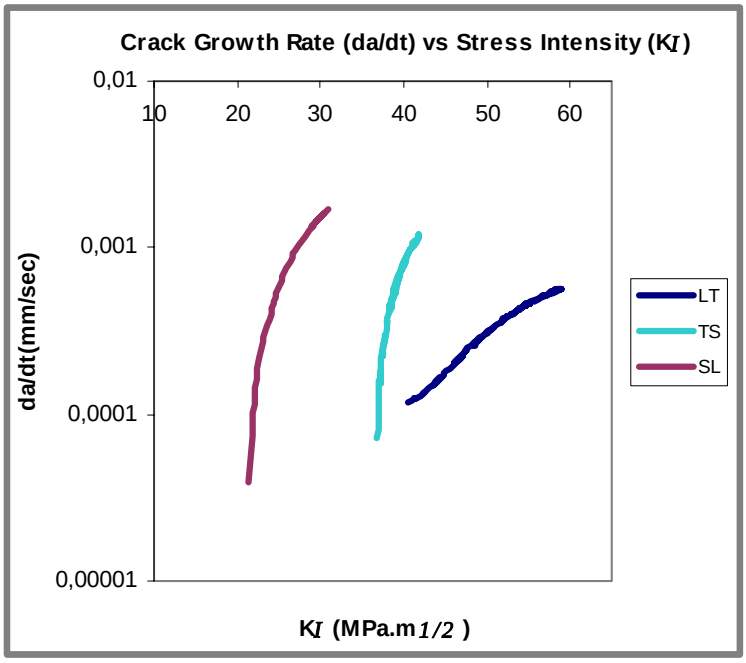

Figure 4.15 The da/dt-K_I curves of 7050-T73651 alloy in LT, TS and SL orientations.

It is worth noting that stage III is not observed in the da/dt-K_I curves. It is reported in literature that in commercial aluminum alloys stage III crack growth is absent under SCC conditions (11).

As seen in Figures 4.13 to 4.15, all the specimens have shown a steep stage I crack growth region which is an indication of a strong stress intensity dependency of the crack propagation rate. At higher stress intensities, a visible decrease in the K_I dependency of the alloy is observed. This behaviour can be attributed to a transition from the stage I to stage II. Actually, stage II is the region on the da/dt- K_I curve in which crack growth rate is independent of K_I. From this data, it can be assumed that the unstable fracture occurs at the beginning of stage II under present testing conditions. Of all, the alloy did not show a transition only for TS orientation and in T7651 condition.

It is obvious for all conditions that from SL, TS to LT, the curves shift to higher stress intensities and lower crack growth rates which is an indication of improved SCC resistance. In addition, when the maximum crack velocities and maximum stress intensities are compared from Table 4.1, orientation dependency appears to be highest for the peak aging condition.

When the effect of orientation to SCC resistance is taken into account, the a-t and da/dt-K_I curves correlates well with each other. The results show that when the alloy is stressed in the longitidunal direction and the crack propagates in the long transverse direction (LT orientation) the SCC resistance is the highest. On the other hand, resistance is minimum when the loading direction is short transverse with a crack propagating in the longitudunal direction (SL orientation). For the TS orientation, the resistance to SCC is improved with respect to SL and it is lower than that of the LT orientation.

All these findings correlate well with a previous study on the same alloy by R. Gürbüz. In that study, the corrosion fatigue crack rates were measured for six orientations both in air and in salt water fog environment. He reported that in

salt water fog, the specimens loaded in the rolling direction (LS and LT) showed better resistance while when the cracks propagate in the rolling direction (SL and TL), susceptibility is the maximum (72).

The anisotropy of the SC crack growth phenomena of aluminum alloy 7050 would inevitably attributed to the highly anisotropic microstructure of the alloy (Figure 4.16). The precipitation hardened and partially recrystallized 7050 alloy has a complex microstructure. It typically consists of elongated recrystallized grains, anisotropic stringers of coarse constituent particles (Al_7Cu_2Fe, Al_2CuMg, Mg_2Si, etc.), relatively coarse and closely spaced incoherent η precipitates on the high-angle grain boundaries and PFZs around the high angle boundaries and uniformly distributed fine precipitates of η and η' phases (73).

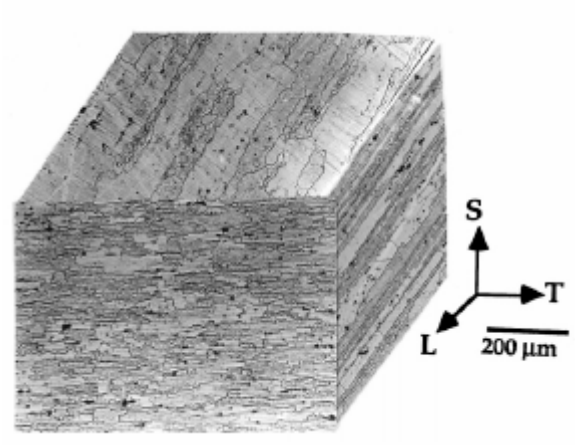

Figure 4.16 Grain structure in 7050 aluminum alloy plate (35).

Since intergranular SCC of high-strength aluminum alloys is usual, more attention has to be paid on grain boundary characteristics. According to Desphande et. al. (73), the probability of crack-tip advancement via local intergranular fracture depends on the probability of finding a high-angle grain

boundary segment perpendicular to the loading direction in the vicinity of the crack-tip, which in turn depends on the total area of the high-angle grain boundaries normal to the loading direction. The same investigators measured the projected area of the high-angle grain boundaries per unit volume of 7050 aluminum alloy. Their study showed that this area is highest on LT plane because the recrystallized grains are elongated along the L direction. It should be noted that LT plane is the fracture plane for the SL oriented specimens. However, the projected area of the high-angle grain boundaries is lowest on ST plane which is the fracture plane of the specimens in LT orientation (74). These findings explain very well why the SCC resistance and fracture toughness of the alloy are minimum when L is the crack propagation direction (i.e. SL specimens) and maximum when L is the loading direction (i.e. LT specimens).

4.3 Fractographic Analysis of the Specimens in Different Orientations

Micrographs of fracture surfaces in three different orientations of 7050 alloy are shown in Figures 4.17 to 4.28. For the purposes of discussion, the T73651 heat treated alloy was selected in order to summmarize the fractographic details at different regions of the fracture surfaces.

A strong dependence of surface texture on orientation was identified by the macro examination of the fracture surfaces under low magnification. From the general view of the fracture surface of TS specimen (Figure 4.17), a strong texture can be identified along the specimen's thickness which is the rolling direction with a fibrous appeareance. In the SL specimen, the appeareance is similar to TS orientation with a fibrous texture (Figure 4.18). In this case, the rolling direction coincides with the crack propagation direction. However, texture is not as strong as in the TS specimen, since grain flattening is less severe in T direction compared to the S. LT specimen did not show such a texture and fibrous appeareance since it is loaded in the longutidunal direction and crack propagation plane is TS (Figure 4.19).

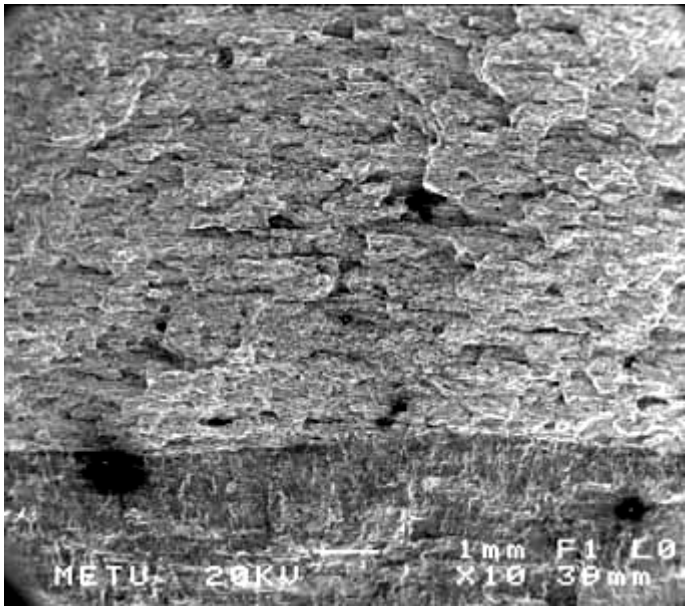

Figure 4.17 General view of fracture surface of 7050-T73651 alloy in TS orientation.

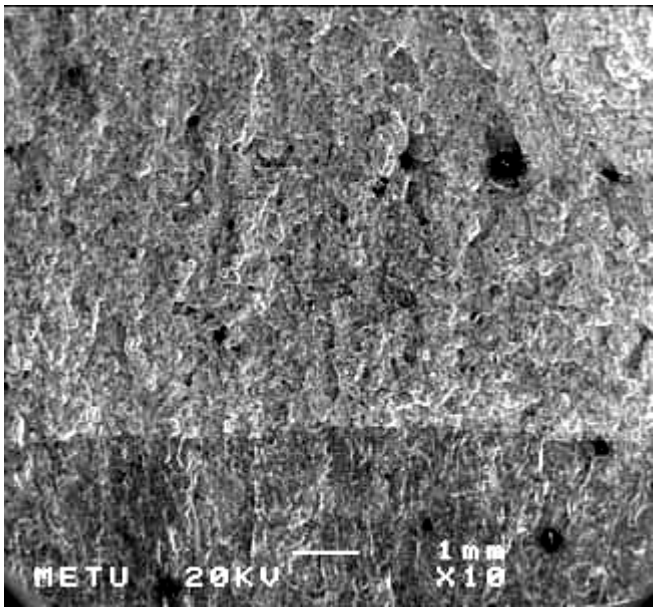

Figure 4.18 General view of fracture surface of 7050-T73651 alloy in SL orientation.

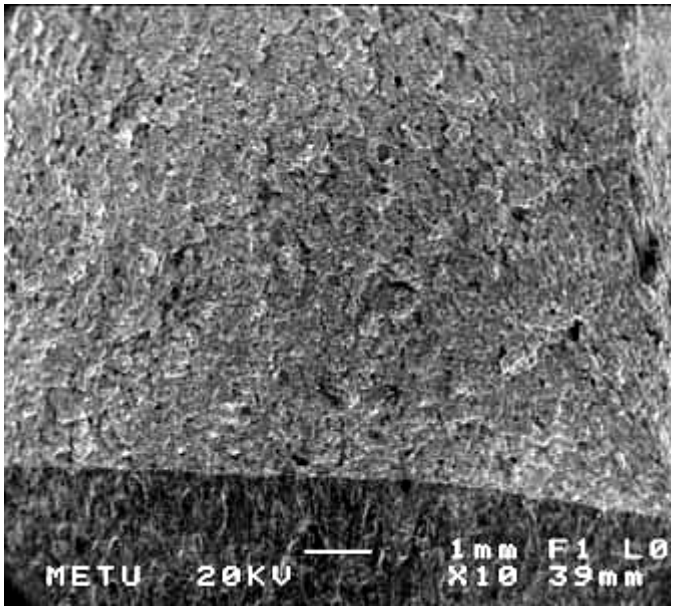

Figure 4.19 General view of fracture surface of 7050-T73651 alloy in LT orientation.

The basic differences in microappearance of fracture surfaces of the fatigue precrack and SC crack can clearly be identified in Figures 4.20 to 4.22. It is worth noting that the texture in fatigue precrack and SC crack regions are specific to the orientation.

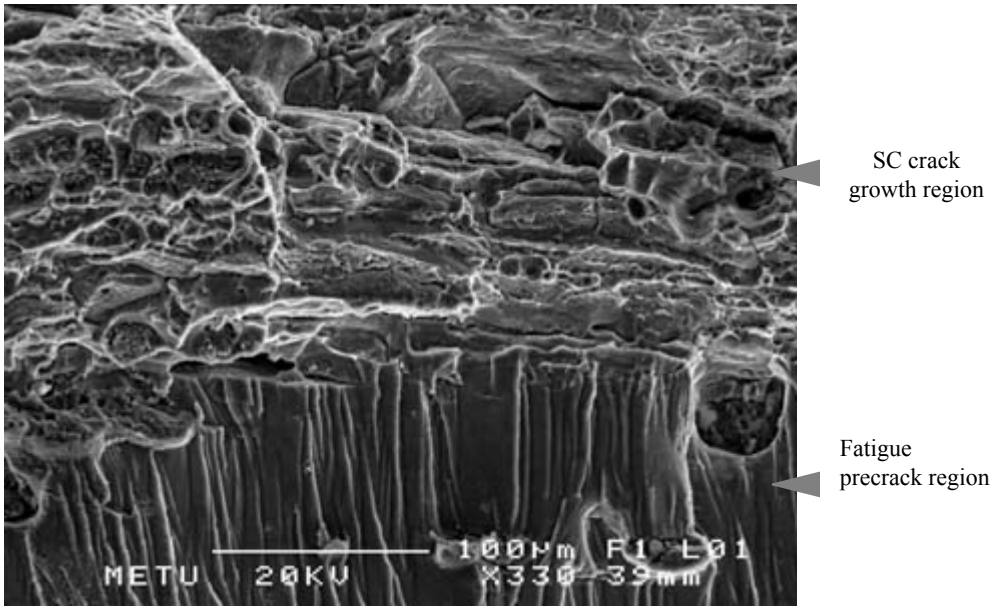

Figure 4.20 Fractograph of 7050-T73651 alloy at the transition region from fatigue precrack to SC crack in TS orientation.

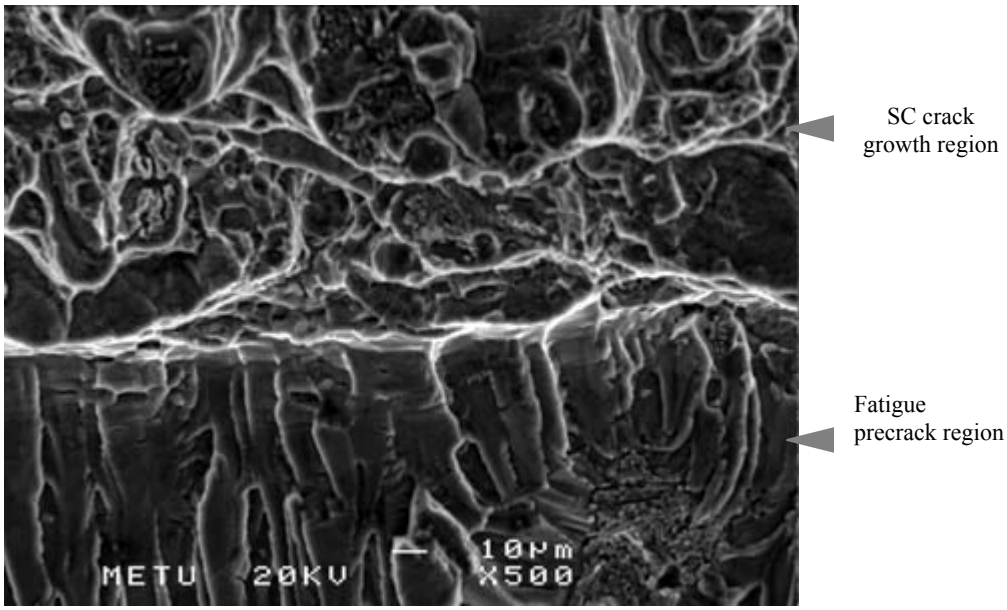

Figure 4.21 Fractograph of 7050-T73651 alloy at the transition region from fatigue precrack to SC crack in SL orientation.

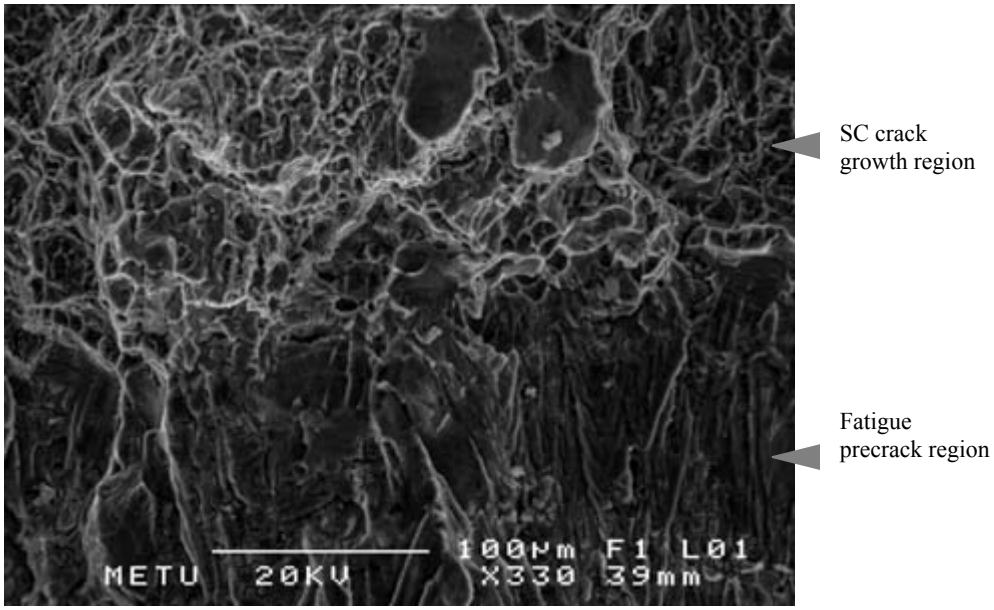

Figure 4.22 Fractograph of 7050-T73651 alloy at the transition region from fatigue precrack to SC crack in LT orientation

Figures 4.23 and 4.24 show fractographs from SC crack growth regions of TS and SL specimens that reveal the fracture of intergranular type, however, another micrograph of SC crack in LT orientation (Figure 4.16) is characterized basically by the mode of transgranular fracture together with the small size dimples.

Micrographs from the fast fracture regions of the same specimens are depicted in Figures 4.26 to 4.28. Transgranular areas in TS and both transgranular and intergranular features in SL specimen are accompanied with dimples. On the other hand, completely ductile failure is observed in LT specimen.

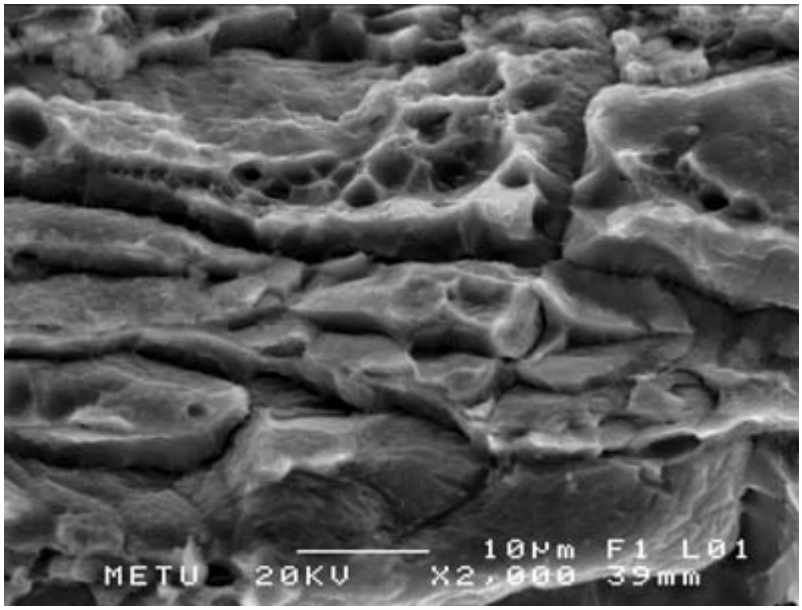

Figure 4.23 Fractograph from SC crack region of 7050-T73651 alloy in TS orientation.

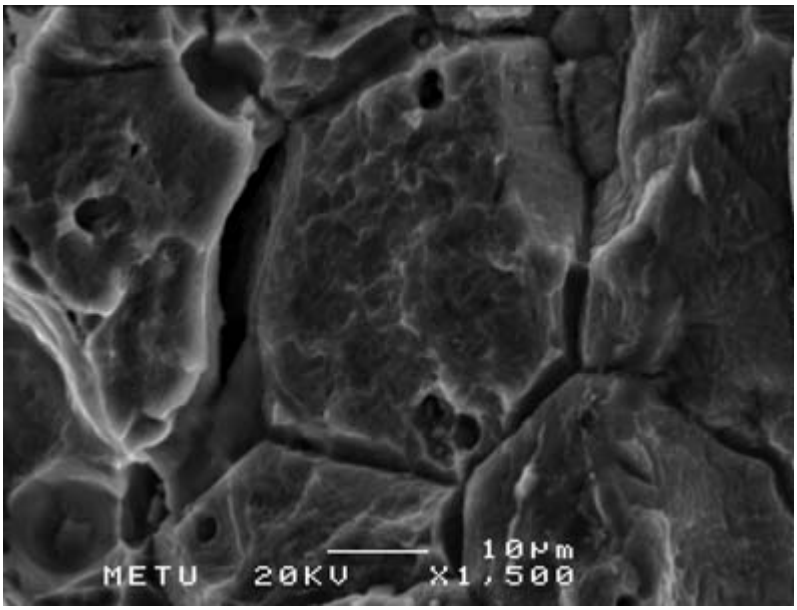

Figure 4.24 Fractograph from SC crack region of 7050-T73651 alloy in SL orientation.

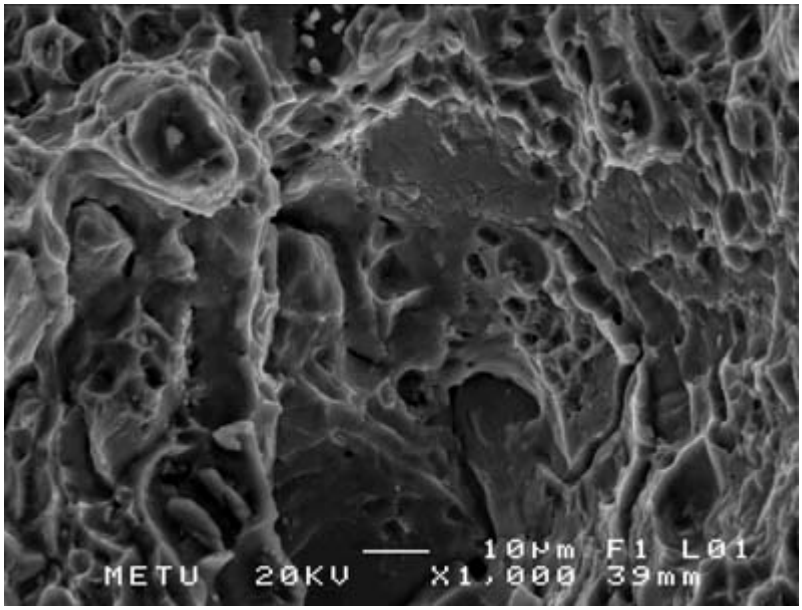

Figure 4.25 Fractograph from SC crack region of 7050-T73651 alloy in LT orientation.

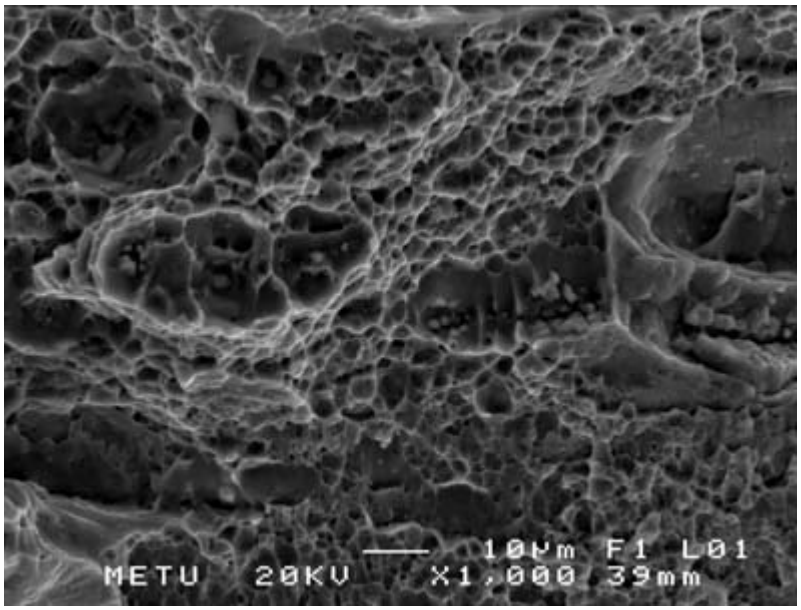

Figure 4.26 Fractograph from fast fracture region of 7050-T73651 alloy in TS orientation.

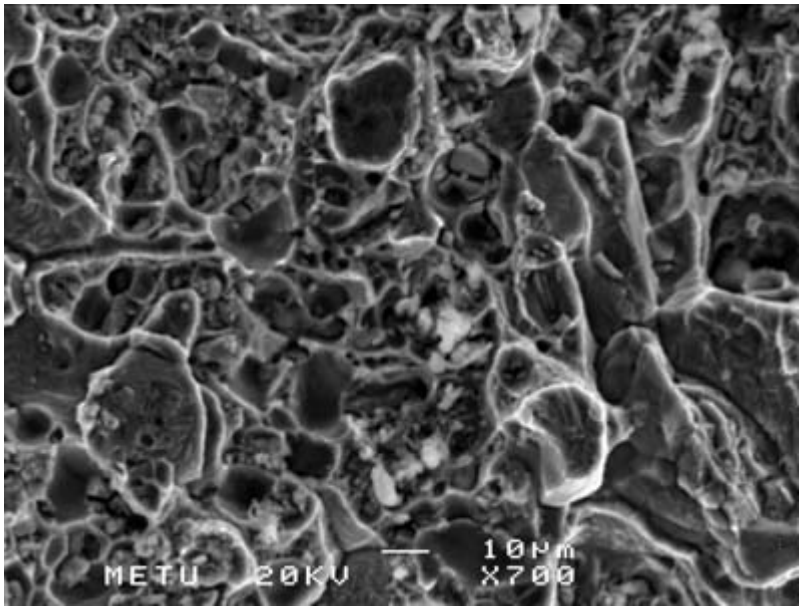

Figure 4.27 Fractograph from fast fracture region of 7050-T73651 alloy in SL orientation.

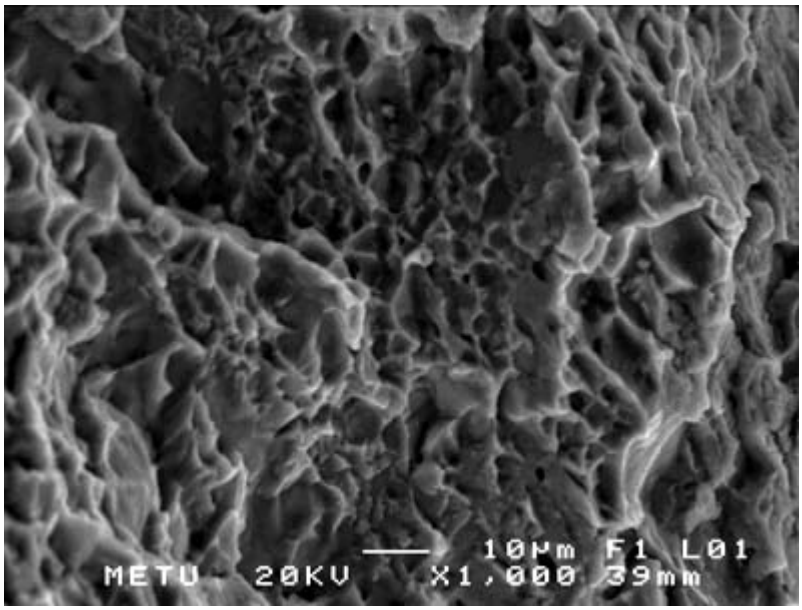

Figure 4.28 Fractograph from fast fracture region of 7050-T73651 alloy in LT orientation.

4.4 Effect of Heat Treatment on SCC Charateristics of 7050 Aluminum Alloy

The crack length versus time curves of T651, T7651 and T73651 conditions are plotted on the same graphs for SL, LT and TS orientations as depicted in Figures 4.29 to 4.31 respectively.

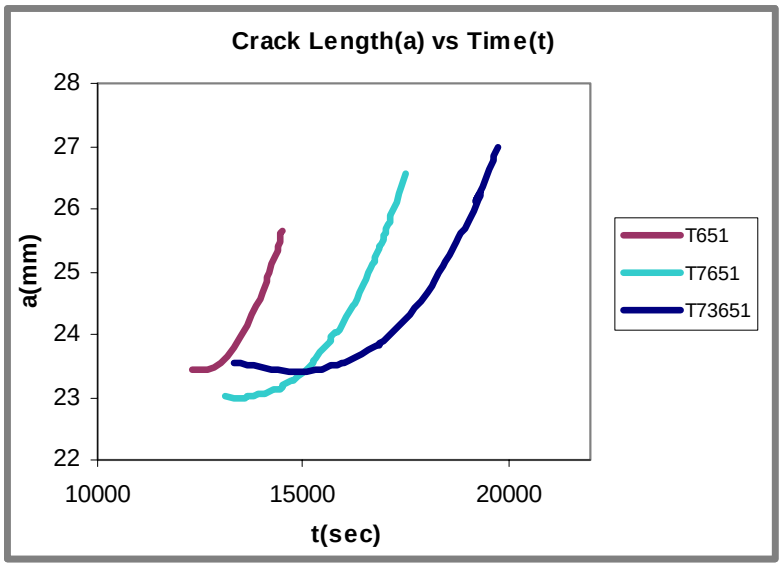

Figure 4.29 The a-t curves of 7050 alloy in SL orientation at T651, T7651 and T73651.

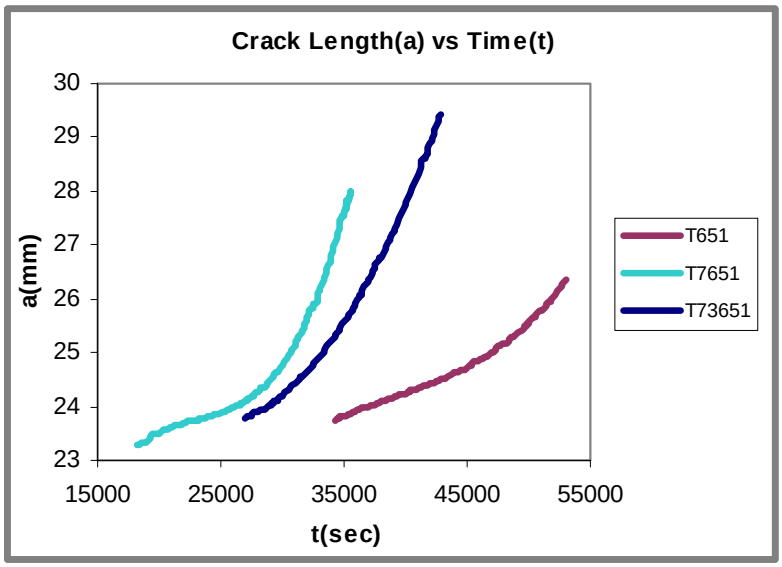

Figure 4.30 The a-t curves of 7050 alloy in LT orientation at T651, T7651 and T73651.

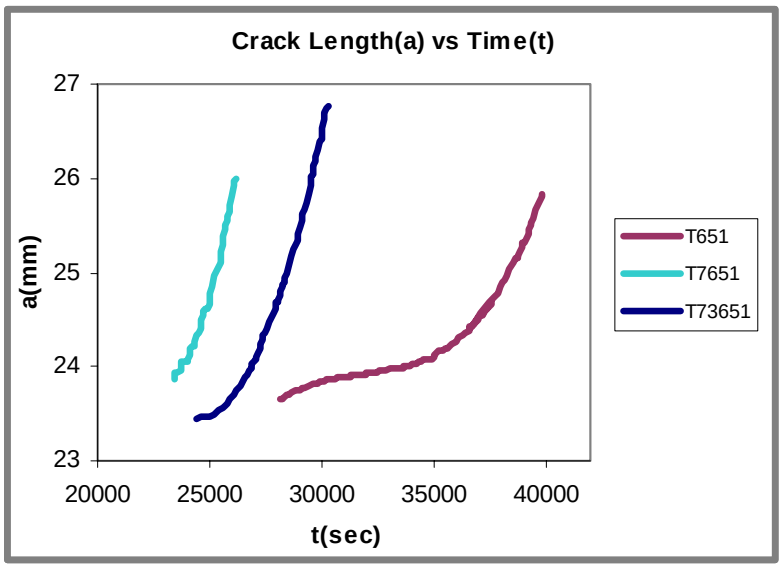

Figure 4.31 The a-t curves of 7050 alloy in TS orientation at T651, T7651 and T73651.

From data in Table 4.1 and Figure 4.29, it can be stated that alloy tested in SL orientation is more resistant to stress corrosion cracking in T73651 heat treatment (the t_f for T73651 condition is 5,5 hours and is 4,9 and 4 hours for T7651 and T651 conditions respectively). As consistent with the literature, the alloy is more susceptible to SCC in the peak aged condition. Over aging at 121° C for 96 hours, T7651, has resulted in quite resistant state of the alloy whereas the two step over aging process has induced a further improvement in SCC resistance.

The a-t curves for LT orientated specimens are depicted in Figure 4.30. Different from SL, the alloy behaves more resistant to SCC in the peak aged condition in LT orientation (the t_f values are 14,7, 9,8 and 11,9 hours for T651, T7651 and T73651 respectively). According to this data, alloy seems to be more susceptible to SCC in T7651 when loaded parallel to the rolling direction and the crack propagates in the long transverse direction.

In Figure 4.31 the a-t curves of TS orientation in different heat treatments are shown. Based on data included in this figure and in Table 4.1 (the t_f is 11,1, 7,3 and 8,4 hours for T651, T7651 and T73651 respectively), it can be concluded that TS orientation gives good SCC resistance in the peak aged condition. When aging time was increased to 96 hours, the resistance was reduced. But when a two step aging was applied, the susceptibility was lowered compared to T7651 condition.

The da/dt-K_I curves for SL orientation for three heat treatments are given in Figure 4.32. As deferred from this figure, when the alloy is peak aged, crack propagation occurred at lower stress intensities accompanied with higher velocities. When the overaging was applied, the da/dt-K_I curve is shifted to higher stress intensities and lower crack growth rates. In case of two-step over aging, the SCC resistance was found to be superior to T7651 and T651 conditions.

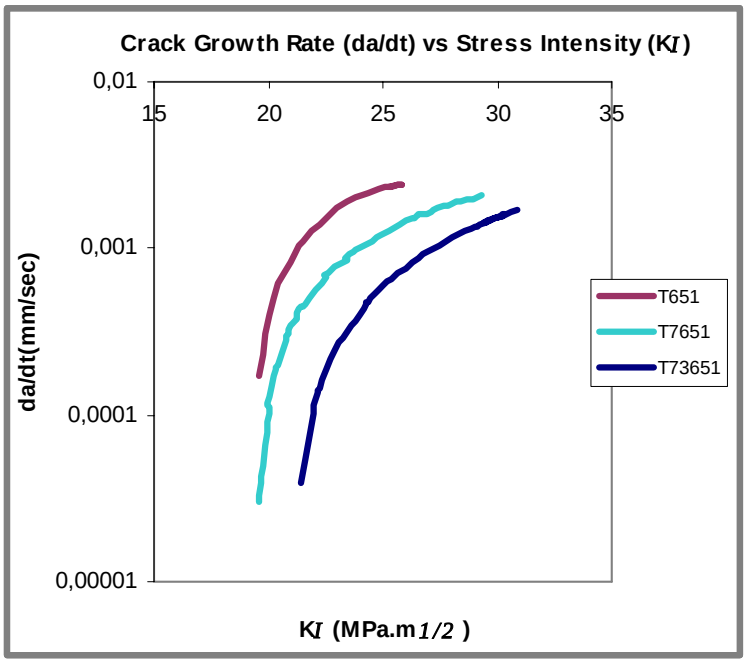

Figure 4.32 The da/dt-K_I curves of 7050 alloy in SL orientation at T651, T7651 and T73651.

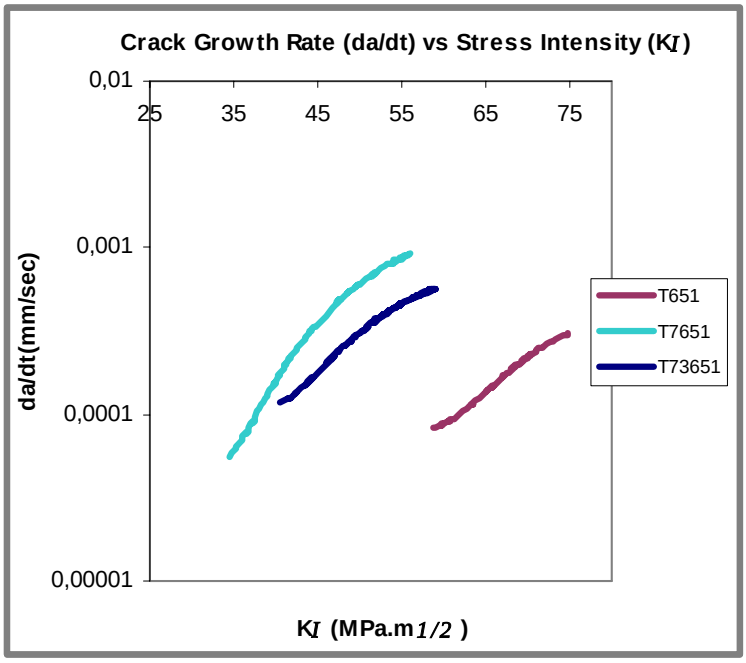

Figure 4.33 The da/dt-K_I curves of 7050 alloy in LT orientation at T651, T7651 and T73651.

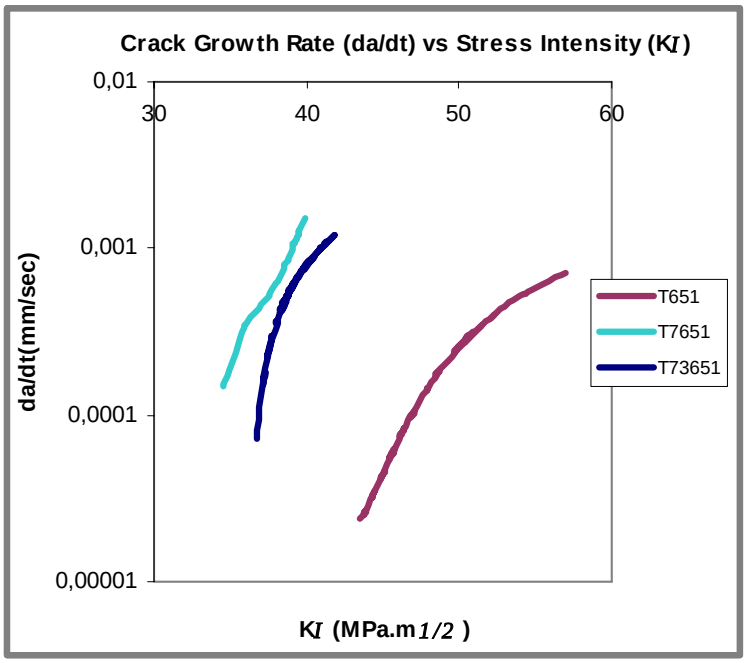

Figure 4.34 The da/dt-K_I curves of 7050 alloy in TS orientation at T651, T7651 and T73651.

The peak aged specimens in the LT and TS orientations showed crack propagations at high stress intensities accompanied with low crack velocities which is again an indication of high SCC resistance (Figures 4.33 and 4.34). However, the T7651 treatment resulted in the most susceptible condition in the same orientations. The T73651 aging improves the SCC resistance of the alloy compared to that observed with T7651 condition.

4.5 Mechanisms for SCC

The crack growth behaviour of the alloy in SL orientation as a function of aging type is in agreement with the previous studies (11). As aging proceeds, the SCC resistance increases. And if a two step over aging, T73651 is applied, a further improvement is achieved in the most SCC susceptible orientation.

Due to the complex microstructure and grain boundary characteristics of the alloy, there may be several reasons for the increase in SCC resistance by over aging. However two points of views seem to explain the phenomena well.

The first one depends on the anodic dissolution mechanism which is reported to be the governing mechanism of SCC in 7000 series alloys. Anodic dissolution was described as: anodic dissolution occurs at the grain boundaries which are anodic with respect to the grain interiors as a result of which crack propagates. The effect of stress is to rupture the surface film at the crack tip and thus to create a fresh surface for new corrosion attack. This sequence is repeated until fracture (12). Sprowls and Brown (50) measured the potentials of the grain boundary regions and grain interior of 7075 alloy at differenet tempers and the results showed that the difference in potentials between these regions decreased by over aging with respect to the peak aging condition. They attributed the improvement of SCC resistance by over aging to relatively similar potentials of grain boundary regions and the grain interior.

The second approach deals with the slip mode. This approach suggests that the overall distribution and nature of precipitates within the matrix is important to determine the SCC susceptibility because of their interaction with dislocations during plastic deformation (47). The slip is usually in long straight bands that terminate at grain boundaries at the high susceptibility condition of the alloy. In this situation most of the stress is concentrated at the grain boundary and this aids intergranular SCC via slip dissolution mechanism. In the over aged samples cross slip occurs more easily and dislocations become tangled around grain boundary precipitates. This change decreases the stress concentration at the grain boundaries (61).

These two approaches are quite coincide with the results of the SL orientation, however the trend is different in TS and LT orientations. They showed better resistance in the peak aged state. At this point, a question may arise that whether other mechanisms act during SCC. Actually there are two other

mechanisms proposed for SCC in high strength aluminum alloys; hydrogen embrittlement and film induced cleavage.

It has been well documented in literature that anodic dissolution is not the single mechanism contributing to SCC but a localized competition between anodic dissolution and hydrogen effects (29, 30, 31, 33). Also it is reported that, by conducting slow strain rate tests and SEM examinations, both anodic dissolution and hydrogen embrittlement operate during SCC process of 7050 aluminum alloy stressed in NaCl solution; the main role of anodic dissolution is to produce critical defects which promote subsequently localized hydrogen discharge, entry and embrittlement (33). However, in some cases, cathodic formation of hydrogen and subsequent measured entry into the metal lattice may stop growing SC cracks by cathodic polarization with accompanying hydrogen evolution (36).

The film induced cleavage model was proposed to explain the discontinuous transgranular crack growth and high transgranular crack growth rates (36, 37). FIC postulates the presence of brittle surface films to include dealloyed films and oxides. According to the FIC mechanism, a low anodic current at a strained surface can foster rapid, discontinuous, brittle cracking (36). In fractographic points of view, Pugh attributed the step formation between the parallel, but displaced, primary cleavage facets to FIC (37). However, there is no a priori reason to expect that surface films or layers are sufficiently brittle to support a brittle crack or that a crack will be sustained after crossing the interface into the underlying ductile matrix. Most passive films are very thin and hydrated. While they can be ruptured, it seems unlikely that they would be sufficiently brittle to verify the suppositions of FIC. Dealloyed layers are unlikely to have sufficient adhesion to the substrate or inherent brittleness to sustain cracking (36).

The inhomogenity in the response to aging processes in different orientations can be explained by proposing different dominant mechanisms at different

orientations. In this study, it seems that mostly the anodic dissolution is responsible for the SCC mechanism in SL orientation. On the other hand, in TS and LT orientations anodic dissolution is not, at least the only, mechanism causing SCC, rather HE and/or FIC may also be involved. Actually, it is not assumed that completely different mechanisms act at different orientations at the same heat treatments but the dominant mechanism may change in different orientations and also at different aging conditions. In addition to the enhancement of SCC by AD, HE or FIC, the probability of cathodic protection by hydrogen and blunting of the crack tip during FIC may also be taken into account to explain the slow crack velocities at high stress intensity levels for 7050-T651 alloy in TS and LT orientations.

4.6 Fractographic Analysis of the Specimens in Different Heat Treatments

Micrographs from fracture surfaces of the alloy in SL orientations at T651, T7651 and T73651 tempers are depicted in Figures 4.35 to 4.39. The mode of cracking is mainly intergranular including little indications of transgranular cracking in all heat treatments (Figures 4.35 to 4.37). The prediction about SL specimens made in the previous part can be supported with these fractographs. The almost completely intergranular cracking can be attributed to failure of the alloy by anodic dissolution mechanism. In Figure 4.38, the grain boundary seperation by intergranular SCC is seen where the rod-like precipitates (possibly η phase, $MgZn_2$) can be identified clearly. Figure 4.39 shows the coarse constituent particles at the SC crack propagation region. Figure 4.40 indicates the elemental analysis for these particles that may be identified as Al_7Cu_2Fe and/or Al_2CuFe compounds.

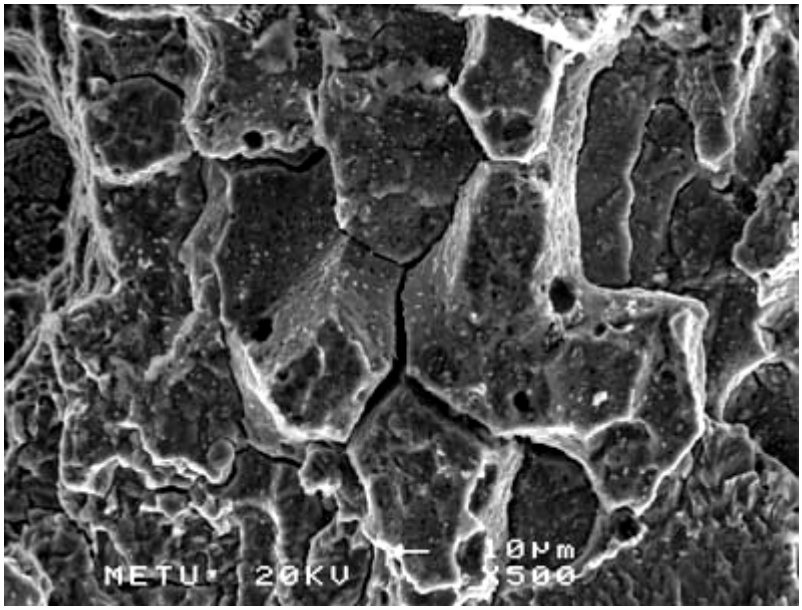

Figure 4.35 Intergranular SC cracks in 7050-T651 alloy in SL orientation.

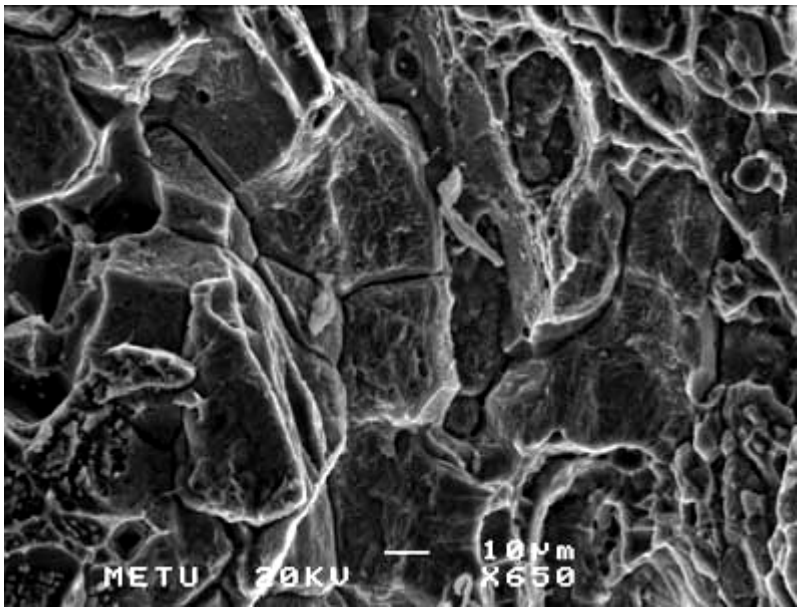

Figure 4.36 Intergranular SC cracks in 7050-T7651 alloy in SL orientation.

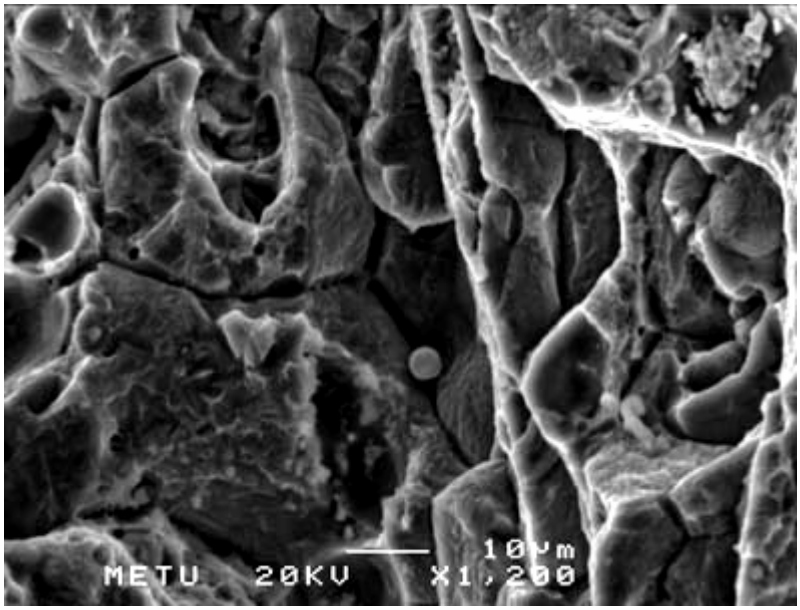

Figure 4.37 Intergranular SC cracks in 7050-T73651 alloy in SL orientation.

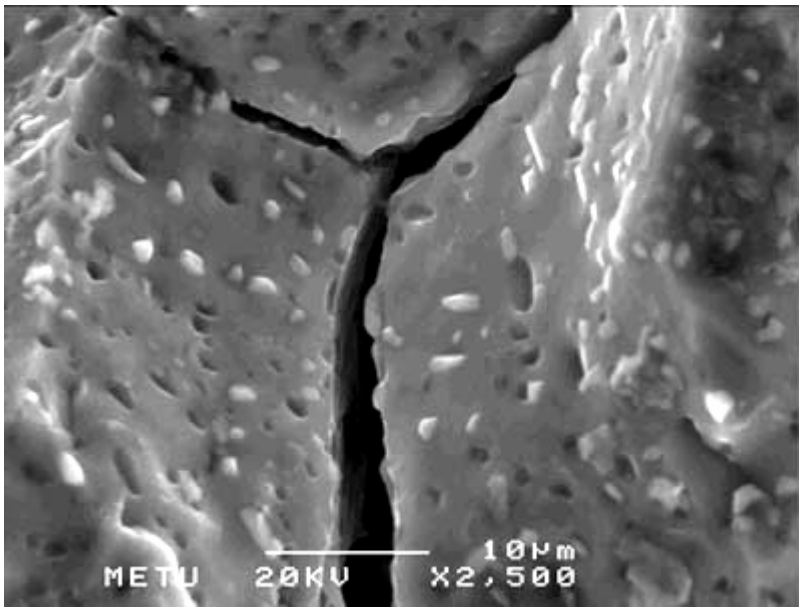

Figure 4.38 Grain boundaries and rod-like precipitates in 7050-T651 alloy in SL orientation.

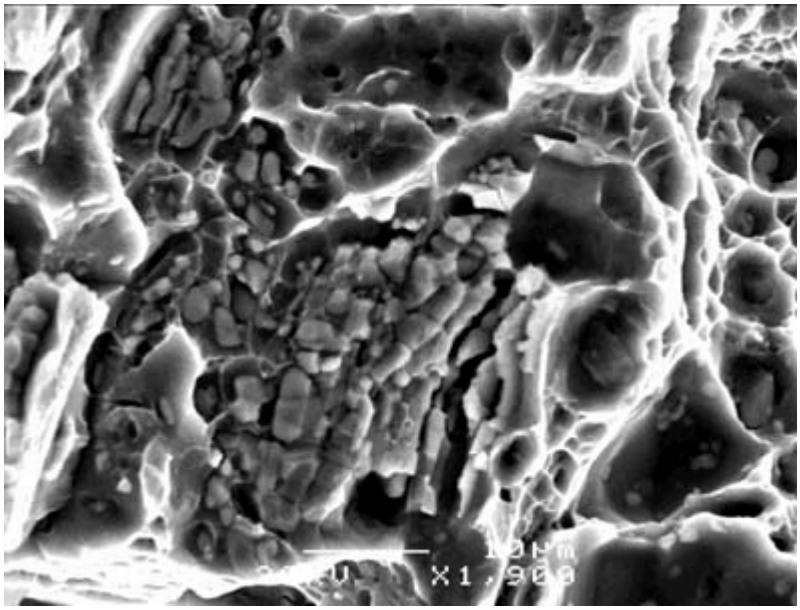

Figure 4.39 Coarse constituent particles at the SC crack propagation region of 7050-T651 alloy in SL orientation.

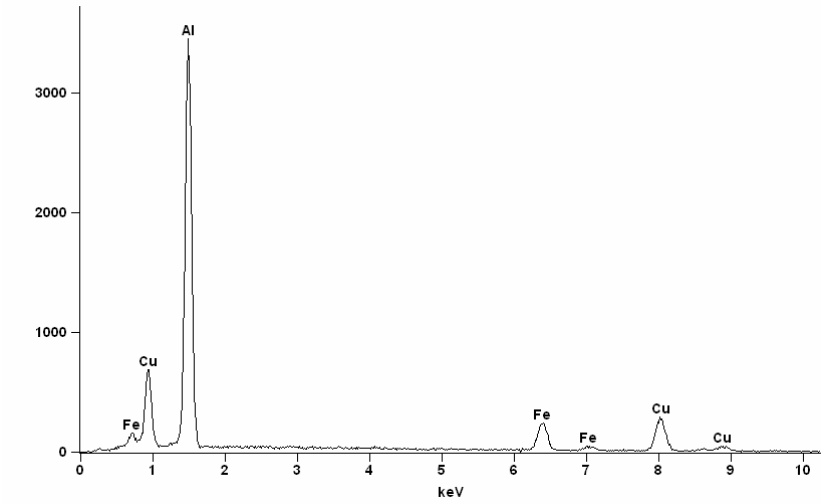

Element	*Weight Conc %*	*Atom Conc %*
Al	61.51	78.34
Fe	11.36	6.99
Cu	27.13	14.67

Figure 4.40 Elemental analysis of coarse constituent particles at the SC crack propagation region of 7050-T651 alloy in SL orientation.

Intergranular type SC crack in 7050-T651 alloy in TS orientation with little indication of transgranular fracture as depicted in Figure 4.41. The seperated grain boundaries together with coarse precipitates are shown in Figure 4.42 in high magnification. In Figure 4.43, the stepped cleavage planes of transgranular region surrounded by intergranular cracks are illustrated. As told before, Pugh attributed this behaviour to FIC. He also suggested that the repeated crack arrest during propagation is presumedly caused by lagging of the step formation process behind the cleavage crack tip. The resulting unfractured ligaments become increasingly load-bearing, reducing the stress at the crak tip until it falls below the value necessary for continued propagation. Step formation continues after crack arrest, redistributing the stress to the crack tip, but further environmental action is necessary to reinitiate the blunted crack (37).

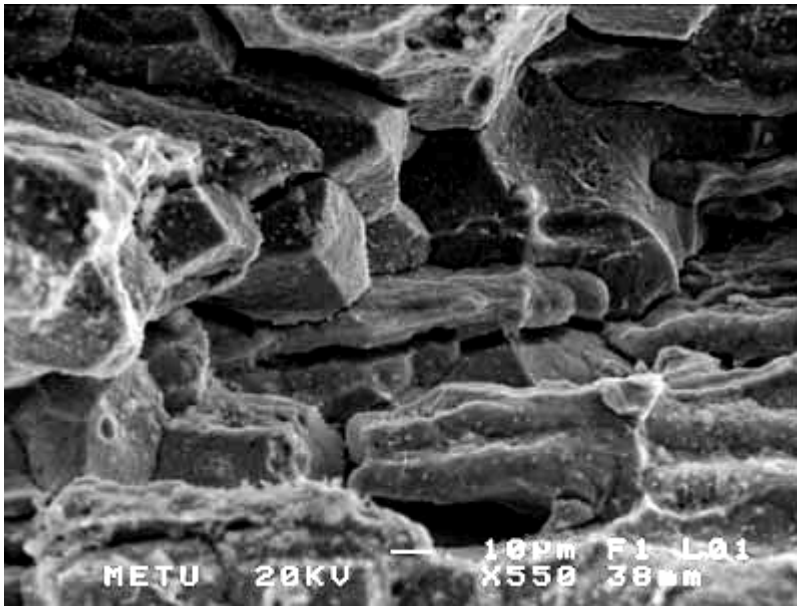

Figure 4.41 Intergranular SC crack of 7050-T651 alloy in TS orientation.

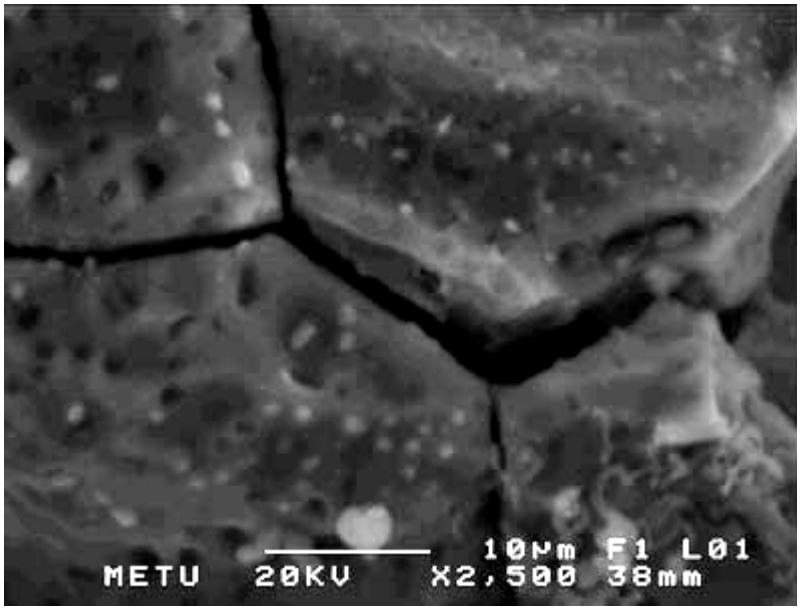

Figure 4.42 Grainboundaries and grain boundary precipitates of 7050-T651 alloy in TS orientation.

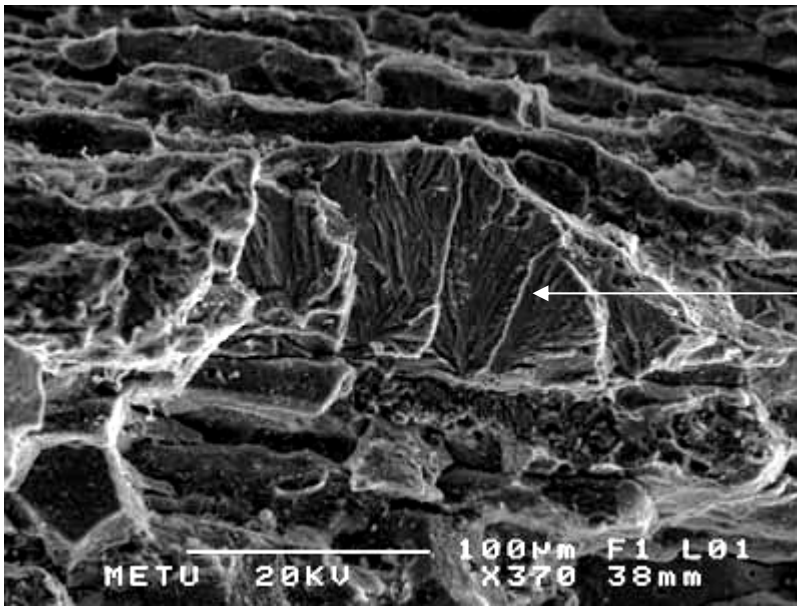

Figure 4.43 Step formation in TS orientated specimen of 7050-T651 alloy.

Micrograph from the intergranular SC crack region is shown in Figures 4.44 and in Figure 4.45 a cleavage plane of transgranular crack propagation can be identified in LT specimen in T651 condition. Figure 4.46 illustrates the oxide particles at the SC crack propagation region.

Figures 4.47 and 4.48 reveals intergranular type of SC crack in TS and LT specimen of 7050-T7651 alloy, respectively. The coarse constituent particles are also observed at these surfaces. Figure 4.49 shows the transgranular and intergranular SC cracks in TS specimen at T7651 temper. And, the transgranular crack propagation region of LT specimen at T7651 temper is visible in photograph given in Figure 4.50.

An intergranular fracture surface of the alloy tested in TS orientation in the two stage overaged state, T73651, is shown in Figure 4.51. Constituent particles can also be observed in this figure. Figure 4.52 shows a mixed fracture features of the same treatment and orientation. Again a mixed type of fracture is observed in LT specimen with T73651 temper as in Figure 4.53. A transgranular fracture surface of the same orientation and temper was previously shown in Figure 4.25.

All these fractographic studies are consistent with the previous discussions. In summary, the alloy has showed almost invariably intergranular type of cracking when tested in SL orientation regardless of the aging type, proposing a failure by anodic dissolution mechanism. However, both intergranular and transgranular type of fracture were observed in TS and LT specimens including cleavage step formation at T651 temper in TS orientation. Hence, these findings can be related to some other mechanisms, such as hydrogen embrittlement and film induced cleavage, operating during SCC of aluminum alloy 7050 in 3,5% NaCl solution. Evidently, there has to be some differences in the relative roles of these mechanisms at different tempers leading to different SC crack growth characteristics.

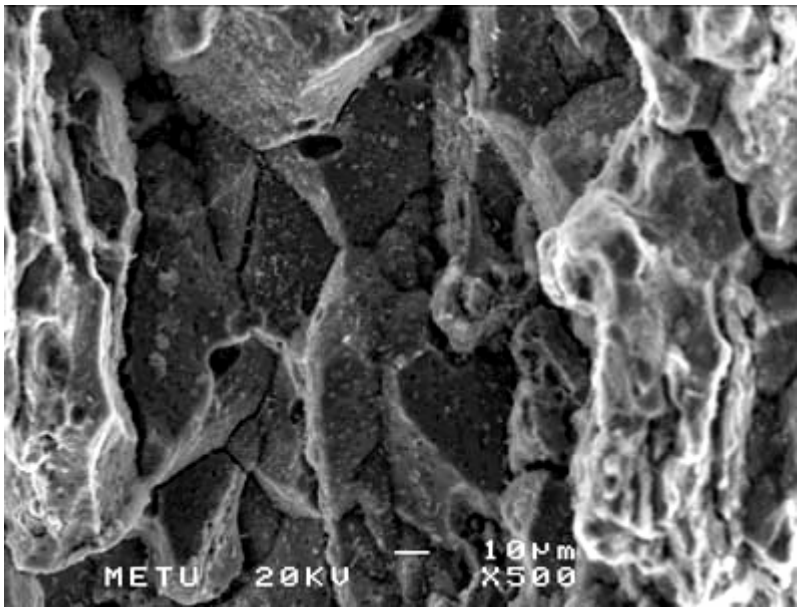

Figure 4.44 Intergranular SCC of 7050-T651 alloy in LT orientation.

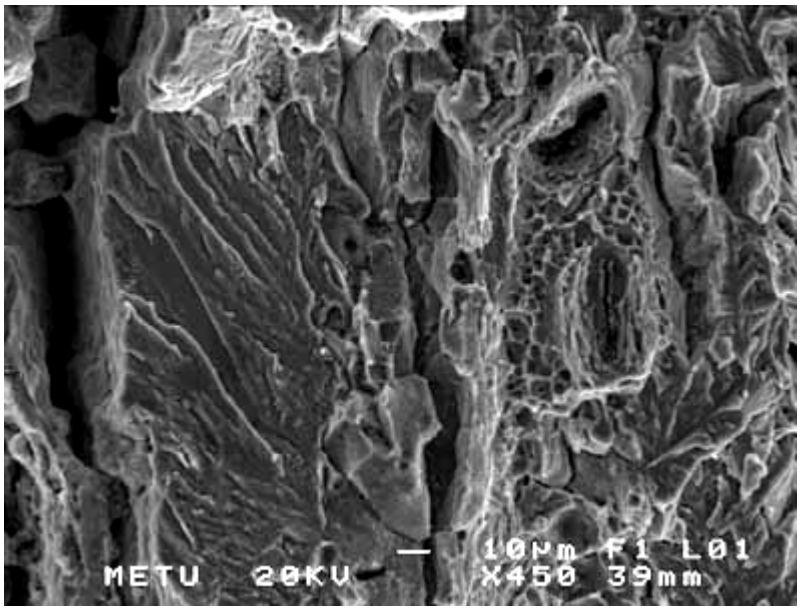

Figure 4.45 Transgranular type of cracking including some dimples in 7050-T651 alloy in LT orientation.

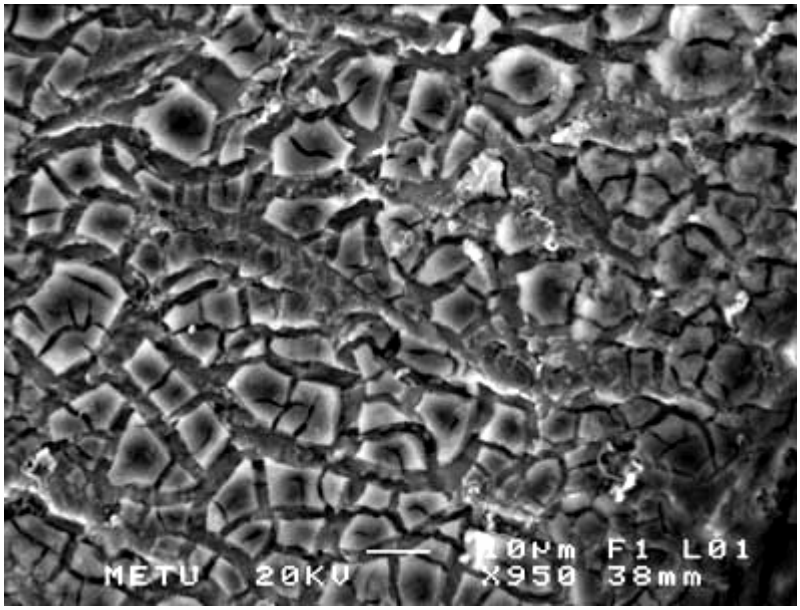

Figure 4.46 The fracture surface covered with oxide particles LT specimen at T651 temper.

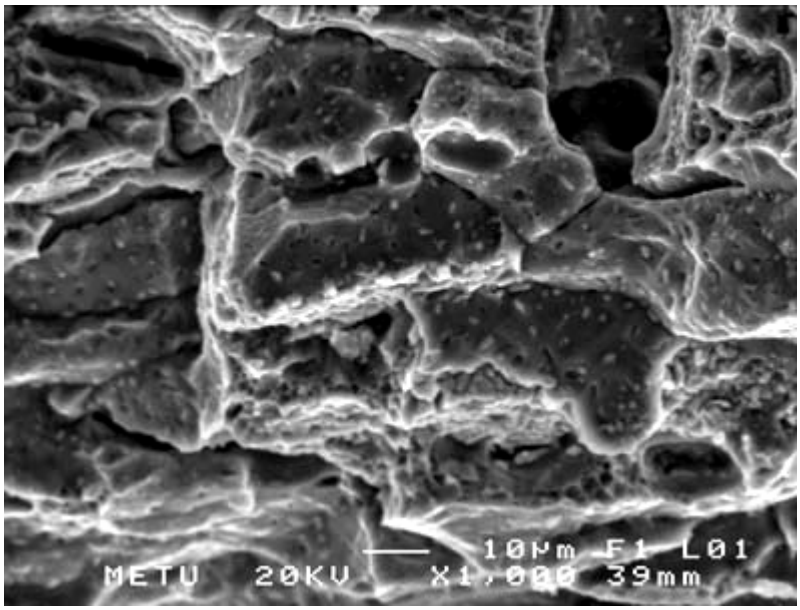

Figure 4.47 Intergranular type of SC crack in TS specimen of 7050-T7651 alloy.

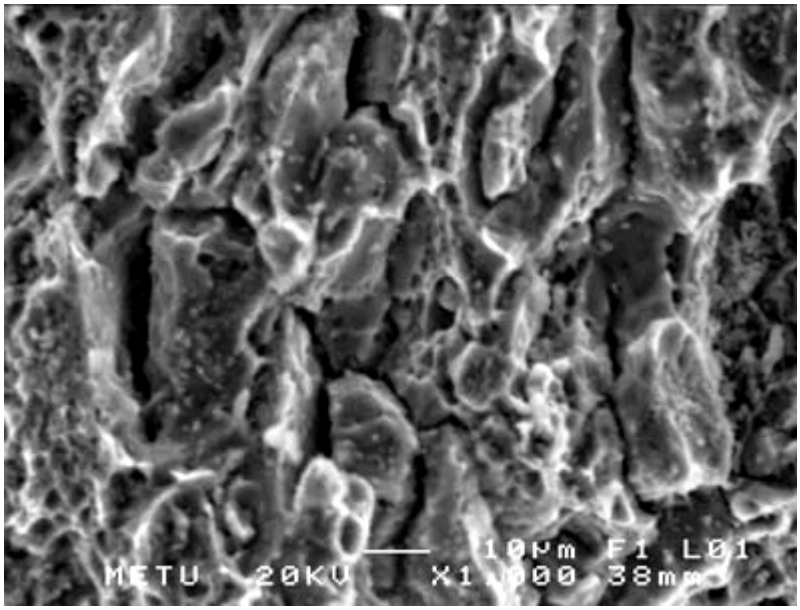

Figure 4.48 Intergranular type of SC crack in LT specimen of 7050-T7651 alloy.

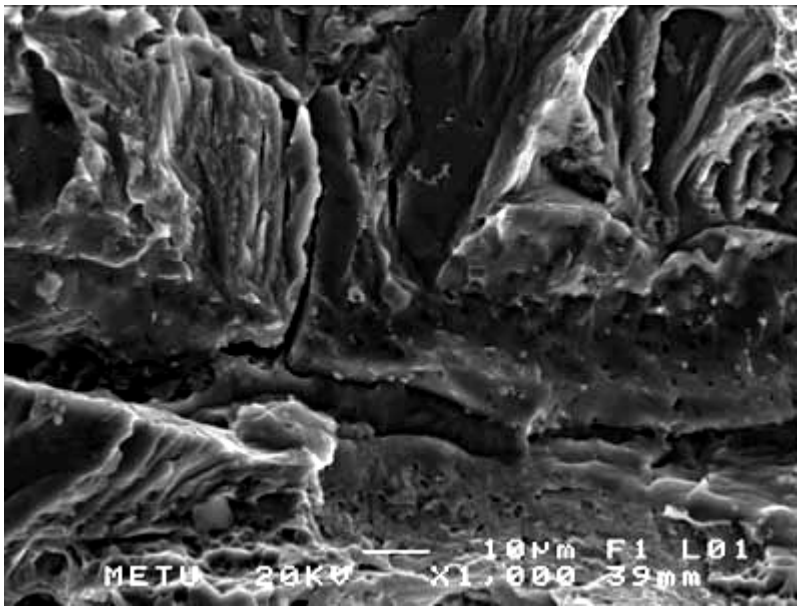

Figure 4.49 Transgranular and intergranular type of SC cracks in TS specimen of 7050-T7651 alloy.

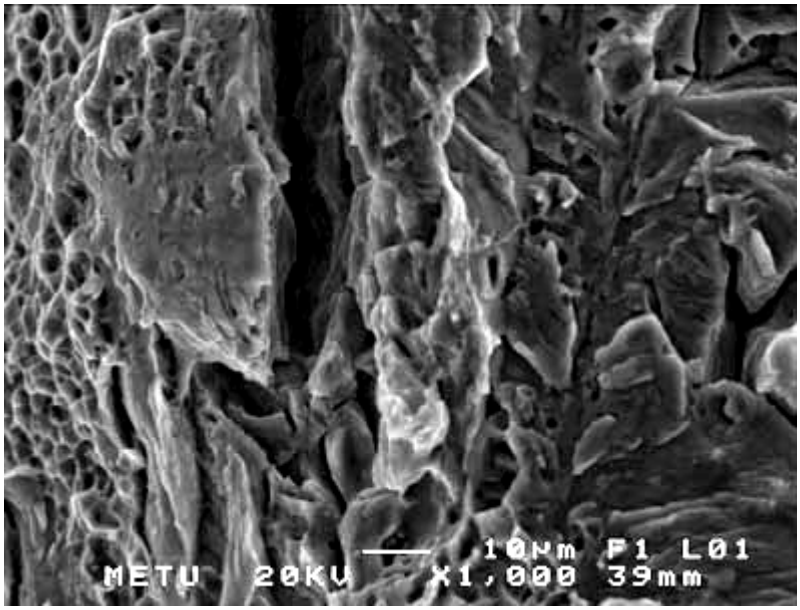

Figure 4.50 Transgranular type of SC cracks in LT specimen of 7050-T7651 alloy.

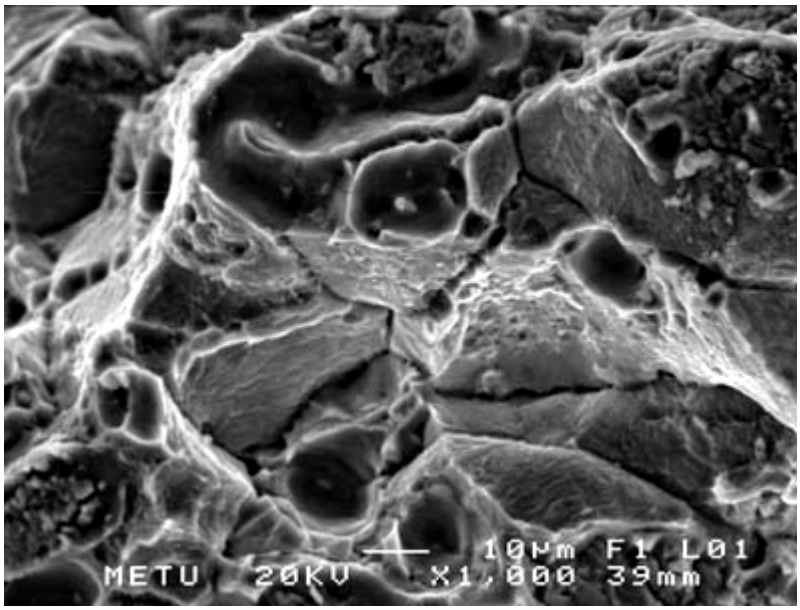

Figure 4.51 Intergranular cracks in SCC region of 7050-T73651 alloy tested in TS orientation, including coarse sonstituent particles.

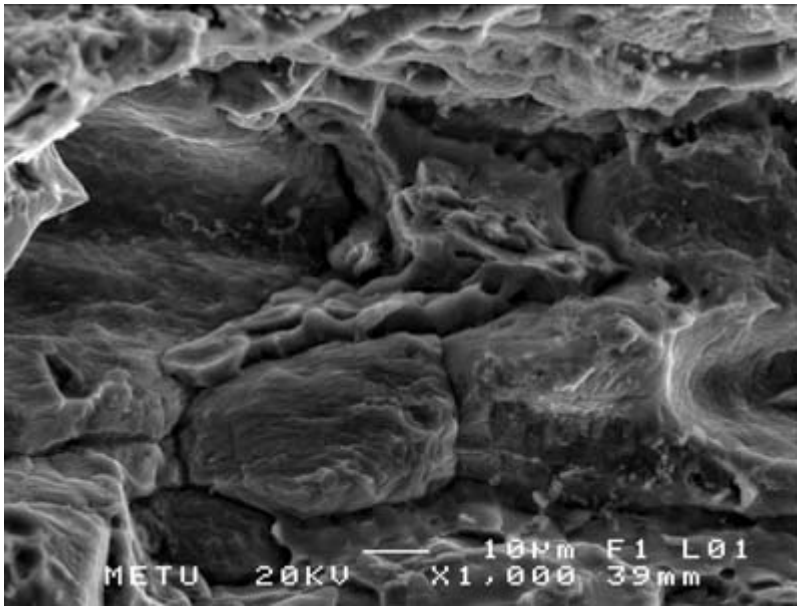

Figure 4.52 Mixed type of fracture surface of 7050-T73651 alloy tested in TS orientation.

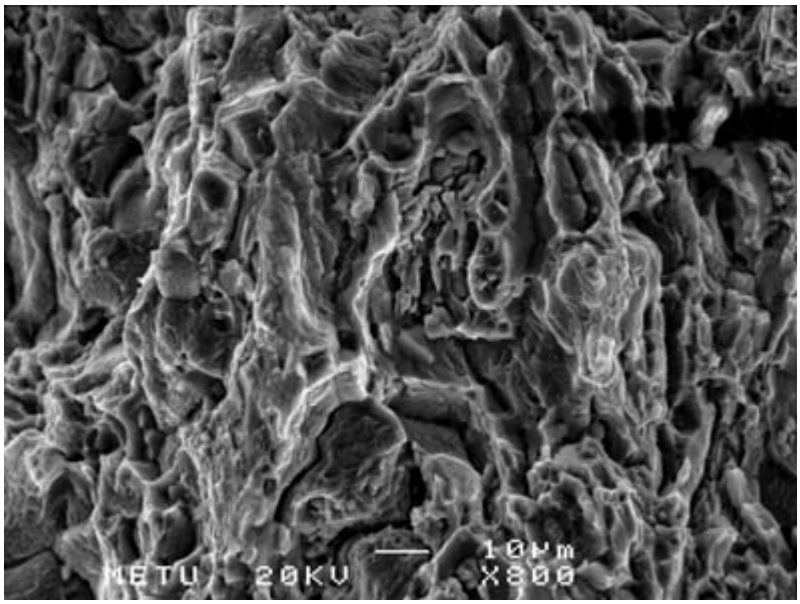

Figure 4.53 Mixed type of fracture surface of 7050-T73651 alloy tested in LT orientation.

4.7 Some Remarks on Experimental Techniques used in this study

In this work, CERT was applied to precracked CT specimens to determine the SCC characteristics of the alloy 7050 in different heat treatments and specimen orientations. Results have shown that this test method is practical for the purpose of its use. By the application of the method, a large number of specimens could be tested in a reasonable period of time leading to a rich database which helped also to arrive at valuable predictions regarding the mechanisms of SCC of Alloy 7050.

CERT provides time-saving although the duration of the tests varied between 4 to 15 hours which may be regarded as long periods for laboratory testing. However, when compared to the constant load and constant deflection tests which require weeks or months to complete, CERT is quite fast method. Since CERT is not terminated after an arbitrary period of time, testing always ends with specimen fracture. So the critical parameters at the fracture point can be used in designing materials for use.

In CERT, since the severity of cracking is a function of strain rate, there is a critical range in which SCC occurs. Maximum severity is observed for strain rates of the order 10^{-6} sec^{-1} for many material-solution systems (56). In this work an extension rate of $5{,}66.10^{-5}$ mm/sec was used which corresponds to a strain rate of $1{,}13.10^{-6}$ sec^{-1} (for a 50 mm long specimen) which falls into the assigned range. Ductile failure occurs at too rapid strain rates before significant SCC is observed. On the other hand, if the rate is slower compared to the critical range, SCC will be suppressed by the repassivation at the crack tip (56,57). Effect of strain rate on the fracture behaviour was shown in Figure 2.12 (2).

The DCPD technique is a practical way to measure the crack lengths during fracture mechanics tests. The first advantage of the method is that visual inspection which may result in reading errors is eliminated. Since the crack

length is evaluated in the plane of crack propagation, the crack front curvature is also included in the measurements.

In this work, the resolution was valuable at a constant current of 15 A. The resolution was 30 μV for 1 mm change in the crack length. This value was found to be quite beneficial for evaluating the SC crack growth behaviour. The calibration technique applied provides an feasable way to accurately determine the crack lengths from the EPD readings. Since the conductivity of the aluminum alloys is much larger than that of the NaCl solution, the error induced by the presence of environment remained at ignorable level.

CHAPTER 5

CONCLUSIONS

1. The SCC resistance of the alloy is maximum when loaded in the longitudinal direction, i.e. LT orientation. Since 7050 alloy is more susceptible to SCC in the SL orientation where the crack propagates parallel to the rolling direction, in all heat treatments, the use of the alloy in this orientation should be avoided.
2. The reason for different SCC characteristics in different orientations of the alloy is the highly anisotropic microstructure of the alloy.
3. The highest resistance in LT orientation and the lowest in the SL are attributed to the total area of the high-angle grain boundaries oriented perpendicular to the loading direction which is less in amount for LT as compared to the SL orientation.
4. Application of peak aging treatment T651 results in the most susceptible condition in the SL orientation. As aging proceeds to T7651, the SCC resistance increases. And if a two step over aging, T73651 is applied, a further improvement is achieved in the most SCC susceptible orientation.
5. Alloy shows highest resistance to SCC in TS and LT orientations in the peak aged state. And the susceptibility decreases in T73651 with respect to T7651.
6. Based on the experimental results and fractographic analysis the dominant mechanism of SCC in SL orientation would be predicted to be the anodic dissolution. In SL specimens, the improvement of SCC resistance with T7651 and T73651 may be attributed to the decreased potential difference between the grain boundary regions and the grain interior; or the change in the slip mode with over aging treatments.

7. As evidenced by results obtained with specimens in TS and LT orientations, it may be concluded that not only anodic dissolution but also hydrogen embrittlement and film induced cleavage may take place in competition during SCC.
8. Constant extension rate testing was applied successfully as a relatively rapid method to evaluate the SCC characteristics.
9. Direct current potential drop technique was found as a sufficiently accurate technique to measure the crack lengths of CT specimens.

REFERENCES

1. B. F. Brown, "Stress-Corrosion Cracking in High Strength Steels and in Titanium and Aluminum Alloys", Naval Research Laboratory, Washington D.C., 1972.
2. ASM Metals Handbook, Ninth Edition, Vol. 8, pp 495-532.
3. R.P. Wei, S.R. Novak, and D.P. Williams, "Some Important Considerations in Stress Corrosion Cracking Test Methods", Materials Research and Standards. MTRSA, Vol.12, No. 9, p.25, 1972.
4. "Review of Full Structural Materials" T.Mills, G.Clark, C.Loader, P.K.Sharp, and R.Schmidt, Airframes and Engines Division, Aeronautical and Maritime Research Lab. Aerostructures Technologies, Pty.Ltd.
5. J.C. Scully, "Stres Corrosion Cracking: Introductory Remarks", The theory of Stres Corrosion Cracking, NATO Science Commitee, Research Evaluation Conference, 1971.
6. T.D. Burleigh, Corrosion, Vol. 47, pp.89-98, 1991.
7. J.Kruger, "Failure by Stress Corrosion Cracking-Current Approaches Toward Failure Prediction", Stress Corrosion Cracking, J.Yahalom, A.Aledyew, Freund Publishing House, Tel-Avis, 1980.
8. Hertzberg, A. Richard, "Deformation and Fracture Mechanics of Engineering Materials", Third Edition, John Wiley & Sons Inc., Newyork, 1989, pp. 421-454.
9. R. C. Newman, in Corrosion Mechanisms in Theory and Practice, edited by P. Marcus, J. Oudar, p.311, Marcel Dekker, Inc., New York, 1995.

10. V.S. Sinyavskii and A.M. Semenov, Protection of Metals, Vol. 38, No.2, pp132-140, 2002.

11. M.O. Speidel, "Current Understanding of Stress Corrosion Crack Growth in Aluminum Alloys", The Theory of Stress Corrosion Cracking in Alloys, J.C. Scully, NATO, Scientific Affairs Division, Brussels, 1971.

12. E. Dix, American Society of Metals, Vol.42, p.1057,1950.

13. R. Mears, R. Brown and E. Dix, Jr., In Symposium on Stress Corrosion Cracking of Metals, p.323 , ASTM-AIME, Philadelphia, 1945.

14. U. R. Evans, The Corrosion and Oxidation of Metals, pp 665-93, Ed. Arnold, London (1960).

15. R. N. Parkins, J. Iron and Steel Inst., V172, p149, 1972.

16. T. P. Hoar, Corrosion, V19, p. 331, 1963.

17. L. Graf, 2nd International Congress on Metallic Corrosion, NACE, Houston, 1963.

18. T. Hoar and J. West, Nature, V181, p.835, 1958.

19. A. Baumell and H: Engell, Archiv. F. Eisenhuttenw., V 32, p. 379, 1961.

20. S. Maitra, G.C. English, Metallurgical Transactions A, Vol13, I1, pp. 161-166,1982

21. A. Joshi, C. R. Shastry, M. Levy, Metallurgical Transactions A, V12, I6, pp. 1081-1088, 1981.

22. D. A. Hardwick, A. W. Thompson, I. M. Bernstein, Metallurgical Transactions A, V 14, pp. 2517-2526, 1983.

23. R. G. Song, M. K. Tseng, B. J. Zhang, J. Liu, Z. H. Jin, K. S. Shin, Acta Materialia, V44, No.8, pp. 3241-3248, 1996.

24. P. N. Adler, G. Geshwind, Metallurgical Transactions, V 3, pp. 3191-3200, 1972.

25. T.C. Tsai, T.H. Chuang, Materials Science and Engineering A225, pp. 135-144, 1997.

26. W.Z. Gruhl, Aluminum, V 54, pp. 323-325, 1978

27. W.Z. Gruhl, Zeitschrift fur Metallkunde, Vo.74, I12, pp. 777-782, 1983.

28. R. Hermann, Corrosion, V 44, I 10, pp. 685-690, 1988.

29. D. Hardie, N. J. H. Holroyd, R. N. Parkins, Metal Science V 13, I 11, pp. 603-610, 1979.

30. E. Kus, Study of Salt-Water Cracking Behaviour of 7050-T73651 Aluminum Alloy Through Slow Strain Rate Testing Under Potentiostatic Control,M.Sc. Thesis in the Department of Metallurgical Engineering, in Middle East Technical University, 2002.

31. T.Magnin and P. Rieux, Scripta Metallurgia and Materialia, V 21, I 7, pp. 907-911, 1987.

32. M. C. Reboul, T. Magnin, T. J. Warner, The 3rd International Conference on Aluminum Alloys, ppp. 453- 460.

33. D. Najjar, T. Magnin, T. J. Warner, Materials Science and Engineering, A 238, pp. 293-302, 1997.

34. S. M. Lee, S.I. Pyun, Y.G. Chun, Metallurgical Transactions A, V 22, pp. 2507-2414, 1991

35. K. Sieradzki and R. C. Newman, Phil. Mag., A 51, pp. 95-132, 1985.

36. D.A. Jones, "Principles and Prevention of Corrosion", Prentice Hall, Second Edition, 1992.

37. E.N. Pugh, Corrosion, V 41, No:19, pp. 517-526, 1985.

38. H. Kanematsu, M. Okido, and T. Oki, J. Japan Inst. Light Metals, V 36, I 6, pp. 333-338, 1985.

39. H. Kanematsu, M. Okido, and T. Oki, J. Japan Inst. Light Metals, V 36, I 5, pp. 255-265, 1985.

40. M.V. Hyatt and M. O. Speidel, "High Strength Aluminum Alloys", in "SCC in High-Strength Steels and in Aluminum Alloys", pp. 147-244, edited by B.F. Brown, Naval Research Laboratory, Washington D. C., 1972.

41. M. Yoda, Engineering Fracture Mechanics, Vol. 30, No. 4, pp. 461-467, 1988.

42. M. O. Speidel, Metallurgical Transactions A, Vol. 6A, pp. 631-651, 1975.

43. B.J. Connolly and J.R. Scully, Scripta Materialia, Vol.42 pp. 1039-1045, 2000.

44. A. Conde, J.J. de Damborena, Corrosion Science, Vol.41, pp. 10791088, 1999.

45. I. J. Polmear, J. Australian Inst. Met.,Vol. 89, p193, 1960.

46. A. J. Sedriks, P. W. Slattery, and E. N. Pugh, Trans. ASM Vol. 62, p 238, 1969.

47. M. O. Speidel, Fundamental Aspects of SCC, edited by R. W. Stahle, A. J. Forthy and D. Van Rooyen, p. 638, NACE Houston, 1969.

48. A. J. Deardo and R. D. Townsend, Metallurgical Transactions., Vol.1, p 2573, 1970.

49. R. W. Hertzberg, Deformation and Fracture Mechanics of Engineering Materials, 4th Edition, John Wiley and Sons Inc., 1996

50. D.O. Sprowls, R.H. Brown, "Stress Corrosion Mechanisms for Aluminum Alloys", Proc. Conf. On Fundeamental Aspects of Stress Corrosion Cracking, NACE, Houston, Texas, p.466, 1969.

51. I.L. Rosenfeld and I.K. Marshakov, Shurn. Fizic. Khimii, V31, p. 2328, 1969.

52. W.T. Tsai, J.B., Duh, J.J. Yeh, J. Lee, Y. Chang, Corrosion, Vol.46, No.6, pp.444-449,1990.

53. W. J. Helfrich, "Influence of Stress and Temperature on Short-Transverse Stress Corrosion Cracking of an Al-4.2Zn-2.5Mg Alloy", Stress Corrosion Testing, ASM STP 425, 1966.

54. B. F. Brown, Stress Corrosion Cracking Control Measures, National Bureu of Standards Monograph 156, U.S. Department of Commerce, June 1977.

55. W. R. Wearmouth, G. P. Dean and R. N. Parkins, Role of Stress in the Stress Corrosion Cracking of a Mg-Al Alloy, Corrosion, Vol. 29, No. 6, pp. 251-258, 1973.

56. R. N. Parkins, Development of Strain Rate Testing and Its Implications, in Stress Corrosion Cracking – The Slow Strain-Rate Technique, STP 665, edited by G. M. Ugiansky and J. H. Payer, ASTM, pp. 5-25, Philadelphia, 1979.

57. R.N. Parkins, "Stress Corrosion Test Methods-Physical Aspects", The Theory of Stress Corrosion Cracking in Alloys, J.C. Scully, NATO, Scientific Affairs Division, Brussels, 1971.

58. J.H.Payer,W.EBerry,W.K. Boyd, "Constant Strain Rate Technique for Assesing Stress-Corrosion Susceptibility", Stress Corrosion-New Approaches, ASTM STP 610, ASM, pp. 82-93,1976.

59. L.F. Mondolfo, "Al-Alloys Structure and Properties", London, Boston,Butterworths, 1976.

60. ASM Speciality Handbook, "Aluminum and Aluminum Alloys".

61. C.L. Briant, "Metallurgical Aspects of Environmental Failures", Materials Science Monographs 12, Elseiver, 1985.

62. ASM Speciality Handbook, Aluminum and Aluminum Alloys, Heat Treating of Aluminum Alloys pp. 675-718.

63. Metals Handbook, Vol.2 - Properties and Selection: Nonferrous Alloys and Special-Purpose Materials, ASM International 10th Ed. 1990.

64. Nr. Bericht TF-621.3 Bauteilspezifische Wekstoffuntersuchungen, Untersuchungen an Halbzeug 7050-T73651, Bruchzahigkeit and Ermudungsverhalten, IABG,1976.

65. ASTM E 399-90, Standard Test Method for Plane-Strain Fracture Toughness of Metallic Materials.

66. J.K Donald, J.Ruscau, "Direct Current Potential Difference Fatigue Crack Measurement Techniques, Fatigue Crack Measurement: Techniques and Applications, EMAS Publication, 1990

67. M.A. Hicks and A.C. Pickard, International Journal of Fracture, Vol.20, pp. 91-101,1982

68. W. Dietzel, K.H. Geesthaht, Material Prüfun, Band 28, No.11 pp, 368-372,1986.

69. G.H.Aronson,R.O.Ritchie, Journal of Testing and Evaluation, Vol.7, No.4, pp. 208-215, 1979.

70. G.A. Hartman and D.A. Johnson, "DC Electric Potential Method Applied to Thermal/Mechanical Fatigue Crack Growth", Experimental Mechanics, pp. 106-112, March 1987.

71. W.R. Catlin, D.C. Lord, T.A. Prater, L.F. Coffin, "The Reversing DC Electrical Potential Method", Automated Test Methods for Fracture and Fatigue Crack Growth, ASTM STP 877, American Society for Testing and Materials, Philadelphia, PA, 1985.

72. R. Gürbüz, Effect of Orientation on Salt Water Fog Enhanced Fatigue Crack Growth Beahviour of 7050-T73651 Alloy, Ph.D. Thesis in the Department of Metallurgical Engineering, in Middle East Technical University,1987.

73. N.U. Deshpande, A.M. Gökhale, D.K.Denzer, and John Liu, Metallurgical and Materials Transactions A, V29A, April 1998, pp1141-1201.

74. A.M. Gökhale, N.U. Deshpande, D.K.Denzer, and John Liu, Metallurgical and Materials Transactions A, V29A, April 1998, pp1203-1210.